

# Annexure I

## List of Primers

Gene	Forward (Sequence 5'-3')	Reverse (Sequence 5'-3')
<i>p53</i>	CAGCCAAGTCTGTGACTTGCACGTAC	CTATGTCGAAAAGTGCTTCTGTCATC
<i>BCL-2</i>	ATGTGTGTGGAGAGCGTCAACC	GCATCCCAGCCTCCGTTATC
<i>MDM-2</i>	GTGCTGTAACCACCTCACAGA	TTGGCACGCCAAACAAATCTC
<i>Survivin</i>	AGAACTGGCCCTTCTTGGAGG	CTTTTTATGTTCTCTATGGGGTC
<i>BAD</i>	CTTTAAGAAGGGACTTCCTCGC	GTGGAGTTTCGGGATGTGGA
<i>BID</i>	TGAGTGGCTGAATGACCCCA	TCCCAGTGGCGACAGAATC
<i>BAX</i>	CCTTTTCTACTTTGCCAGCAAAC	GAGGCCGTCCCAACCAC
<i>AIF</i>	GTGCATCAGGGGGCAAATC	TCTGAAGCAGATAACGCGGC
<i>PARP1</i>	GCCCTAAAGGCTCAGAACGA	CTACTCGGTCCAAGATCGCC
<i>cathepsin B</i>	CCAGGGAGCAAGACAGAGA	GAGACTGGCGTTCTCCAAAG
<i>β-catenin</i>	GTCCTGGAATGAGACCGGAG	TAGCCCCCAGAGTGAAAGGG
<i>calpain 2</i>	CGAGAGGGCCATCAAGTACC	GCAGATCTCCGTGGGGC
<i>PCNA</i>	TGTTCTCTCGTTGTGGAGT	TCCCAGTGCAGTTAAGAGCC
<i>caspase 3</i>	ACATGGCGTGTCAATAAATACC	CACAAAGCGACTGGATGAAC
<i>caspase 9</i>	CCAGAGATTCGCAAACCAGAGG	GAGCACCGACATCACCAAATCC
<i>caspase 7</i>	GGAGCGCACTACCCCGA	ATCATCTGCCATCGTTCCCA
<i>caspase 8</i>	AGAGTCTGTGCCCAAATCAAC	GCTGCTTCTCTCTTTGCTGAA
<i>cytochrome c</i>	GAACAAAGGCATCATCTGGGG	GGCAGTGGCCAATTATTACTCA

<b><i>TRADD</i></b>	CGCTCTGTGGGTCTCAAATGGC	AGTCCTCTGCCAGGCTGGTGA
<b><i>FADD</i></b>	TTGGAGAAGGCTGGCTCGTCAG	ACATGGCCCCACTCCTGTTCTG
<b><i>cyclin D</i></b>	ATGCCAACCTCCTCAACGAC	TCTGTTCCCTCGCAGACCTCC
<b><i>cyclin E</i></b>	CCATCATGCCGAGGGAGC	TTATTGTCCCAAGGCTGGCT
<b><i>CDK 4</i></b>	CCTCTCTAGCTTGCGGCCTG	CTCAGATCAAGGGAGACCCTCAC
<b><i>CDK 2</i></b>	GCATCTTTGCTGAGATGGTGAC	GTAACCTCCTGGCCACACCAC
<b><i>HIF-1<math>\alpha</math></i></b>	AGAGGTTGAGGGACGGAGAT	GACGTTCAGAACTTATCCTACCAT
<b><i>IL-8</i></b>	GCTCTGTGTGAAGGTGCAGTT	TTTCTGTGTTGGCGCAGTGT
<b><i>TGF-<math>\beta</math></i></b>	CGACTCGCCAGAGTGGTTAT	CGGTAGTGAACCCGTTGATGT
<b><i>IL-10</i></b>	CGAGATGCCTTCAGCAGAGT	GGCAACCCAGGTAACCCTTA
<b><i>iNOS</i></b>	TGCCCTCCTCTCGACAAAAC	TTGAGTTCATCCCCTTCGCC
<b><i>MMP9</i></b>	GTCTCCTGGCTCATGCCTTT	TTTACCACCTGGCCCTCTC
<b><i>MMP2</i></b>	GCCTTCAAGGTGTGGAGTGA	ATCCCCGTGGTCAGCTTTTC
<b><i>E cadherin</i></b>	AGGCCAAGCAGCAGTACATT	GGGGGCTTCATTACATCCA
<b><i>N cadherin</i></b>	ATCAAGCCTGTGGGAATCCG	CTCTATGGGCCAGGTTTTCTCA
<b><i>vimentin</i></b>	GACCAGCTGACCAACGACAA	GAGGCATTGTCAACATCCTGTC
<b><i>snail 1</i></b>	CGAACGCACACTGGTGAAAA	CATACGGGAGAAAGTCCGGG
<b><i>snail 2</i></b>	AGGACTCACACCTTGCCTTG	GTAGGTGAGCCCTGAGGTTG
<b><i>TIMP2</i></b>	ACTACGCCTGCATCAAGAGG	GGCGTGGACCAGTCTAACAT
<b><i>TIMP4</i></b>	AAAGCTATACGGGCACCAGG	CAAAGCTGTGAGCGTGCAAT
<b><i>claudin 3</i></b>	GCCACCAAGGTCGTCTACTC	CCCTGCGTCTGTCCCTTAGA
<b><i>claudin 4</i></b>	TCTCCTCTGTTCCGGGTAGG	CGTCCATCCACTCTGCACTT

<b><i>VEGF-<math>\alpha</math></i></b>	CTCCACCATGCCAAGTGGTC	GCAGTAGCTGCGCTGATAGA
<b><i>AKT</i></b>	CAGCCTGGGTCAAAGAAGTCA	ATGTACTIONCCCCTCGTTTGTGC
<b><i>KDR</i></b>	GCTTGCTTTTTGCCGGATGA	TGCCGACCTCTGCATGTTAG
<b><i>ZEB1</i></b>	CGTTCATAAGGGAGGACGGG	AGTGGGAGCACTCATAGGGT
<b><i>18s rRNA</i></b>	GGCCGTTCTTAGTTGGTGGA	TCAATCTCGGGTGGCTGAAC

# A synthetic coumarin derivative (4-flourophenyacetamide-acetyl coumarin) impedes cell cycle at G0/G1 stage, induces apoptosis, and inhibits metastasis via ROS-mediated p53 and AKT signaling pathways in A549 cells

Shweta Umar<sup>1</sup> | Rina Soni<sup>2</sup> | Sunil D. Durgapal<sup>2</sup> | Subhangi Soman<sup>2</sup> | Suresh Balakrishnan<sup>1</sup> 

<sup>1</sup>Department of Zoology, Faculty of Science, The M. S. University of Baroda, Vadodara, India

<sup>2</sup>Department of Chemistry, Faculty of Science, The M. S. University of Baroda, Vadodara, India

## Correspondence

Suresh Balakrishnan, Department of Zoology, Faculty of Science, The M. S. University of Baroda, Vadodara 390002, Gujarat, India.  
Email: b.suresh-zoo@msubaroda.ac.in

## Funding information

Department of Biotechnology, Ministry of Science and Technology, India,  
Grant/Award Number: BT/PR11467/MED/31/270/2014; Science and Engineering Research Board, Grant/Award Number: SB/SO/AS-008/2014

## Abstract

New chemotherapeutic agents with minimum side effects are indispensable to treat non-small-cell lung cancer (NSCLC) since the mortality rate of patients suffering from NSCLC remains high despite receiving conventional medication. In our previous study, many coumarin derivatives were screened for their anticancer properties in A549, an in vitro NSCLC model. One of these, 4-flourophenyacetamide-acetyl coumarin (4-FPAC), induced cytotoxicity at a concentration as low as 0.16 nM. Herein, initially, the cytotoxic potential of 4-FPAC was tested on a noncancerous cell line NIH3T3 and was found safe at the selected dose of 0.16 nM. Further, we investigated the mechanism by which 4-FPAC induced cytotoxicity and arrested the progression of cell cycle as well as metastasis in A549. Results of ethidium bromide/acridine orange (EtBr/AO), 4,6-diamidino-2-phenylindole, comet, and lactate dehydrogenase assays revealed that 4-FPAC caused cytotoxicity via reactive oxygen species-induced p53-mediated mechanism, which involves both extrinsic and intrinsic pathways of apoptosis. Dichlorodihydrofluorescein diacetate, rhodamine 123, and AO staining confirmed the involvement of both mitochondria and lysosome in inducing apoptosis. However, flow cytometric analysis revealed that it causes cell cycle arrest at the G0/G1 phase by modulating p21, CDK2, and CDK4 expression. Aggregation, soft-agar, clonogenic, and scratch assays as well as gene expression analysis collectively confirmed that 4-FPAC minimizes the metastatic property of A549 by downregulating Snail, matrix metalloproteinase 9, and interleukin-8. Additional studies reaffirmed the above findings and substantiated the role of PI3K/AKT in achieving them. The cell-type-specific selective cytostatic and antimetastatic properties shown by 4-FPAC indicate its potential to emerge as a drug of choice against NSCLC in the future.

## KEYWORDS

apoptosis, coumarin derivative, epithelial-mesenchymal transition, non-small-cell lung cancer, reactive oxygen species

## 1 | INTRODUCTION

Cancer is a complex disease characterized by rapidly proliferating transformed cells that have got enormous invasion as well as metastatic abilities.<sup>[1]</sup> However, despite all the available modern medical interventions, cancer therapy is still a major challenge. Further, it has been reported that of all the cancers known worldwide, lung cancer most frequently occurs in men, with a conspicuously high mortality rate. Moreover, out of the total incidents of lung cancer, non-small-cell lung cancer (NSCLC) alone accounts for around 80% to 85%, of which adenocarcinoma is the most common type, claiming for 40% of the total occurrences.<sup>[2]</sup> NSCLC is observed in many individuals irrespective of their dietary habits. However, the present medical advances like surgery, immunotherapy, and chemotherapy are insufficient for its complete alleviation. On the contrary, the latter adds to the complications by aggravating the side effects, and causes deleterious effects on surrounding healthy cells. Therefore, it is imperative to find a chemotherapeutic agent with the least plausible side effects and higher specificity.

Coumarin is one such phytopharmacological agent that is widely known for its anticancer, anti-inflammatory,<sup>[3]</sup> and anticoagulant properties.<sup>[4]</sup> These compounds and some of their derivatives are found naturally in tonka beans and cinnamon, but they are present in a lesser amount, which makes the extraction process cumbersome. Therefore, chemical analogs of natural coumarin were synthesized. Some of these analogs were marketed as fixatives, blood thinners, and as drugs for the treatment of osteoporosis. However, due to attendant side effects these molecules are not approved by Food and Drug Administration in the United States.<sup>[5]</sup> One of the derivatives, which was used for treating lymphoedema in few European countries also got disapproved, due to its hepatotoxicity.<sup>[6]</sup> Such drawbacks of the available coumarin derivatives, lead to more concerted efforts to chemically synthesize better derivatives with selective anticancer properties, along with least evasive effects.

In one such attempt, we synthesized as many as twenty derivatives of coumarin by adding various pharmacophores to different positions of benzopyrone ring. They were then tested for potential cytotoxicity by using A549 cell line, a widely accepted in vitro model for NSCLC. The result of this study revealed that one of these derivatives, 4-fluorophenylacetamide-acetyl coumarin (4-FPAC), induced significant cytotoxicity at a very low concentration of 0.16 nM.<sup>[7]</sup> To ponder the mechanistic details of this observation the current study was envisaged wherein the antiproliferative, anti-metastatic, and antiangiogenic properties of 4-FPAC at a concentration of 0.16 nM was evaluated using A549 cell line.

## 2 | MATERIAL AND METHOD

### 2.1 | Chemical and reagent

The reagents were purchased from Sisco Research Laboratories (India), Gibco, or Sigma-Aldrich. After ascertaining the purity of the compound, as detailed in our previous study,<sup>[7]</sup> a stock solution of

4-FPAC was prepared in dimethylformamide (DMF). Various dilutions of the derivative were prepared in phosphate-buffered saline (PBS) wherein the final concentration of DMF was not more than 0.5% in any of the chosen aliquots.

### 2.2 | Cell line selection, procurement, and maintenance

The focus of the study was to check the effectiveness of 4-FPAC as an anticancer agent against the adenocarcinoma subtype of NSCLC, which accounts for 40% to 70% of the total NSCLC.<sup>[2]</sup> Therefore, as a prelude, we screened the efficacy of 4-FPAC, through 3-(4,5-dimethylthiazol-2-yl)-2,5-diphenyltetrazolium bromide (MTT) assay, in two additional representative cell lines of NSCLC namely, NCI-H23 and NCI-H522 (refer the Supporting Information Data for details) other than A549. The result revealed that 4-FPAC curtailed cell cycle progression only at very high concentration for NCI-H23 and NCI-H522 cell lines (half minimal inhibitory concentration [IC<sub>50</sub>] 26.08 ± 2.03 μM and 19.68 ± 3.98 μM, respectively) as compared with the IC<sub>50</sub> value of 0.16 nM recorded for A549 cell line.<sup>[7]</sup> Therefore, the human lung adenocarcinoma cell line A549 was selected as an in vitro NSCLC model to study the anticancer property of 4-FPAC.

Additionally, to evaluate the safety of 4-FPAC, MTT assay was performed on mouse fibroblast cell line NIH3T3, which is a widely used noncancerous cell line for safety evaluation of new chemical entities. All the cell lines were purchased from National Centre for Cell Science (Pune, India). Cell lines were maintained in Dulbecco's modified Eagle's medium (DMEM) supplemented with 2 mM of L-glutamine and 10% fetal bovine serum (FBS) with 1% antibiotic solution (penicillin and streptomycin). The cells were maintained at 37°C with 5% CO<sub>2</sub> in a humidified CO<sub>2</sub> incubator (Thermo Fisher Scientific).

### 2.3 | Dose and duration of treatment

In all the experiments, barring the ones that warranted a range of doses, a concentration of 0.16 nM of 4-FPAC was used since at this concentration significant reduction in cell viability was observed in A549. Further, a time-lapse study was conducted wherein after challenging A549 cells with a single dose of 0.16 nM of 4-FPAC, the cell viability was checked at an interval of 6, 12, 24, 48, and 72 hours (refer the Supporting Information Data for details). The result revealed that 4-FPAC exerted a maximum inhibitory effect at 48-hour posttreatment. Therefore, all the further analyses were performed after 48 hours of treatment with 0.16 nM of 4-FPAC.

### 2.4 | MTT assay

As mentioned previously, the IC<sub>50</sub> of 4-FPAC on A549 cell line was studied using MTT dye, as a part of preliminary screening of synthesized coumarin derivatives, and was found to be 0.16 nM.<sup>[7]</sup> However, to

check the safety of 4-FPAC at a dose of 0.16 nM, MTT assay was performed on mouse fibroblast cell line NIH3T3. These cells were seeded in a 96-well plate ( $1 \times 10^3$  cells per well) overnight in 100  $\mu$ L DMEM media supplemented with 10% FBS. During our initial trials, no significant change in viability was shown by NIH3T3 cells subjected to 4-FPAC even at a concentration of 500 nM. Therefore, a higher dose range of 0.5, 1, 10, 25, 50, 75, and 100  $\mu$ M was selected and the cells were incubated for 48 hours. Subsequently, 20  $\mu$ L of MTT solution (5 mg/mL prepared in PBS) was added, and the plate was incubated for 4 hours. Following incubation, the supernatant was removed and the purple-colored formazan crystals were dissolved in 100  $\mu$ L of acidified isopropanol. The absorbance (abs) was measured using a microplate reader at 570 nm (Metertech  $\Sigma$ 960) and cell viability was calculated using the following formula.

$$\text{Cell viability (\%)} = \left( \frac{\text{average abs. of treated groups}}{\text{average abs. of the control group}} \right) \times 100\%.$$

## 2.5 | Cell viability test

The cell viability test was performed by the dye exclusion test with 0.5% trypan blue. A total of  $1 \times 10^5$  cells per well were seeded in a 12-well plate and kept overnight for attachment. Next day, the cells were treated with 0.16 nM of 4-FPAC and incubated for 48 hours. DMF-treated cells were taken as vehicle control, whereas Triton X-100 treated ones served as a positive control. Following incubation, the cells were trypsinized, and the count was made using a hemocytometer.<sup>[8]</sup> Results are expressed as the percentage of dead cells.

## 2.6 | Cell cycle analysis

The effect of 4-FPAC on cell cycle distribution was analyzed using the BD FACS Aria III flow cytometer. Cells were seeded at the density of  $6 \times 10^7$  cells per T25  $\text{cm}^2$  flask. Cells were synchronized in serum-free media for 24 hours followed by derivative treatment for 48 hours. Since, in all previous experiments, there was no significant change observed between vehicle control and normal control, in the subsequent experiments, only vehicle control (0.2% DMF) was used alongside the treatment group. Cells were trypsinized and washed with PBS. The cell pellet was resuspended and fixed in ice-cold 70% ethanol at  $-20^\circ\text{C}$  for overnight. The next day, cells were centrifuged, collected, and the cell pellet was washed twice with PBS, then incubated with RNAase (100  $\mu\text{g}/\text{mL}$ ) and propidium iodide (50  $\mu\text{g}/\text{mL}$ ) solution for 30 minutes at  $37^\circ\text{C}$ . Moreover, 10 000 events per sub-population were analyzed using BD FACSDIYA software (Becton Dickinson & Co), as described by Chikara et al.<sup>[9]</sup>

## 2.7 | Cell morphology study

The cells from positive control, control, and 4-FPAC-treated group were seeded in a 12-well plate ( $2 \times 10^5$  cells per well). They were

then incubated for 48 hours and observed under  $\times 20$  magnification in Lawrence and Mayo (NIB 100) inverted microscope for their morphology.

## 2.8 | Ethidium bromide/acridine orange staining

A549 cells were treated with 0.16 nM of 4-FPAC and incubated for 48 hours. Cells from both control and treated groups were then washed with PBS, trypsinized, and stained with 10  $\mu$ L of ethidium bromide/acridine orange (EtBr/AO; 100  $\mu\text{g}/\text{mL}$ ). Cells treated with 0.1% Triton X-100 was used as positive control. The ratio of stain to cell ( $1 \times 10^3$ ) was maintained as 1:25  $\mu$ L. Images were taken using a DM2500 fluorescence microscope (Leica, Germany).

## 2.9 | Lactate dehydrogenase assay

Lactate dehydrogenase (LDH) assay was performed to check the necrotic potential of 4-FPAC. However, treatment with 0.16 nM of 4-FPAC did not induce a significant release of LDH. Therefore, a dose range study was conducted to find the concentration at which 4-FPAC induces membrane damage. A549 cells were plated on a 96-well plate ( $1 \times 10^4$  cells per well) for 24 hours in DMEM media without phenol red, followed by addition of 4-FPAC at a concentration of 0, 0.1, 0.5, 1.0, 1.5, 2.0, 2.5, and 3.0 nM. Subsequently, cells were incubated for 48 hours. The assay was performed as per the manufacturer's protocol (Pierce LDH Cytotoxicity Assay; Thermo Fisher Scientific).

## 2.10 | Comet assay

The effect of the 4-FPAC on apoptosis was observed using the comet assay. Derivative treatment with a dose of 0.16 nM was given, as mentioned previously, in a 12-well plate. Cells were harvested in 10  $\mu$ L PBS and mixed with 10  $\mu$ L of 1% low melting point (LMP) agarose and were spread on the slide precoated with 1% normal melting point agarose. Three slides were prepared for each experiment and were kept for 20 minutes at  $4^\circ\text{C}$ , followed by a coating of 0.75% LMP agarose for another 20 minutes at  $4^\circ\text{C}$ . After solidification of the components, slides were submerged in freshly prepared lysis buffer for 4 hours at  $4^\circ\text{C}$ . These were placed in the electrophoretic chamber, filled with freshly prepared tank buffer (pH 8.3), and incubated for 30 minutes at  $4^\circ\text{C}$ . Electrophoresis was conducted at 200 mA/22 V for 20 minutes at  $4^\circ\text{C}$ . Slides were three times washed with neutralization buffer and allowed to dry for 5 minutes in absolute ethanol. Following this, cells were stained with ethidium bromide (20  $\mu\text{g}/\text{mL}$ ). Slides were then observed under a fluorescence microscope. At least 30 cells per slides were evaluated, and components of comet assay were analyzed using CaspLab software version 1.2 (Krzysztof Kořica, CaspLab.com). As suggested by Olive and Banáth<sup>[10]</sup> DNA damage was expressed as % DNA in tail, % DNA in the head, tail length, head length, total comet length, tail moment, and olive tail moment.

## 2.11 | Nuclear morphology study

Change in nuclear morphology and chromatin condensation was observed using 4, 6-diamidino-2-phenylindole (DAPI).<sup>[11]</sup> A total of  $1 \times 10^3$  cells were seeded on coverslips, which were placed in a six-well plate and incubated at 37°C overnight for attachment. Following day, old media was replaced with the fresh one, containing 0.16 nM of 4-FPAC in case of the treatment group and incubated for 48 hours. Further, the cells were washed with PBS and fixed with ice-cold 70% ethanol, followed by permeabilization of the cells using 0.2% Triton X-100. Cells were then stained with 10 µg/mL DAPI solution for 15 minutes at room temperature and images were taken using a fluorescence microscope.

## 2.12 | Analysis of reactive oxygen species

Dichlorodihydrofluorescein diacetate (DCFH-DA) staining was used for the detection of intracellular reactive oxygen species (ROS) levels. Cells were seeded on a six-well plate ( $5 \times 10^5$  cells per well) and treated with 0.16 nM of 4-FPAC for 48 hours, then harvested by trypsinization. Following which, the pellet was washed with PBS and stained with 25 µM of DCFH-DA dye.  $H_2O_2$  was used as a positive control. Stained cells were incubated for 40 minutes. Representative images were captured using a Leica DM2500 fluorescence microscope.

To quantify total ROS, A549 cells ( $5 \times 10^5$  cells per well) were seeded in a six-well plate overnight. Next day, the cells were treated with 0.16 nM of 4-FPAC and incubated for 48 hours. Following incubation, the cells were harvested by trypsinization, washed with PBS, and again resuspended in 100 µL PBS containing 10 µM DCFH-DA and incubated for 40 minutes. An equal number of cells in 100 µL PBS was used as control for each fluorimetry detection. Tubes were read at 480 nm in Qubit 2.0 Fluorometer (Invitrogen), and the graph was plotted against change in ROS level.<sup>[12]</sup>

## 2.13 | Sample preparation for biochemical estimations

A total of 70% to 80% confluent cells were treated with 0.16 nM of 4-FPAC. After 48 hours of incubation, they were trypsinized, and the pellet was washed with prechilled PBS. Pellet was resuspended in extraction buffer (0.1% Triton X 100 and 0.6% sulfosalicylic acid in potassium phosphate EDTA buffer), homogenized and sonicated in ice for 2 to 3 minutes. The lysate was centrifuged at 3000g for 4 minutes at 4°C, and the supernatant was collected in a prechilled tube for following enzymatic assay.

## 2.14 | Glutathione peroxidase

Reaction mixture contained 200 µL phosphate buffer (0.4M pH 7), 100 µL glutathione (2 mM), 200 µL  $NaN_3$  (10 mM), 200 µL  $H_2O_2$

(10 mM), 100 µL water, and 40 µL of supernatant. It is then incubated for 5 minutes at room temperature followed by addition of 200 µL metaphosphoric acid (30 mM). It was further kept in ice for 10 min followed by centrifugation at 2000 rpm for 10 minutes. Of the supernatant collected, 60 µL was incubated with 60 µL of  $Na_2HPO_4$  (0.4M) and 3 µL DTNB following which, reading was taken at 412 nm in a microplate reader. The blank contained all the reagents except the supernatant. The activity of glutathione peroxidase (GPx) was expressed as nM of glutathione oxidized per minute per milligram protein.<sup>[13]</sup>

## 2.15 | Superoxide dismutase

Superoxide dismutase (SOD) activity of supernatant was assayed using a method based on its capacity to inhibit pyrogallol auto-oxidation, under standard assay condition.<sup>[14]</sup> A total of 3 µL of supernatant was added to 50 µL potassium phosphate buffer (0.2M, pH 8) and 5 µL pyrogallol (25 mg pyrogallol in 1 mL of 0.5N HCl), reading was taken at 420 nm in a microplate reader. Blank contained all the reagents except the supernatant.

$$\begin{aligned} \text{Unit of SOD/ml of assay mixture was calculated} \\ = (A - B/A \times 50) \times 100, \end{aligned}$$

where A is the abs of substrate blank and B is the abs of substrate test.

## 2.16 | Catalase

The supernatant was mixed with 50 µL of  $H_2O_2$  (0.2M) and 80 µL PBS (0.01M pH 7), incubated for 1 minute at room temperature then 80 µL dichromic acetic acid reagent (5%  $K_2Cr_2O_7$  in 1:4 glacial acetic acid) was added and boiled for 10 minutes, allowed to cool down, while absorbance was taken at 570 nm in a microplate reader. Blank contained all the reagents except supernatant.<sup>[15]</sup>

$$\text{Catalase activity} = [(\text{sample OD} \times \text{volume of assay})] / \text{aliquot} \times \text{CF},$$

where CF = 0.0041.

Result are expressed as µmol of  $H_2O_2$  decomposed/µg protein.

## 2.17 | Detection of mitochondrial membrane potential

For the detection of mitochondrial membrane potential rhodamine 123, a fluorescent dye that binds only to metabolically active mitochondria, was used as per standard protocol.<sup>[10]</sup> Cells were seeded on a coverslip in a six-well plate and incubated overnight for attachment. Next day, the old media was replaced with fresh media containing 0.16 nM of 4-FPAC and incubated for 48 hours, followed

by washing with PBS. Cells were fixed with ice-cold 70% ethanol and further incubated for 30 minutes at 37°C with 5 µg/mL rhodamine 123. Cells were then washed with PBS and photographed using Leica DM2500 fluorescence microscope.

## 2.18 | Detection of lysosomal membrane permeabilization

Acridine orange, a lysosomotropic weak basic dye was used in this experiment.<sup>[16]</sup> Intact lysosomes stain red. However, lysosomes under stress give green fluorescence. Cells were plated on the coverslip and treated with 0.16 nM of 4-FPAC. After 48 hours, these cells were treated with 5 µg/mL AO solution and incubated for 15 minutes. Representative images were captured using Leica DM2500 fluorescent microscope.

## 2.19 | Clonogenic inhibition assay

For determining colony formation ability of the cell line under the influence of 4-FPAC, clonogenic inhibition assay was performed. Cells were trypsinized at the log phase, and  $1 \times 10^3$  cells/mL were plated on 35 mm plate, followed by treatment with 0.16 nM of the derivative. After 48 hours, the old media was replaced with new, and the cells were further incubated for 10 days. After that, the cells were fixed and stained with 0.1% crystal violet solution. The number of colonies was counted using Image J software (NIH). The surviving fraction was calculated as the ratio of the number of colonies formed after treatment to the product of the number of cells plated and the plating efficiency.<sup>[17]</sup>

## 2.20 | Soft agar assay

Anchorage-independent growth is a decisive property of cancer metastasis and growth. This adhesion independent growth, under the influence of 4-FPAC, was evaluated by using soft agar assay.<sup>[18]</sup> Disc (35 mm) was coated with 0.8% agarose in FBS-free media, once solidified, it was overlaid with 0.4% agarose with cell and left to solidify. Media with 0.16 nM of 4-FPAC was added and incubated for 48 hours. It was then replaced with a fresh one and incubated for 10 days. On the 11th day, the cells were stained with 0.01% crystal violet solution and photographed under the microscope. The number and size (pixels) of the colony were counted using Image J software (NIH).

## 2.21 | Wound-healing assay

Cancer cell migration was analyzed using a wound-healing assay.<sup>[19]</sup> Cells were seeded on six-well plate with a density of  $2 \times 10^5$  cells per well in media supplemented with 10% FBS. Cells were incubated

overnight to adhere and form a monolayer. Once the monolayer reached 90% confluence, it was scratched with the help of a 20 µL pipette tip, then washed with PBS to remove the detached cells completely. After that, the old media was replaced with fresh one containing 0.16 nM of 4-FPAC. The image was taken using an inverted microscope at 0 hour, followed by incubation for 48 hours, in 1% serum media, and was photographed using Lawrence and Mayo inverted microscope and evaluated using Image J software (NIH). Wound area covering was compared using Student's *t* test at 95% significance, wherein, the experiment was done in triplicates with three scratches each, for both, control and treated.

## 2.22 | Hanging drop aggregation assay

Aggregation property of the cell line was analyzed using the hanging drop method. Cells were harvested, centrifuged, and counted. A total of  $2 \times 10^6$  cells/mL were resuspended from stock in media containing 0.16 nM of 4-FPAC, and for control, the same number of cells were incubated in media without derivative. Thirty microliter of cell-suspended media was placed as a droplet on the inner side of the 60 mm Petri dish lid, and 20 droplets per lid were placed and incubated for 48 hours. Ten milliliter of media was poured in the disc to avoid evaporation. The image was taken at 0 and 48 hours for both control and treatment. The total area covered by aggregate was analyzed using Image J software (NIH), and the mean area of aggregate was expressed in pixels.

## 2.23 | Gelatin zymography

A total of  $1 \times 10^6$  cells per well were seeded in a six-well plate and incubated overnight, followed by treatment with 0.16 nM of 4-FPAC. After 48 hours, the media was removed and cells were washed with cold PBS. Thereafter, the cells were homogenized in lysis buffer (Tris-Cl 10mM pH 8, NaCl 150 mM, CaCl<sub>2</sub> 10 mM, and 1% Triton X-100), centrifuged and the supernatant was taken, and concentration of protein was estimated using Bradford reagent. Thirty microgram of protein was used for sodium dodecyl sulfate polyacrylamide gel electrophoresis (SDS-PAGE), containing 2.5% gelatin in resolving gel. Electrophoresis was done at 100 V. The gel was washed twice with a Triton wash buffer followed by two incubation buffer washes of 15 minutes each. It was then left for further incubation overnight at 37°C, followed by staining with 0.25% coomassie brilliant blue for 4 hours and destaining till clear band was seen on blue background.

## 2.24 | Western blot analysis

Protein from treated and control cells was harvested as mentioned for zymography. Forty microgram of protein was used for the SDS-PAGE electrophoresis. The separated sample was transferred onto the polyvinylidene difluoride membrane at 100 mA for 20 minutes.

After that, blocking was done with TBS containing 0.1% Triton X-100% and 5% skimmed milk for 1 hour. After that, the membrane was incubated with primary antibodies which were, monoclonal anti-MMP-9 IgG goat 0.1 µg/mL (Sigma-Aldrich, St Louise, MO), anti-IL-1β IgG rabbit 0.1 µg/mL (Sigma-Aldrich), anti-β-catenin IgG mouse 0.1 µg/mL (Santa Cruz Biotechnology), anti-p53 IgG mouse 0.1 µg/mL (Santa Cruz Biotechnology), anticytochrome c IgG mouse 0.1 µg/mL (Santa Cruz Biotechnology), anti-PCNA IgG rabbit 0.1 µg/mL (Sigma-Aldrich), anticlaved Caspase 3 IgG rabbit 0.1 µg/mL (Sigma-Aldrich), anti-VEGF-α IgG goat 0.5 µg/mL (DSHB IOWA), anti-AKT IgG rabbit 0.1 µg/mL (Sigma-Aldrich), anti-pAKT IgG rabbit 0.1 µg/mL (Sigma-Aldrich), anti-TNF-α IgG mouse 0.1 µg/mL (Sigma-Aldrich), anti-iNOS IgG rabbit 0.1 µg/mL (Sigma-Aldrich), anti-IL-6 IgG mouse 0.5 µg/mL (DSHB IOWA), anti-E-cadherin IgG mouse 0.5 µg/mL (DSHB IOWA), anti-N-cadherin IgG mouse 0.5 µg/mL (DSHB IOWA), antivimentin IgG mouse 0.5 µg/mL (DSHB IOWA), anti-PI3K IgM mouse 0.5 µg/mL (DSHB IOWA), anti-Grb7 IgG mouse 0.5 µg/mL (DSHB IOWA), and anti-β-actin IgG mouse 0.1 µg/mL (Santa Cruz Biotechnology) at 4°C for 16 hours. Followed by three washes with wash buffer (50 mM Tris HCl of pH 7.6, 150mM NaCl and 0.1% Tween 20), and each wash last for 15 minutes. Then, incubated with corresponding biotinylated secondary antibody (0.5 µg/mL) for 45 minutes at room temperature, followed by three washes. After that, the membrane was incubated with alkaline phosphatase-conjugated streptavidin (0.5 µg/mL) for 45 minutes, washed three times, as mentioned earlier. Bands were developed upon the addition of the BCIP-NBT substrate (Sigma-Aldrich).

## 2.25 | Quantitative real-time polymerase chain reaction

Total RNA was isolated from using TRIzol reagent and purity of RNA was checked by the ratio of  $A_{260nm}$  by  $A_{280nm}$ . One microgram of DNAase-free RNA was reverse-transcribed into complementary DNA (cDNA) using cDNA Synthesis Kit (Applied Biosystems). Real-time RT-PCR (LightCycler 96; Roche Diagnostics, Switzerland) was performed using primers for genes viz. *p53*, *p21*, *BCL-2*, *MDM2*, *survivin*, *BID*, *BAX*, *BAD*, *AIF*, *PARP1*, *β-catenin*, *cathepsin B*, *calpain 2*, *PCNA*, *caspase 3*, *9,7, 8*, *cytochrome c*, *TRADD*, *FADD*, *cyclin D1*, *CDK2*, *cyclin E*, *CDK4*, *HIF-1α*, *IL-8*, *TGF-β*, *IL-10*, *iNOS*, *MMP9*, *MMP2*, *TIMP2*, *TIMP4*, *E-cadherin*, *N-cadherin*, *vimentin*, *snail1*, *snail2*, *ZEB1*, *claudin 3 (CLDN3)*, *claudin 4 (CLDN4)*, *VEGF-α*, *VEGF-R/KDR*, and *AKT*. *18sr* RNA was used as an endogenous control for normalization of data. Gel electrophoresis and melt curve analysis were used for confirmation of specific product formation. Fold change was calculated using the Livak method ( $2^{-\Delta\Delta C_q}$ ).<sup>[20]</sup>

## 2.26 | Statistical analysis

All values are reported as mean ± SEM. Experiments were performed in triplicates. The GraphPad Prism 5 software was used for statistical analysis. The difference between groups was analyzed using one-way

analysis of variance or Student's *t* test. The level of significance was kept at 95%.

## 3 | RESULTS

### 3.1 | 4-FPAC induces cytotoxicity in the A549 cell line

The metabolic viability of 4-FPAC on the noncancer cell line (NIH3T3) was evaluated using the MTT assay and the  $IC_{50}$  was found to be  $79.58 \pm 10.24$  µM (Figure 1B). However, 4-FPAC could effectively curb the viability of A549 at a very low concentration of 0.16 nM.<sup>[7]</sup> It is, therefore, prudent to presume that at the selected dose of 0.16 nM, 4-FPAC will not cause any deleterious effect to neighboring noncancer cells.

In trypan blue exclusion assay, treatment with 0.16 nM of 4-FPAC showed 28% death in the A549 cell line. In contrast, no significant difference in cell death was observed between control and vehicle control groups (Figure 1C). However, the reported metabolic viability in MTT assay was found to be 50% at this concentration,<sup>[7]</sup> which highlights the quiescent stage of the cells, wherein the cells are not dead, but elicit arrested growth. Therefore, it could be deduced that 4-FPAC was not only showing cytotoxic but also cytostatic property.

### 3.2 | 4-FPAC causes cell cycle arrest at the G0/G1 phase

The effect of 4-FPAC on cell cycle was analyzed using propidium iodide staining through flow cytometry. The proportions of control A549 cells in various stages of the cell cycle are representative of an untreated, healthy cell population, with a large majority of the cells (>90%) caught in either of the G0/G1, S or the G2/M phases. Sub G0/G1, which often reflects DNA fragmentation, a hallmark of apoptotic death, had a minute proportion of cells. The 4-FPAC-treated sample, however, had a very large proportion of cells in the sub G0/G1 region of the plot (40.9%), which points toward a high apoptotic rate. Moreover, among the normal stages of the cell cycle, majority of the treated cells were found in the G0/G1 phase. This is likely a result of most cells not being able to cross the G1 cell cycle checkpoint, which is the major decision point for a cell to enter the cell cycle and of which, DNA integrity check is one of the criteria (Figure 2).

The cell cycle genes, including checkpoint genes viz. *cyclin D*, *CDK2*, *CDK4*, *cyclin E*, *PCNA*, *p21*, *p53*, were analyzed using quantitative reverse transcription polymerase chain reaction (qRT-PCR) and at the transcript level, a significant increase was observed in the expression of *p53*, *p21*, and *PCNA*. However, the expression of *CDK4*, *cyclin D (CCND)*, *CDK2*, and *cyclin E (CCNE)* were found significantly decreased (Figure 3A). Nonetheless, a concomitant Western blot analysis revealed a definite increase in the expression of p53 with no change in the expression pattern of proliferating cell nuclear antigen (PCNA), a well-known marker of cell proliferation (Figure 3B).

Genes	Forward (sequence 5'-3')	Reverse (sequence 5'-3')
p53	CAGCCAAGTCTGTGACTTGACACGTAC	CTATGTCGAAAAGTGCTTCTGTCATC
BCL-2	ATGTGTGTGGAGAGCGTCAACC	GCATCCCAGCCTCCGTTATC
MDM-2	GTGCTGTAACCCACCTCACAGA	TTGGCACGCCAAACAAATCTC
Surviving	AGAACTGGCCCTTCTTGGAGG	CTTTTTATGTTCTCTATGGGGTC
BAD	CTTTAAGAAGGGACTTCTCTCGC	GTGGAGTTTCGGGATGTGGA
BID	TGAGTGGCTGAATGACCCCA	TCCCAGTGGCGACAGAATC
BAX	CCTTTTCTACTTTGCCAGCAAAC	GAGGCCGTCCCAACCAC
AIF	GTGCATCAGGGGGCAAATC	TCTGAAGCAGATAACGCGGC
PARP1	GCCCTAAAGGCTCAGAACGA	CTACTCGGTCCAAGATCGCC
cathepsin B	CCAGGGAGCAAGACAGAGA	GAGACTGGCGTTCTCCAAAG
$\beta$ -catenin	GTCTGGAATGAGACCGGAG	TAGCCCCAGAGTGAAAGGG
calpain 2	CGAGAGGGCCATCAAGTACC	GCAGATCTCCGTGGGGC
PCNA	TGTTCTCTCGTTGTGGAGT	TCCCAGTGCAGTTAAGAGCC
caspase 3	ACATGGCGTGCATAAAATACC	CACAAAGCGACTGGATGAAC
caspase 9	CCAGAGATTGCAAAACCAGAGG	GAGCACCGACATCACCAAATCC
caspase 7	GGAGCGCACTACCCCGA	ATCATCTGCCATCGTTCCCA
caspase 8	AGAGTCTGTGCCCAAATCAAC	GCTGCTTCTCTTTTGTGAA
cytochrome c	GAACAAAGGCATCATCTGGGG	GGCAGTGGCCAATTATTACTCA
TRADD	CGCTCTGTGGGTCTCAAATGGC	AGTCTCTGCCAGGCTGGTGA
FADD	TTGGAGAAGGCTGGCTCGTCAG	ACATGGCCCCACTCCTGTTCTG
cyclin D	ATGCCAACCTCTCAACGAC	TCTGTTCTCGCAGACCTCC
cyclin E	CCATCATGCCGAGGGAGC	TTATTGTCCCAAGGCTGGCT
CDK 4	CCTCTTAGCTTGCGGCTG	CTCAGATCAAGGGAGACCCTCAC
CDK 2	GCATCTTTGCTGAGATGGTGAC	GTAACCTCTGGCCACACCAC
HIF-1 $\alpha$	AGAGGTTGAGGGACGGAGAT	GACGTTCAGAACTTATCTACCAT
IL-8	GCTCTGTGTGAAGGTGCAGTT	TTTCTGTGTTGGCGCAGTGT
TGF- $\beta$	CGACTCGCCAGAGTGTTAT	CGGTAGTAACCCGTTGATGT
IL-10	CGAGATGCCTTCAGCAGAGT	GGCAACCCAGGTAACCCCTTA
iNOS	TGCCCTCCTCTGACAAAAC	TTGAGTTCATCCCCTTCGCC
MMP9	GTCTCCTGGCTCATGCCTTT	TTTACCACCTTGGCCCTCTC
MMP2	GCCTTCAAGGTGTGGAGTGA	ATCCCCGTGGTCAAGCTTTTC
E cadherin	AGGCCAAGCAGCAGTACATT	GGGGGCTTCATTACATCCA
N cadherin	ATCAAGCCTGTGGGAATCCG	CTCTATGGGCCAGGTTTTCTCA
Vimentin	GACCAGCTGACCAACGACAA	GAGGCATTGTCAACATCCTGTC
snail 1	CGAACGCACACTGGTAAAA	CATACGGGAGAAAGTCCGGG
snail 2	AGGACTCACACCTTGCCTTG	GTAGGTGAGCCCTGAGGTTG
TIMP2	ACTACGCTGCATCAAGAGG	GGCGTGGACCAGTCTAACAT
TIMP4	AAAGCTATACGGGCACCAGG	CAAAGCTGTGAGCGTGCAAT
claudin 3	GCCACCAAGGTCTGCTACTC	CCCTGCGTCTGTCCTTAGA
claudin 4	TCTCCTCTGTTCCGGGTAGG	CGTCCATCCACTCTGCACTT
VEGF- $\alpha$	CTCCACCATGCCAAGTGTC	GCAGTAGCTGCGCTGATAGA
AKT	CAGCCTGGGTCAAAGAAGTCA	ATGTACTCCCCTCGTTTGTGC
KDR	GCTTGCTTTTTGCCGATGA	TGCCGACCTCTGCATGTTAG
ZEB1	CGTTCATAAGGGAGGACGGG	AGTGGGAGCACTCATAGGGT
18s rRNA	GGCCGTTCTTAGTTGGTGA	TCAATCTCGGGTGGCTGAAC

### 3.3 | 4-FPAC induces apoptosis in A549 cell line

Morphology of A549 cells was observed after 48h of 4-FPAC treatment at a dose of 0.16 nM. Apoptotic features like granulation, rounding of cell, and detachment from substratum were frequently observed in the 4-FPAC-treated group (Figure 4C). No visible change in morphology was observed in DMF-treated cells (Figure 4B), which indicates that the vehicle caused no significant alteration in cell morphology. However, Triton X-100, which served as a positive control, resulted in a more substantial loss of attachment and more rounding of the cell (Figure 4D).

Subsequently, cell death and its mechanism were analyzed by dual staining method using EtBr/AO dye. It gives green color if cells are alive, orange/yellow if cells are in early or late stage apoptosis, and red if cells are under necrosis. In control (Figure 4E) and vehicle control groups (Figure 4F), most of the cells were green when compared with 4-FPAC-treated group (Figure 4G), where maximum cells were in the early or late apoptotic stage as exemplified by the yellow/orange color. However, all cells in the positive control were red (Figure 4H). The current result indicates that 4-FPAC-treated cells were undergoing an apoptotic type of cell death.

Additionally, to ensure that cell death observed in the treatment group is not due to necrosis, the LDH assay was performed. The result revealed that a statistically relevant increase in membrane permeability and therefore the release of LDH was observed in A549 cells that received a minimum concentration of 0.5 nM 4-FPAC. At the selected concentration of 0.16 nM, no significant release of LDH

was noticed, hence consolidating the fact that at this concentration 4-FPAC induced cell death only by apoptosis (Figure 4I).

### 3.4 | 4-FPAC induces genotoxicity in A549 cell line

The genotoxic effect of 4-FPAC was analyzed by comet assay and the DNA damage was represented in the form of comet tail length. The result revealed that unlike control (Figure 5A) and vehicle control groups (Figure 5B), 4-FPAC-treated cells (Figure 5C) showed ample signs of DNA damage, which were quite comparable to that of positive control (Figure 5D). The percentage head DNA, percentage tail DNA, tail moment, and olive tail moment in A549 are presented in Table 1.

The morphological evidence of apoptosis-like chromatin condensation, nuclear fragmentation, and margination of the nucleus was further confirmed by DAPI staining. No visible sign of chromatin condensation and margination was observed in control (Figure 6A) and vehicle control group (Figure 6B), whereas in 4-FPAC-treated cells, chromatin condensation could be seen frequently (Figure 6C).

### 3.5 | 4-FPAC treatment hampers the balance between ROS and antioxidant enzymes

ROS plays a very critical role in cancer cell proliferation, as well as in cellular toxicity. Many chemotherapeutic agents induce apoptosis in

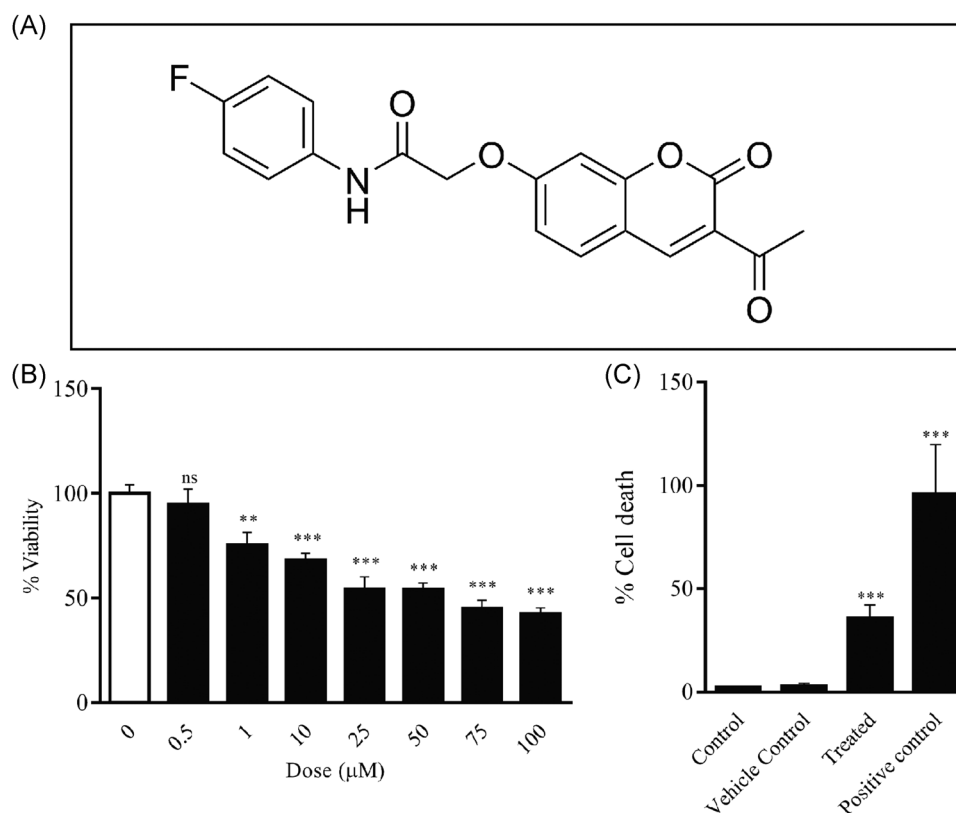


**FIGURE 1** Structure of 4-FPAC and its cytotoxic effect: (A) chemical structure of derivative 4-FPAC. Cytotoxicity study (B) cell viability assay for NIH3T3 cell line and (C) trypan blue dye exclusion assay in A549 cell line. \*\*\* $P \leq .001$ , \*\* $P \leq .01$ . 4-FPAC, 4-fluorophenylacetamide-acetyl coumarin; ns, not significant

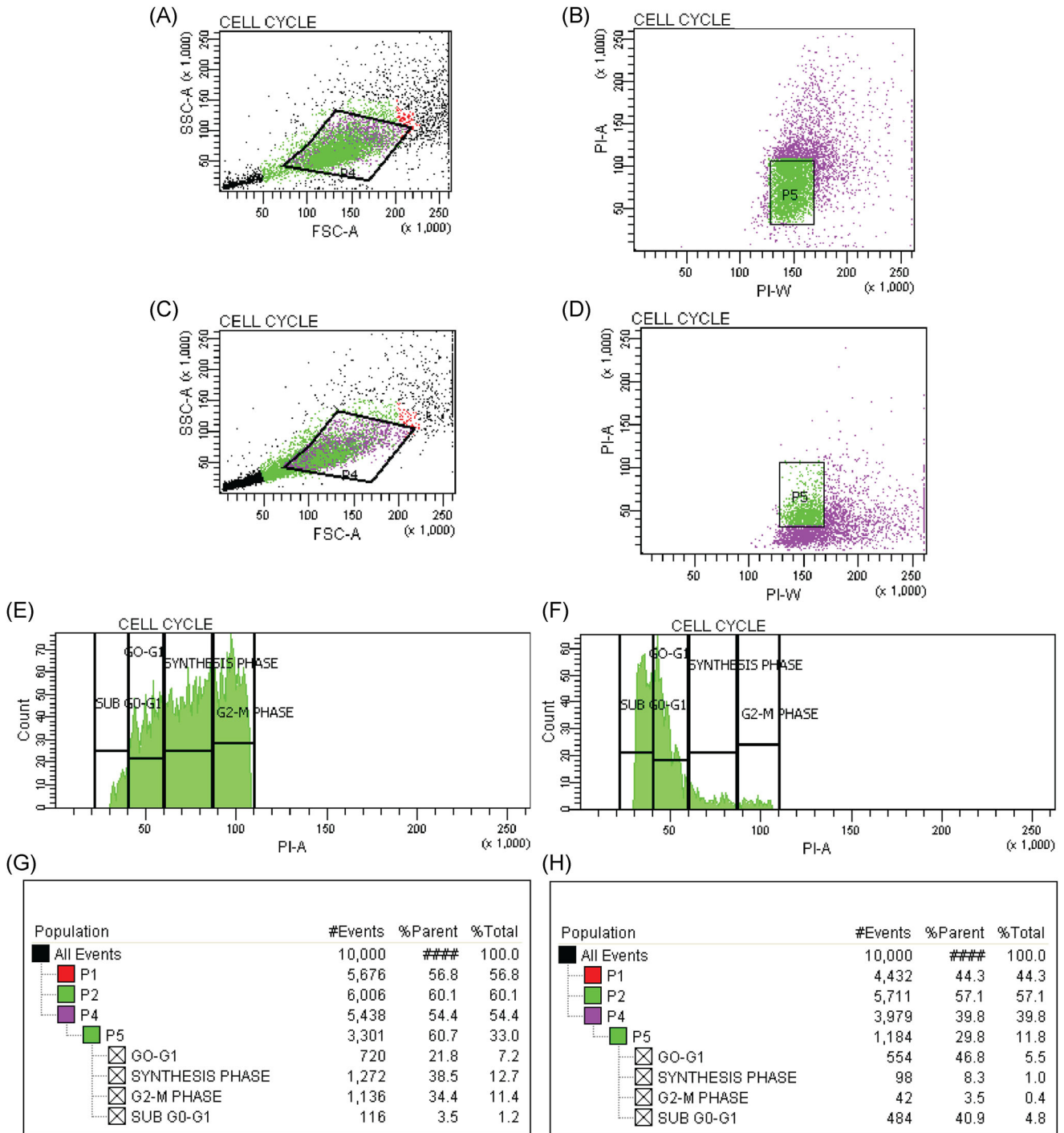


**FIGURE 2** Flow cytometric analysis of cell cycle distribution in A549 cell line. Histogram represents forward scatter (FSC-A) vs side scatter (SSC-A) of control group (A) and treated group (C). Histogram represents pulse width (PI-W) vs pulse area (PI-A) of control group (B) and treated group (D). Graph represents percentage of cell under various phases of cell cycle in control (E) and treated (F). Table represents number and percent of cell under various phases of cell cycle in control (G) and treated (H)

cancer cells by augmenting the intracellular ROS concentration beyond the threshold level.<sup>[21]</sup> The antioxidant enzyme system, which regulates ROS concentration and maintains the cellular redox equilibrium, includes SOD, catalase (CAT), and GPx. These antioxidant enzymes act by

metabolizing the free radicals, which might damage the cell.<sup>[22]</sup> Herein, the ROS level was measured using a fluorimeter (Figure 7D).

Further, the morphology of the cell was analyzed to ascertain that the ROS generation was not due to cellular damage. There

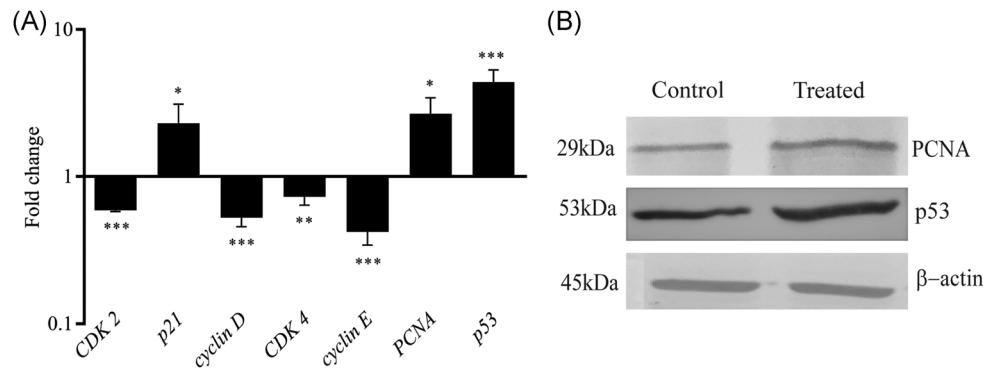


**FIGURE 3** Effect of 4-FPAC on genes involved in cell cycle regulation in A549 cell line. A, Values are expressed as mean  $\pm$  SEM. Fold change values for control is 1. \*\*\* $P \leq .001$ , \*\* $P \leq .01$ , \* $P \leq .05$ . B, Western blot analysis of PCNA and p53 in control and treated group,  $\beta$ -actin was taken as internal control. 4-FPAC, 4-fluorophenylacetamide-acetyl coumarin; PCNA, proliferating cell nuclear antigen

was an increase in fluorescence of the treated cells (Figure 7B) as compared to the control one (Figure 7A), which revealed a significant increase in the intracellular ROS level. 4-FPAC might be exerting its cytotoxic effect on A549 cells via increased intracellular ROS concentration as it plays a significant role in the induction of apoptosis.

The activities of SOD, CAT, and GPx were also evaluated in the treated as well as control cells at 24 and 48 hours. The analysis of the result revealed that at 24 hours, the activities of the studied antioxidant enzymes in the 4-FPAC-treated cells remained at the basal level except for that of GPx (Figure 8B), which registered a significant increase. However, at 48 hours, a considerable decrease in the activities of CAT and GPx were observed (Figure 8A,B). However, no change in SOD was observed when compared to the control (Figure 8C).

### 3.6 | 4-FPAC treatment disrupts membrane potential in mitochondria and lysosome

Rhodamine 123 (RH-123) fluorescent dye was used for evaluating mitochondrial membrane potential. RH-123 is a cationic dye, which electrophoretically accumulates into the mitochondrial matrix. However, 4-FPAC-treated cells (Figure 9B) when stained with RH-123 showed less fluorescence compared to the control cells (Figure 9A), indicating that derivative treatment depolarized the mitochondrial membrane (Figure 9C). In a parallel study, AO was used to analyze the lysosomal membrane integrity. AO is a weak base, which accumulates in lysosomes where it gets protonated and entrapped. However, when the lysosomal membrane gets permeabilized, AO relocates itself into the cytosol and gives green fluorescence. It has been observed that the cells treated with 0.16 nM of 4-FPAC (Figure 9D) emitted intense green fluorescence from the cytosol compared to control cells (Figure 9E). The results herein vividly exemplify that 4-FPAC at the given concentration disrupted the integrity of both mitochondria as well as lysosomal membranes presumably because of the increased oxidative stress as described previously.

### 3.7 | 4-FPAC affects genes regulating apoptotic pathway

Major genes of intrinsic and extrinsic pathways of apoptosis were analyzed in A549 cells treated with 0.16 nM of 4-FPAC. The results revealed that at the transcript level, the expression of proapoptotic genes of an intrinsic pathway like *BAD*, *BAX*, *cytochrome c*, *caspace 9*, *BID*, and so forth, was upregulated in the treated cells compared to controls, nonetheless, *caspace 7* expression remained unaltered (Figure 10A). In addition, the anti-apoptotic gene like *survivin* and *BCL2* were found significantly downregulated, along with the negative regulator of *p53* like *MDM2* and  *$\beta$ -catenin*, in the 4-FPAC-treated cells (Figure 10B). A parallel Western blot analysis revealed heightened expression of cytochrome *c*, a marker protein of mitochondria-mediated apoptosis (Figure 10C). Moreover, the study also revealed that compared to control cells, the transcript level expression of *AIF* and *PARP-1* remained low in the 4-FPAC-treated cells (Figure 10B), which reaffirms that 4-FPAC does not activate any pathway that can lead to necrosis.

Further, transcript level analysis of the extrinsic pathway of apoptosis revealed that *FADD*, *TRADD*, and *caspace 8* was triggered by 4-FPAC treatment (Figure 10A). Thus, it can be construed that in 4-FPAC-treated A549 cells, both the mitochondria-mediated intrinsic, as well as the TRADD/FADD-mediated extrinsic pathways are involved in inducing apoptosis, wherein *BID* acts as a mediator between these two pathways and *caspace 3* acts as a dominant effector caspase. The significant upregulation of caspase 3, at protein and transcript level, in the 4-FPAC treated cells (Figure 10C) further indicates that the derivative induced apoptosis by p53-mediated caspase-dependent pathway.

Moreover, since 4-FPAC was found adversely affecting lysosomal as well as mitochondrial membrane integrity, it was thought necessary to study the involvement of these organelles in cell death and, hence the transcript levels of cathepsin B, a lysosomal protease and calpain 2, a cysteine protease localized to the cytosol as well as

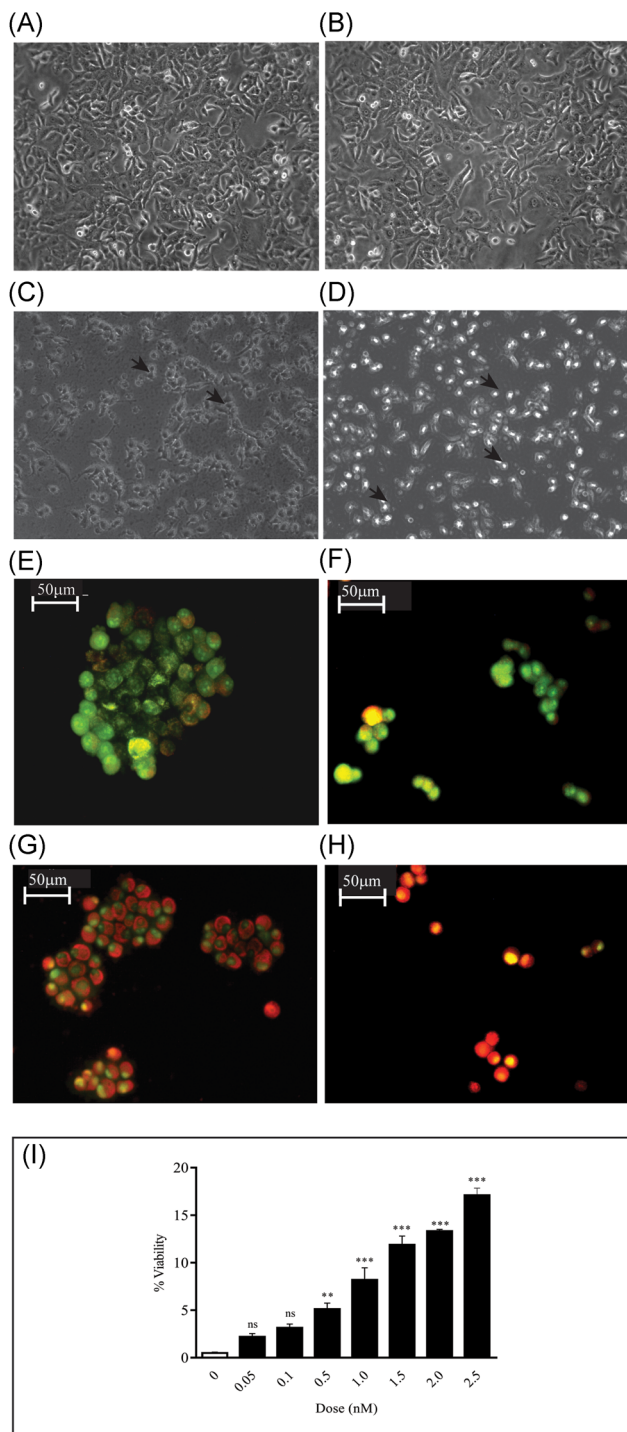


**FIGURE 4** 4-FPAC induced apoptosis in A549. Cell morphology of control (A), vehicle control (B), treated (C), and positive control (D) groups, dead cells are marked with black arrow. AO/EtBr staining for control (E), vehicle control (F) treated (G), and positive control (H) groups. I, Percentage LDH release in A549 under different concentrations (nM) of 4-FPAC. \*\*\* $P \leq .001$ , \*\* $P \leq .01$ . 4-FPAC, 4-flourophénylacétamide-acétyle coumarine; EtBr/AO, éthidium bromide/acridine orange. LDH, lactate déhydrogénase

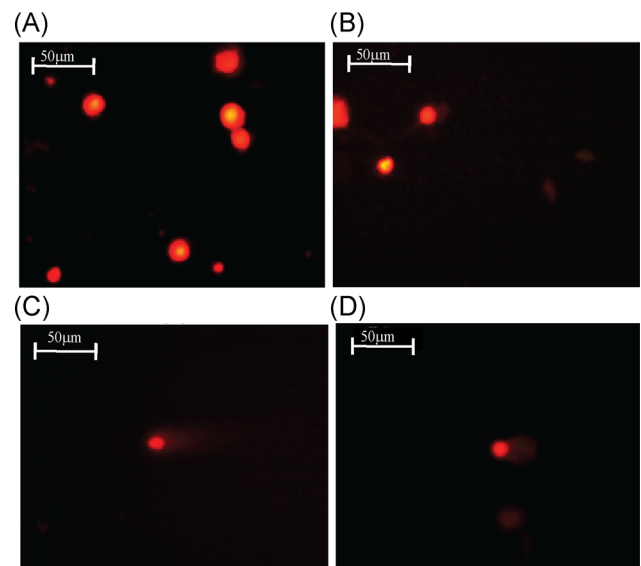


**FIGURE 5** Comet assay in control (A), vehicle control (B), treated (C), and positive control (D)

mitochondria were checked. Results revealed that the expression of *calpain2* went down in the 4-FPAC-treated cells, whereas that of *cathepsin B* was significantly upregulated (Figure 10B), indicating the possibility of both lysosomal and mitochondrial-mediated pathways in inducing apoptosis.

### 3.8 | 4-FPAC treatment reduces metastasis in A549 cell line

Cancer cell migration plays a decisive role in establishing metastasis and is a frequently used feature to evaluate the anticancer property of any novel derivative. It initiates, with the remodeling of ECM components, and is followed by migration to the distant niche. This remodeling is mostly governed by matrix metalloproteinases (MMPs), which degrade type-VI collagen, the main component of ECM.<sup>[23]</sup> Here, we observed the effect of 4-FPAC at the selected dose on MMP-9 and MMP-2, the critical players of invasion and metastasis of cancer. At the transcript level, there was a significant decrease in *MMP9* and *MMP2* (Figure 11C). A similar decreasing trend of *MMP-9* was noticed at protein (Figure 11A) and activity level (Figure 11B) too, hence reaffirming the inhibitory role of 4-FPAC on matrix remodeling. Moreover, there was an upregulation in the expression of *TIMP2* and *TIMP4* (Figure 11C), the negative regulators of MMPs, which further support the downregulation of MMPs thereby, minimizing the ECM degradation in the presence of a derivative.

With the onset of ECM remodeling, tumor cells are known to change their typical phenotype so as to aid metastasis. First, cancer cell loses its anchorage dependency, cell-cell interaction, and

	Control	Vehicle control	Treated	Positive control
Total comet length	98 ± 5.09	112 ± 11.09	204 ± 12.67	186 ± 4.43
Head length	93 ± 4.19	105 ± 12.05	139 ± 12.37	133 ± 1.891
Tail length	5 ± .034	7 ± 0.901	65 ± 9.05	53 ± 1.891
% head DNA	92.98 ± 3.92	99.40 ± 18.91	64.68 ± 1.5	54.45 ± 3.275
% tail DNA	7.5 ± .018	0.591 ± .003	35.31 ± 2.85	45.53 ± 2.677
Tail moment	0.37 ± .03	0.0413 ± .0001	58.26 ± 0.33	24.31 ± 1.334
Olive tail moment	0.311 ± .03	2.367 ± .021	41.61 ± 6.49	37.57 ± 1.491

**TABLE 1** Comet assay parameters: genotoxic effect of 4-flourophenylacetamide-acetyl coumarin on A549 cell line

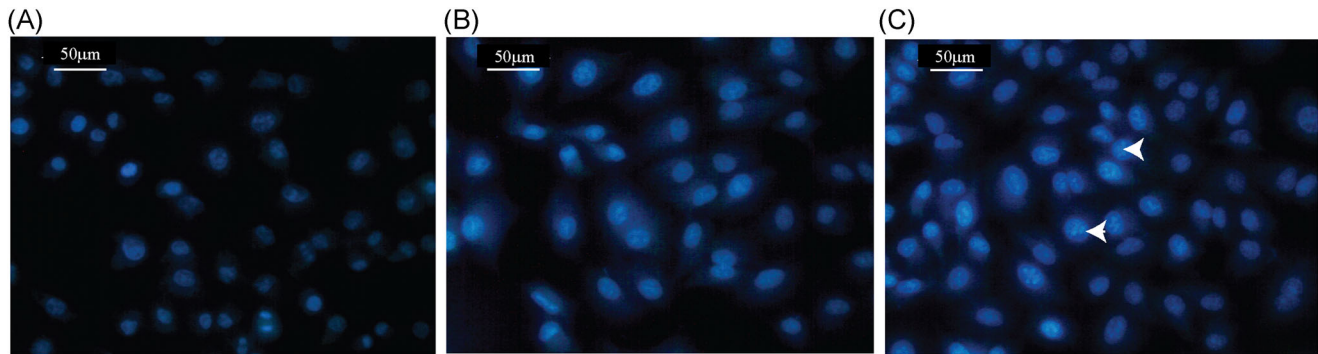


**FIGURE 6** Nuclear staining with 4,6-diamidino-2-phenylindole in control (A), vehicle control (B) and treated (C). White arrow head indicates chromatin condensation

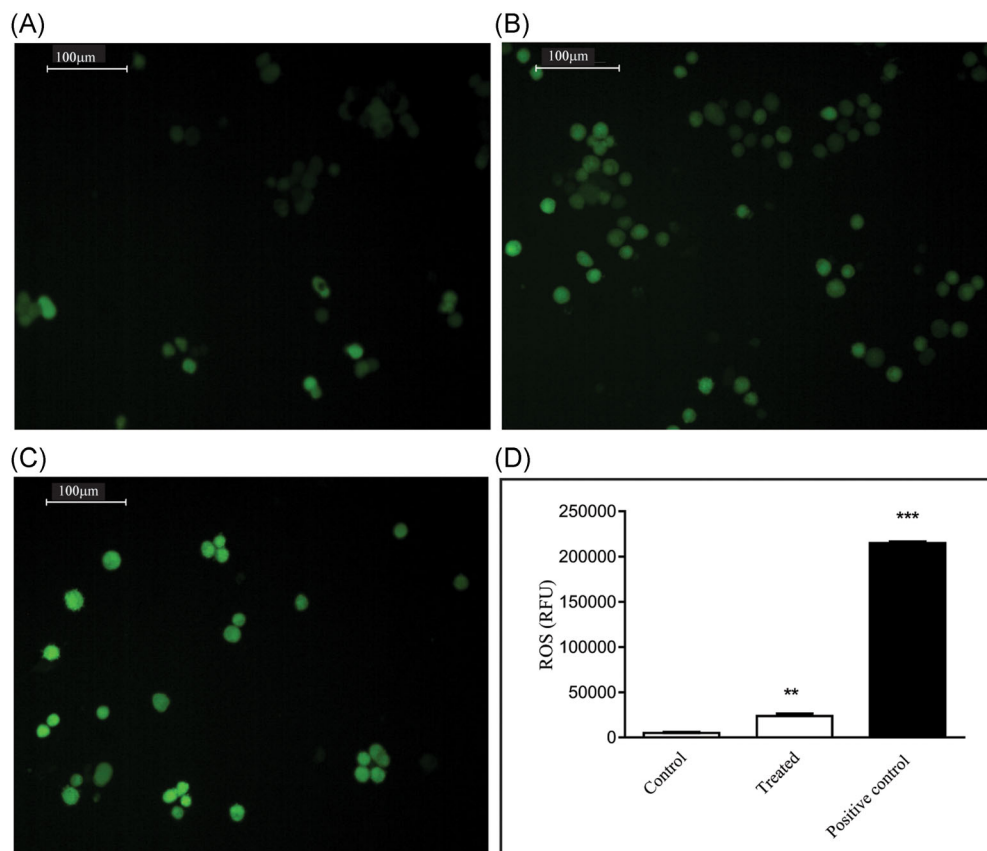


**FIGURE 7** DCFH-DA staining in control (A), treated (B), and positive control (C). D, Estimation of ROS by DCFH-DA assay. \*\*\* $P \leq .001$  and \*\* $P \leq .01$ . DCFH-DA, dichlorodihydrofluorescein diacetate; ROS, reactive oxygen species

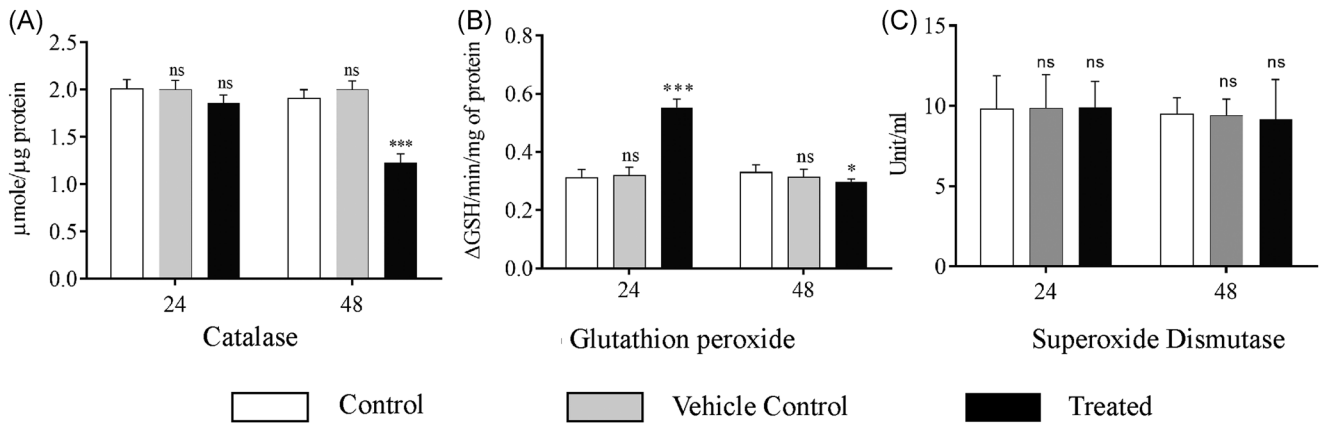


**FIGURE 8** Effect of 4-FPAC on antioxidant enzyme levels in A549 cell line at 24 and 48 hours post treatment: (A) catalase (B) glutathione peroxidase, and (C) superoxide dismutase. Data are represented as mean  $\pm$  SD. \*\*\* $P \leq .001$  and \* $P \leq .05$ . 4-FPAC, 4-fluorophenylacetamide-acetyl coumarin

establishes rapid proliferation. These properties of cancer cells were evaluated by soft agar, aggregation, and clonogenic assay. Soft agar assay was done for optimizing the anchorage-independent growth of the cell. The result showed that control cells (Figure 12C) had proliferated at an average rate on the agar layer and formed a larger colony. However, cells treated (Figure 12D) with 4-FPAC, when observed after 48 hours incubation, showed an apparent reduction in

the size of the colony (Figure 12F). Nevertheless, no significant difference was observed in the number of colonies as compared to control (Figure 12G). This outcome was reaffirmed with the clonogenic assay and found that the derivative is negatively affecting the clonogenic property of the cancer cell line (Figure 12E). Therefore, from both experiments, it was confirmed that in the presence of 4-FPAC, the anchorage-independent growth and proliferation

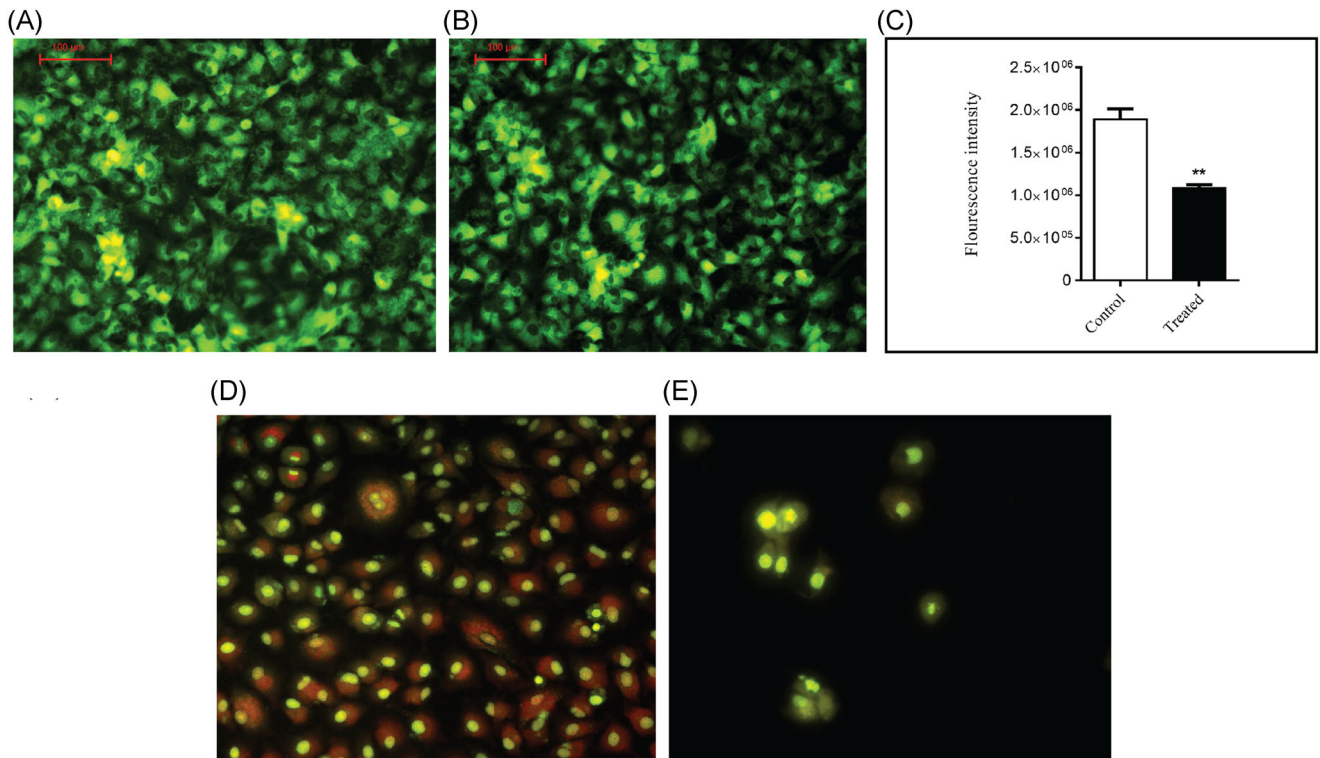


**FIGURE 9** Effect of 4-FPAC on membrane integrity and potential in A549 cell line: rhodamine staining for mitochondrial membrane potential in control (A) and treated (B). C, Represents the quantitative measurement of mitochondrial membrane potential. \*\* $P \leq .01$ . Acridine orange staining to detect lysosomal membrane permeabilization in control (D) and treated (E). 4-FPAC, 4-fluorophenylacetamide-acetyl coumarin

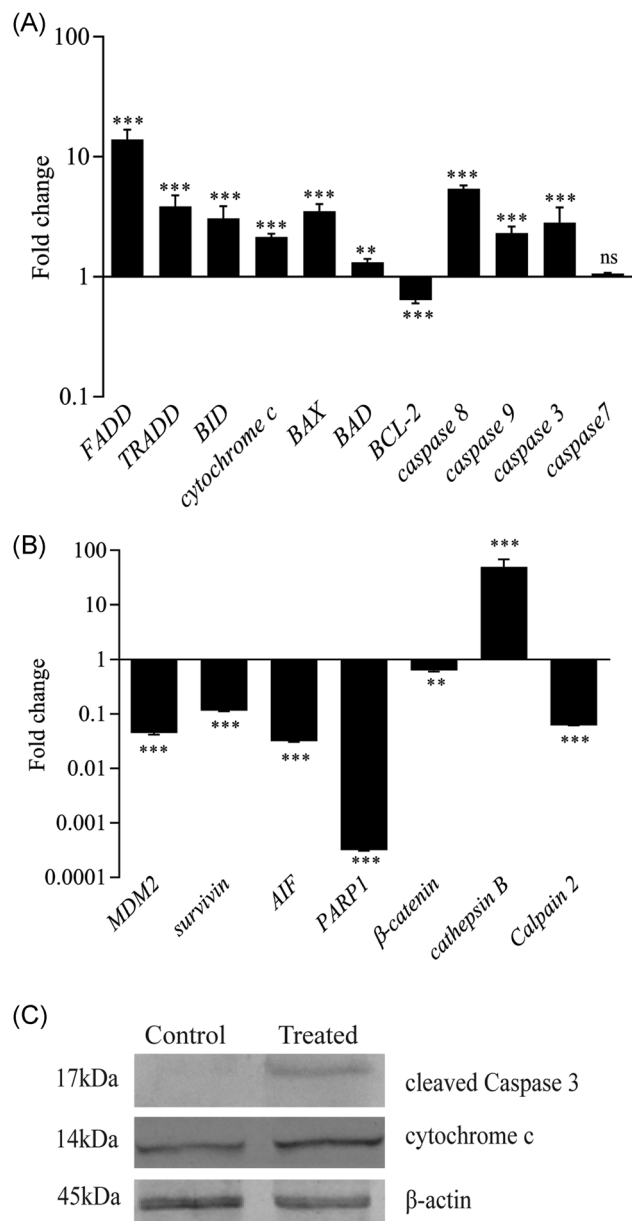


**FIGURE 10** Analyzing apoptosis at the molecular level: quantitative reverse transcription polymerase chain reaction of genes involved in apoptosis depicted in (A, B). Values are expressed as mean  $\pm$  SEM. Fold change values for control is 1. \*\*\* $P \leq .001$  and \*\* $P \leq .01$ . C, Western blot analysis of cleaved caspase 3 and cytochrome c in control and treated group,  $\beta$ -actin was taken as internal control

capacity of the cancer cell was reduced. Nonetheless, a significant increase in the aggregate size of cancer cells was observed when treated with 0.16 nM of 4-FPAC (Figure 13C). The average size of cell aggregate in case of the control group was 60 601 pixels (Figure 13A) but when treated with derivative, the mean size of aggregate was increased to 237 339 pixels (Figure 13A), which showed that 4-FPAC increases the aggregation property of cancer cell and minimizes the metastasis property of cancer cell line in vitro.

At the molecular level, during metastasis of cancer cell, down-regulation of E-cadherin, an epithelial cell surface adhesion molecule, upregulation of N-cadherin, a mesenchymal cell surface adhesion molecule and vimentin, an intermediate filament protein were observed. All these are usually associated with epithelial to mesenchymal transition (EMT), which helps cancer cells to migrate from one niche to other.<sup>[24]</sup> Therefore, we checked the expression of E-cadherin, N-cadherin, and vimentin at messenger RNA (mRNA) and protein levels. At the transcript level, a significant decrease in N-cadherin and an increase in vimentin, as well as E-cadherin, was observed (Figure 14A). Whereas, at the protein level, there was a minor increase in the expression of E-cadherin but a decrease in vimentin and no significant change in N-cadherin was observed (Figure 14D). Which, further illustrated that the derivative at the selected dose resists the morphological changes associated with EMT in A549 cells by increasing the epithelial property by increasing the levels of E-cadherin. It also minimizes the mesenchymal property of the cells by reducing vimentin. Downregulation of transcription factors namely Snail1, Snail2, and ZEB1 was also observed in treated cells (Figure 14C), which are known to repress E-cadherin and facilitate cell migration.<sup>[25]</sup>

Further, the effect of 4-FPAC on migration property of cancer cell line was estimated by in vitro wound-healing assay. The result showed a significant reduction in percentage wound coverage in treated disc compared to control cells after 48 hours of treatment (Figure 15).

### 3.9 | 4-FPAC reduces the expression of angiogenesis regulating genes and cytokines

Angiogenesis is the critical stage for metastasis, and many putative factors are known to influence it. Herein, we analyzed the transcript level expression of these factors and found that in 4-FPAC-treated cells, there was a significant increase in *TGF- $\beta$* , *iNOS*, *VEGF- $\alpha$* , and *kdr* (Figure 14A,B). However, though a significant decrease was observed in the level of *IL-8* and *IL-6*, no significant change was noted in the level of *IL-10* (Figure 14B). At the protein level, *TNF- $\alpha$*  and inducible nitric oxide synthase (*iNOS*) were found to be upregulated whereas, interleukin 1 $\beta$  (*IL-1 $\beta$* ) and *IL-6* were downregulated and no significant change was observed in vascular endothelial growth factor  $\alpha$  (*VEGF- $\alpha$* ; Figure 14D).

### 3.10 | 4-FPAC reduces the expression of PI3K and Akt

PI3K is the key regulator of cell division,<sup>[26]</sup> cell survival,<sup>[27]</sup> apoptosis,<sup>[28]</sup> EMT,<sup>[29]</sup> and angiogenesis.<sup>[30]</sup> The result of the qRT-PCR analysis did not show any significant change in the expression of *AKT* in the 4-FPAC-treated cells compared to that of control (Figure 16A). Nonetheless, analysis of the Western blot images revealed an

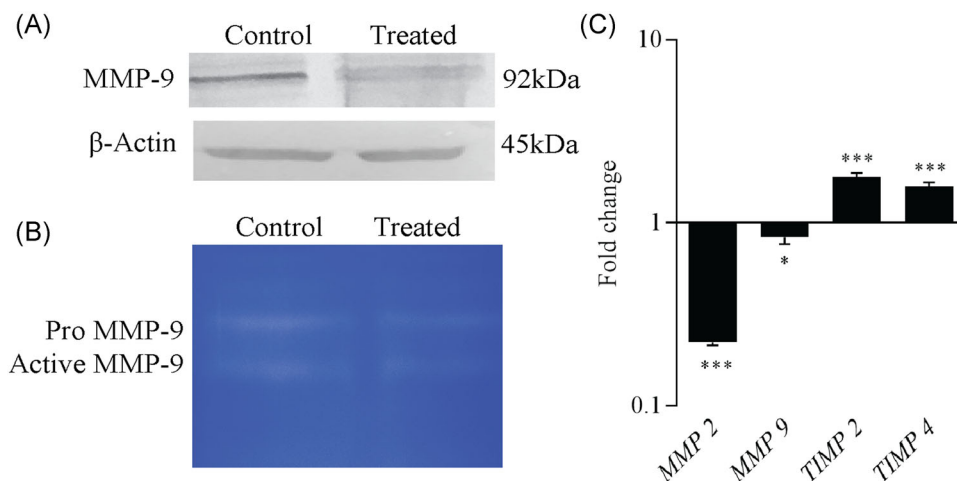


**FIGURE 11** Effect of 4-FPAC on cell migration in A549. A, Western blot analysis of MMP9 in control and treated group,  $\beta$ -actin was taken as an internal control. B, Gelatin zymogram for MMP9 activity. C, Quantitative reverse transcription polymerase chain reaction of genes involved in migration. Values are expressed as mean  $\pm$  SEM. Fold change values for control is 1. \*\*\* $P \leq .001$  and \* $P \leq .05$ . 4-FPAC, 4-flourophenylacetamide-acetyl coumarin; MMP, matrix metalloproteinase

appreciable reduction in the expression of AKT, pAKT, and PI3K in the treated cells (Figure 16B). Moreover, no significant change in the protein level expression of Grb7, an upstream regulator of PI3K, was noticed in the treatment group (Figure 16B), which vividly indicates that the derivative is affecting the pathway downstream of Grb7 at PI3K level.

## 4 | DISCUSSION

As a prelude to this study, a string of coumarin derivatives was synthesized with different substituents and the antiproliferative property of each derivative was evaluated. Among these, 4-FPAC showed lowest median inhibitory concentration in A549—a human

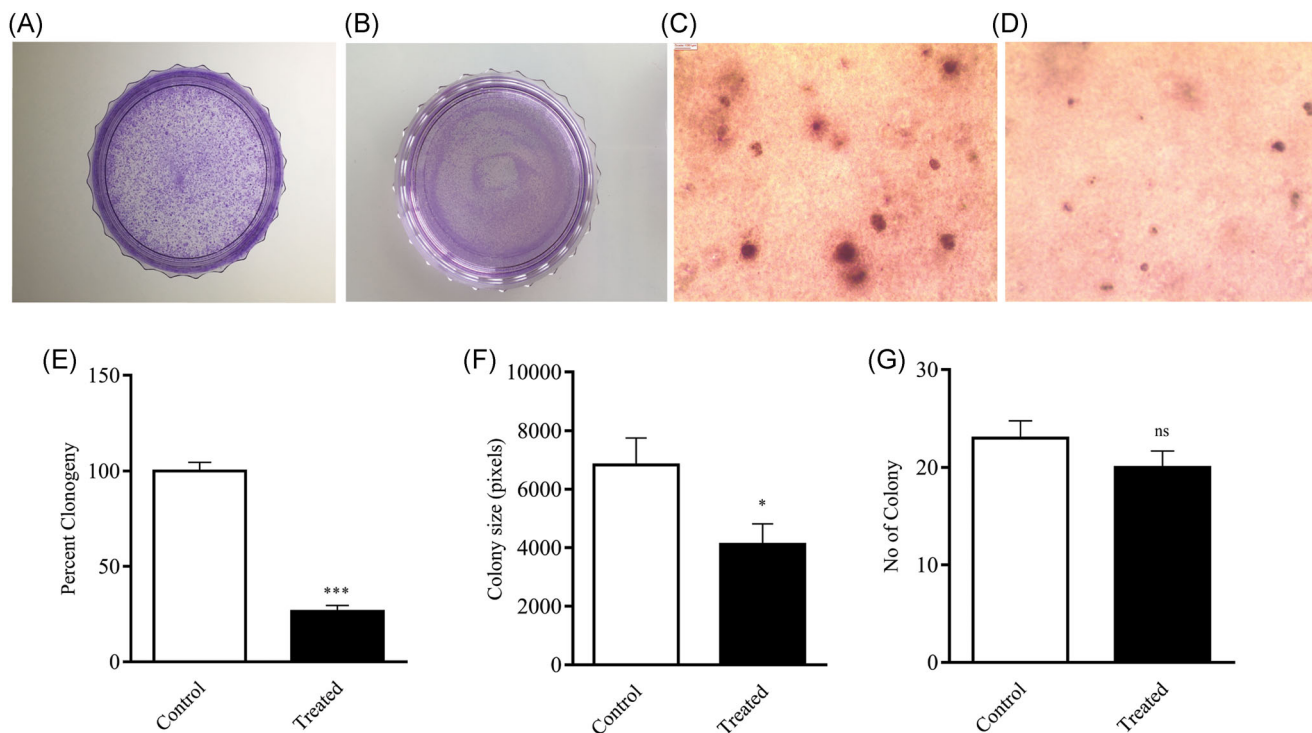


**FIGURE 12** Effect of 4-FPAC on anchorage independent growth and clonogenic property of A549 cell line. Clonogenic assay depicting control (A) and treated (B) colonies at 48 hours post treatment. E, Graph represents clonogenic inhibition in treated condition,  $n = 5$ . Soft agar assay for control (C) and treated (D) cell lines, at 48 hours post treatment. Graphs representing size of colony (F) and number of colony (G) on agar. \*\*\* $P \leq .001$  and \* $P \leq .05$ . 4-FPAC, 4-flourophenylacetamide-acetyl coumarin

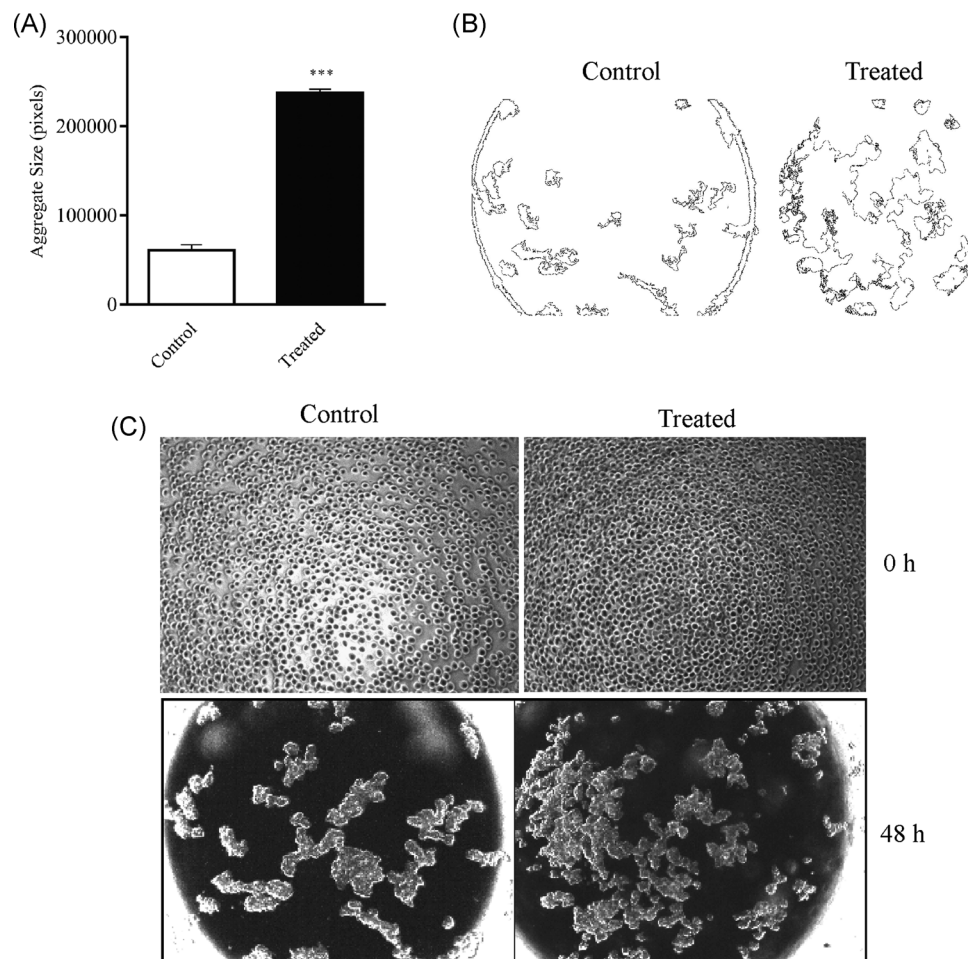


**FIGURE 13** Hanging drop assay. A, Graph represents aggregate size (in pixels). B, Images of aggregate in control and treated cell at 48 hours. C, Photomicrographs of hanging drop assay for control and treated at 0 and 48 hours. \*\*\* $P \leq .001$

adenocarcinoma lung cell line.<sup>[7]</sup> What particularly triggered our interest in this molecule was its negligible cytotoxicity toward NIH3T3 cells—a noncancerous mouse fibroblast line. The present study looks into the effects of 4-FPAC on different aspects of metastasis in the A549 cell line. The observations stated herein have been made after incubation of A549 with 0.16 nM of 4-FPAC for a 48-hour period, since it exerted maximum inhibitory effect for this duration of exposure.

First, a trypan blue exclusion assay in A549 revealed approximately 28% cell death at the selected dose of 0.16 nM of 4-FPAC, whereas an MTT assay showed 50% loss of metabolic viability at the same dose.<sup>[7]</sup> Since loss of metabolic viability reflects both cell death as well as quiescence, it could be deduced from the results of trypan blue and MTT assays that 4-FPAC was not only showing cytotoxic but also cytostatic property. Further, flow cytometric analysis revealed that 4-FPAC arrests cell cycle at the G<sub>0</sub>/G<sub>1</sub> phase in a large proportion of cells. This indicates an inability of cells to cross the G<sub>1</sub> cell cycle checkpoint, which may indicate the presence of DNA damage.<sup>[31]</sup> Indeed, a comet assay performed at the same concentration of 4-FPAC confirmed significant DNA damage. It was evident from Western blot results that the p53 protein was induced in the A549

cells in response to incubation with 0.16 nM of 4-FPAC. This is likely a result of DNA damage. p53 leads to the activation of p21, a downstream target of p53, and a known inhibitor of CDK2, CDK4, and PCNA. When activated p21 binds to PCNA, it inhibits the latter's activity, which was evident from the low protein level expression of PCNA in the 4-FPAC-treated cells. Besides, the inactivation of PCNA by p21 might prevent DNA repair and hence induce cell cycle arrest at the G<sub>1</sub> phase.

Moreover, it has been reported that activated p21 inhibits G<sub>1</sub> phase progression by inhibiting CDK4-cyclin complex.<sup>[32]</sup> Furthermore, it is documented that CDK2, in combination with cyclin E, helps the cell to pass G<sub>1</sub> phase.<sup>[33]</sup> In the present study, the 4-FPAC treatment resulted in significant downregulation of CDK2 expression, rendering it unavailable for CDK2-cyclin E complex formation, resulting in cell cycle arrest at the G<sub>0</sub>/G<sub>1</sub> phase and ultimately inducing cell death in A549 cells.

It is well-known that necrosis and apoptosis are the two major pathways that converge to cell death when treated with a cytotoxic compound. As necrosis is an uncontrolled process, it leads to sudden cell rupture, plasma membrane damage, adenosine triphosphate depletion, and enhanced ROS generation, which causes damage to

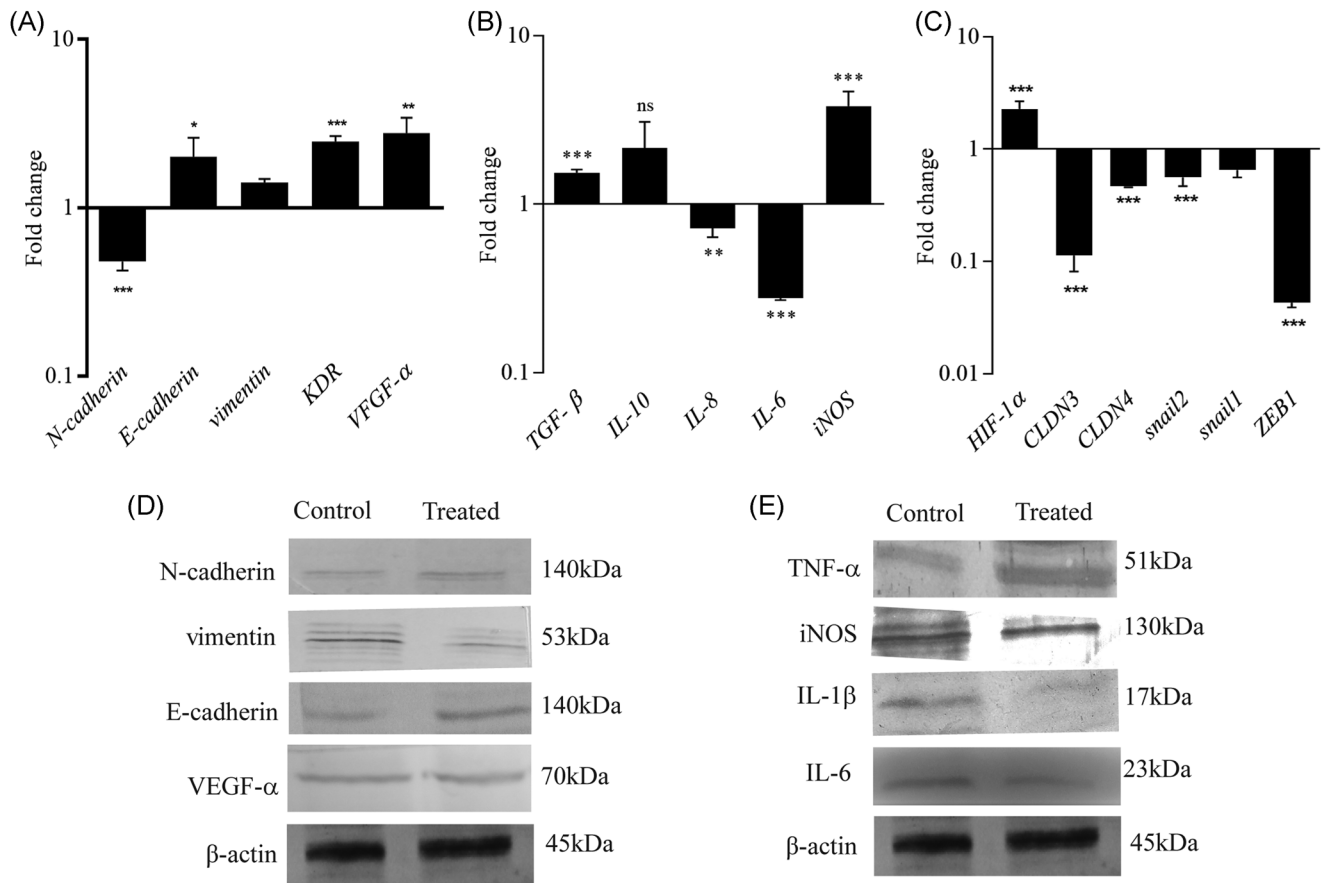


**FIGURE 14** Analysis of metastasis and angiogenesis in A549 cell line. Quantitative reverse transcription polymerase chain reaction of genes involved in metastasis and angiogenesis are depicted in (A-C). Values are expressed as mean ± SEM. Fold change values for control is 1. \*\*\* $P \leq .001$ , \*\* $P \leq .01$ , and \* $P \leq .05$ . C-E, Western blot analysis of key proteins involved in metastasis and angiogenesis in control and treated group, β-actin was taken as internal control

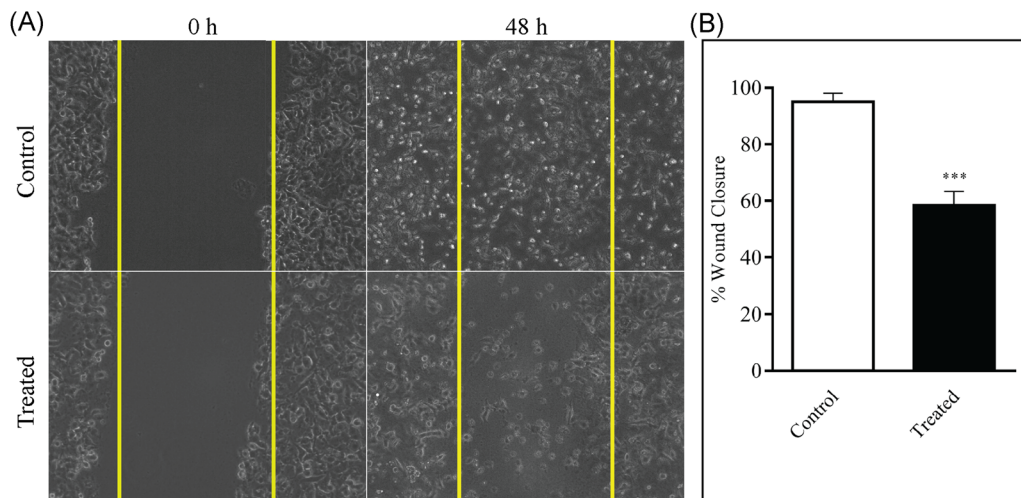


**FIGURE 15** Wound closure assay for A549 cell line upon treatment with 4-FPAC. A, Photomicrograph of control and treated cells at 0 and 48 hours. B, Graph represents % wound area cover in control and treated cell line. \*\*\* $P \leq .001$

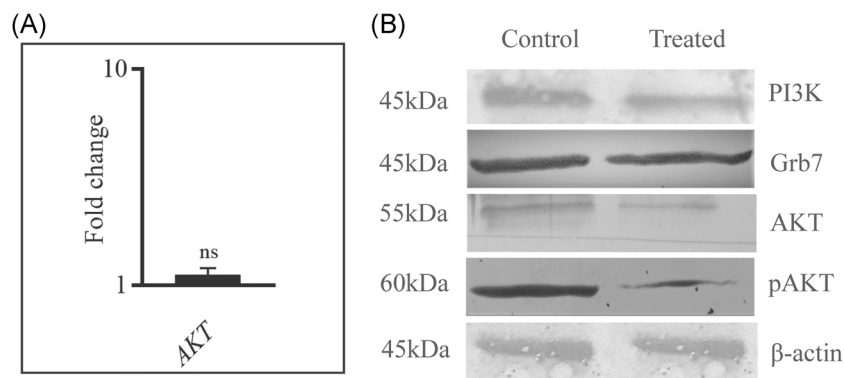


**FIGURE 16** 4-FPAC affects PI3K/AKT signaling pathway. (A) Quantification of AKT at transcription level by quantitative reverse transcription polymerase chain reaction. Graph represents fold change of AKT. Expression level of control messenger RNA was assigned as 1.0. Experiment was performed in triplicate. Data are represented as mean  $\pm$  SEM. B, Western blot analysis of PI3K, AKT, pAKT, and Grb7 in control and treated cell line. 4-FPAC, 4-fluorophenylacetamide-acetyl coumarin; ns, not significant

neighboring cells as well. However, apoptosis is characterized by cell rounding, membrane blebbing, and finally removal of cells through the formation of apoptotic bodies, which would be engulfed by phagosome and further eliminated from the system without damaging neighboring cells.<sup>[34]</sup> Herein, the mechanism of cell death was analyzed in 4-FPAC-treated A549 cells by EtBr/AO staining, DAPI staining, LDH release assay, and comet assay. The microscopic analysis revealed apoptotic signs like cell rounding and membrane blebbing in the treated cells. The 4-FPAC-treated cells also exhibited additional markers of apoptosis like chromatin condensation and DNA damage, as evident from the results of EtBr/AO, DAPI, and comet assay. Moreover, only the basal level of LDH, a sign of necrosis, was found to be released from cells treated with 0.16 nM of 4-FPAC. The above result, therefore, indicates that 4-FPAC induces apoptosis in A549 cells at the selected dose.

Most of the known chemotherapeutic agents exert their cytotoxicity by elevating the ROS beyond a threshold limit.<sup>[35]</sup> Hence, the intracellular ROS level was investigated by DCFH-DA assay and a significant elevation in ROS concentration in cells treated with 0.16 nM of 4-FPAC was found. This elevated ROS may be responsible for apoptotic death observed in 4-FPAC-treated A549 cells. As ROS is a universal intracellular metabolite, it regulates several cellular cascades, in cancer as well as in noncancer cells, including cell survival, cell death, metastasis, and angiogenesis.<sup>[36,37]</sup> Whenever ROS is elevated by a pharmacological compound, it induces apoptosis by disrupting the mitochondrial membrane potential that results in the release of cytochrome *c* and formation of the apoptosome, which activates caspase cascade.<sup>[38]</sup> As well, it has been reported that Fas ligand also elevates ROS, and that signals the Fas-associated death domain that further activates caspase-8-mediated apoptosis.<sup>[39]</sup> Other than intrinsic and extrinsic pathway regulators, p53, a redox-sensitive transcription factor, is also involved in cell death, survival, and DNA repair.<sup>[40]</sup> It has been observed that ROS-mediated DNA damage activates p53-mediated apoptosis in cancer cells.<sup>[41]</sup> The present observations like loss of mitochondrial membrane potential, elevated levels of *FADD*, *cytochrome c*, *caspase 3*, and *p53* confirm that

ROS plays a pivotal role in the induction of apoptosis in 4-FPAC-treated A549 cells.

Failure of the antioxidant system leads to ROS induction that further stimulates p53-mediated apoptosis. Here, in this study, a significant decrease in the activity of antioxidant enzymes such as CAT and GPx were observed in A549 cells at 48 hours of treatment with 0.16 nM of 4-FPAC compared to that of control. Therefore, it can be deduced that the reduction in the activities of these antioxidant enzymes might be the main reason for the observed elevation of intracellular ROS in the treated cells.

It is stated that the elevated ROS is responsible for the loss of mitochondrial as well as the lysosomal membrane potential. Hence, we investigated the mitochondrial membrane potential by rhodamine 123 staining and lysosomal membrane potential by AO staining. The results vividly showed that both of the organelles lost the membrane potential when treated with 0.16 nM of 4-FPAC. Mitochondrial membrane permeabilization leads to the release of *cytochrome c* and *AIF*, in which *cytochrome c* causes caspase-dependent, whereas *AIF* is responsible for caspase-independent cell death.<sup>[42]</sup> The transcript level analysis showed that *AIF* is downregulated, and *cytochrome c* is upregulated in the 4-FPAC-treated cells. Hence, it can be deduced that cell death in treated A549 is caspase-dependent. The upregulated expression of *caspase 9*, *caspase 8*, and *cleaved caspase 3* in the treated cells further consolidate this notion.

Moreover, Cirman et al<sup>[43]</sup> have opined that lysosomal membrane damage leads to the release of cathepsins, which subsequently activates Bid, Bax, and Bad, and releases cytochrome *c* from the mitochondria. Additionally, it was reported that Bax directly affects lysosome when translocated from cytosol to lysosomal membrane.<sup>[44]</sup> Therefore, lysosomal and mitochondrial membrane damage act as a positive feedback loop for the release of cathepsin, activation of Bid, and subsequent release of cytochrome *c*, and all these three were found upregulated in the A549 cells treated with 0.16 nM of 4-FPAC.

Furthermore, it has been documented that like ROS, iNOS too acts in a concentration-dependent manner and differentially regulates various cellular functions.<sup>[45]</sup> At low concentration, iNOS acts

as a signaling molecule and facilitates cell survival, proliferation, metastasis, and angiogenesis, whereas, at high concentrations, it exerts antitumor activity.<sup>[46]</sup> Moreover, the regulatory role of iNOS was reported in various types of cancers, including brain tumor, melanoma, and breast cancer.<sup>[47–49]</sup> The dual role of iNOS is dependent on cell type, the concentration of therapeutic, and cellular environment. Chemo-preventive agents like 5-fluorouracil and fenretinide are known to induce apoptosis in cancerous cells by activating iNOS.<sup>[50,51]</sup> The typical markers of iNOS-mediated cytotoxicity are caspase-dependent apoptosis, chromatin condensation, DNA fragmentation, p53 phosphorylation, and cytochrome c release from mitochondria.<sup>[52]</sup> Since the levels of these markers were found high in 4-FPAC-treated cells compared with controls, we can conclude that the observed hike in the level of iNOS has contributed its bit in inducing apoptosis in the treated A549 cells.

Parallely, the efficacy of 4-FPAC was tested for its potent antimetastatic property. Metastasis is a complex process that involves multiple steps like rapid proliferation, EMT, invasion, cell migration, and angiogenesis. When A549 cells were treated with 0.16 nM of 4-FPAC, a significant reduction in the aggregation property, clonogenic capacity, and anchorage dependency for growth and migration was observed. To understand the molecular events behind these phenomena, specific markers of the pathway that facilitate various processes of metastasis, as mentioned above, were studied in 4-FPAC-treated A549 cells at transcript and protein levels. Results revealed significant reduction in the expression of major transcriptional regulators of EMT like Snail1, Snail2, and ZEB1 in the A549 cells treated with 4-FPAC. The Snails and ZEB1 are known to induce EMT by downregulating the cell adhesion molecules and upregulating intermediate filaments that facilitate cell migration.<sup>[53,54]</sup> Moreover, the reduced expression of PCNA, a proliferation marker, further substantiates the reduction in clonogenic capacity exhibited by A549 cells subjected to 4-FPAC. Besides, reduction in the levels of adhesion molecules like claudin 3 and claudin 4 was also observed in the treated cells, which could be a function of Snail-mediated expression of a transcriptional inhibitor named ZEB1. Similar observations by Lin et al.<sup>[55]</sup> give credence to the present result. It is reported that when p53 expression increases, it degrades Snail2 via MDM2 interaction.<sup>[56]</sup> Therefore, it is prudent to presume that the observed hike in p53 expression might be the reason behind the reduction in *snail 2* levels in the treated cells. Moreover, the compromised expression of *snail 2*, in turn, influences the expression of ZEB1, a downstream modulator of the Snail pathway, resulting in a substantial reduction of EMT in A549 cells challenged with 4-FPAC. Further study on other transcription factors is required to unlock the complete phenomenon of EMT. Therefore, it could be inferred that 4-FPAC affects the EMT initiation process by upregulating E-cadherin via Snail-activated downregulation of ZEB1 in the 4-FPAC-treated A549 cells.

However, once EMT is initiated, the process will be maintained by the autocrine loop of growth factors like transforming growth factor  $\beta$  (TGF- $\beta$ ).<sup>[57]</sup> The TGF- $\beta$  chiefly support EMT by activating

transcription factors like Twist, Snail1, and ZEB1, which downregulates E-cadherin and upregulates vimentin and N-cadherin.<sup>[58]</sup> TGF- $\beta$  is also known to induce ROS by reducing the levels of antioxidant enzymes like GPx, SOD, and CAT.<sup>[59]</sup> It is also reported that tumor cells undergoing EMT secrete MMPs under the influence of Snail, which is activated by TGF- $\beta$  and hypoxia.<sup>[60]</sup> The MMPs further degrades the basement membrane, and cells start the migration from one site to another via lymph node. The activated Snail induces IL-8 and VEGF- $\alpha$ , which initiates neovascularization near tumor cells.<sup>[61,62]</sup> VEGF- $\alpha$  also activates EMT via hypoxia-inducible factor 1 $\alpha$  (HIF-1 $\alpha$ )-mediated Snail pathway.<sup>[63]</sup> It was observed that 4-FPAC increases the expression of TGF- $\beta$ , which leads to the augmentation of ROS and upregulation of HIF-1 $\alpha$ . Nonetheless, this upregulation was not enough to prevent Snail degradation and release of MMP-2 and MMP-9, as both were found to be decreased in treated cells. At the same time, a decrease in protein level expression of IL-8 was also observed, which might be because of the downregulation of *snail* and MMPs, as reported by Lewis et al.<sup>[64]</sup> Moreover, p53 is known as a negative regulator of VEGF- $\alpha$  promoter activity,<sup>[65]</sup> and in the treated cells, there was a significant reduction in the expression of p53. Therefore, it can be inferred that p53 and Snail were the major angiogenesis inhibitors in the A549 cells treated with 4-FPAC.

Other factors have also been suggested to be involved in the initiation and maintenance of metastasis, including IL-6, IL-10, TNF- $\alpha$ , and IL-1 $\beta$ , which, too, were studied herein to corroborate the earlier described antimetastatic property of 4-FPAC in A549 cells. IL-10 is reported to be a suppressor of metastasis and angiogenesis.<sup>[66]</sup> However, in most of the lung cancer cases, IL-6 remained upregulated to assist survival, proliferation, invasion, metastasis, and EMT.<sup>[67,68]</sup> Most of the NSCLC secrete IL-6 and TNF- $\alpha$ , which promotes EMT, invasion, and metastasis.<sup>[68]</sup> IL-1 $\beta$ , which is produced by cancer cells itself, acts on cancer cells by establishing a cross-talk with autocrine factors like MMPs, VEGF- $\alpha$ , IL-8, IL-6, and TNF- $\alpha$ , and hence facilitate invasion and angiogenesis.<sup>[69]</sup> In this study, a significant elevation in the transcript levels of IL-10 and a concomitant reduction in the mRNA levels of IL-6 and IL-1 $\beta$  was observed in 4-FPAC-treated A549 cells, which reiterate the antimetastatic potential of the compound in question. Nonetheless, the expression of TNF- $\alpha$  was found significantly reduced in the cells subjected to 0.16 nM of 4-FPAC. However, apart from its reported prometastatic property, TNF- $\alpha$  is also an activator of the Fas-mediated apoptotic pathway, and ROS-mediated necrotic pathway,<sup>[70]</sup> hence its increase could assist the extrinsic pathway of apoptosis as described previously.

Furthermore, an attempt was also made to understand the effect of the 4-FPAC on PI3K/AKT pathway, one of the primary mediators of cell survival, EMT, metastasis as well as angiogenesis and hence, a potential target for anticancer therapy. Recently it has been reported that one of the coumarin derivatives successfully hampered the PI3K/AKT pathway in K562 cells.<sup>[71,72]</sup> Moreover, it is stated that upon activation, PI3K phosphorylates AKT, a downstream target and positive regulator of the pathway, which subsequently phosphorylates and inactivates both BAX and BAD,

the two proapoptotic proteins of the intrinsic pathway of apoptosis.<sup>[73]</sup> In addition, phosphorylated AKT is known to enhance the MDM2 expression, and hence counteracts the expression of p53.<sup>[74]</sup> In the present study, a significant reduction in the transcript levels of AKT and MDM2 was observed in the A549 cells treated with 4-FPAC. Moreover, it was also noted that mRNA levels of BAD, BAX, and p53 remained significantly high in the treated cells. Therefore, it is possible that exposure to 4-FPAC might have reduced the expression of AKT, which resulted in the reduction of MDM2 level, leading to the activation of p53, BAD, and BAX, and hence could have induced apoptosis in the 4-FPAC-treated A549 cells.

Additionally, the PI3K/AKT pathway is known to upregulate the potent inducers of EMT namely Snail, TWIST, MMPs, and TGF- $\beta$ .<sup>[75,76]</sup> The ablation of the AKT pathway is also reported to inhibit the nuclear accumulation of  $\beta$ -catenin and thereby EMT.<sup>[77]</sup> Moreover, the overexpression AKT favors angiogenesis by increasing the expression of HIF-1 $\alpha$ .<sup>[78]</sup> In this study, we found that 4-FPAC downregulates the PI3K/AKT pathway, thereby increasing the apoptosis and concomitantly decreasing the EMT, invasion, and angiogenesis in the 4-FPAC-treated A549 cells.

Overall, the present in vitro study vividly exemplified that the coumarin derivative 4-FPAC, at a dose of 0.16 nM, successfully hampered the proliferation, EMT, invasion, migration, and angiogenesis in A549 cells. In particular, 4-FPAC exerts its effect through AKT-mediated inhibition of the p53 pathway. In brief, the derivative caused cell cycle arrest at G0/G1 by p53-induced p21-mediated inhibition of CDK2/CDK4 cyclin complex. Additionally, this derivative also induced apoptotic cell death by ROS-evoked p53-mediated caspase-dependent pathway, which involves both mitochondrial and lysosomal compartments. Further, it was observed that 4-FPAC is effective in curtailing the metastasis and angiogenesis in A549 cells by p53-mediated downregulation of Snail, MMP-2, 9, and IL-8. The currently observed antitumor and antiangiogenic efficacy of 4-FPAC on A549 cells suggest that it has the potential to evolve as a promising novel chemotherapeutic agent against NSCLC.

#### ACKNOWLEDGMENTS

Authors are thankful to Science and Engineering Research Board, New Delhi (Grant number: SB/SO/AS-008/2014), and Department of Biotechnology, New Delhi (Grant number: BT/PR11467/MED/31/270/2014) for supporting the research carried out at the department. Shweta Umar is indebted to the University of Grant Commission, New Delhi, for support in terms of fellowship. We are thankful to the anonymous reviewers for their constructive suggestions that helped us to improve the manuscript.

#### CONFLICT OF INTERESTS

The authors declare that there are no conflict of interests.

#### ORCID

Suresh Balakrishnan  <http://orcid.org/0000-0002-6559-022X>

#### REFERENCES

- [1] C. B. Thompson, *Science* **1995**, *267*, 1456.
- [2] J. Ferlay, I. Soerjomataram, R. Dikshit, S. Eser, C. Mathers, M. Rebelo, D. M. Parkin, D. Forman, F. Bray, *Int. J. Cancer* **2015**, *136*, E359.
- [3] G. J. Finn, E. Kenealy, B. S. Creaven, D. A. Egan, *Cancer Lett.* **2002**, *183*, 61.
- [4] J. Hirsh, J. E. Dalen, D. R. Anderson, L. Poller, H. Bussey, J. Ansell, D. Deykin, *Chest* **2001**, *119*, 8S.
- [5] N. Iwata, M. Kainuma, D. Kobayashi, T. Kubota, N. Sugawara, A. Uchida, S. Ozono, Y. Yamamuro, N. Furusyo, K. Ueda, E. Tahara, *Front. Pharmacol.* **2016**, *7*, 174.
- [6] D. Egan, R. O'Kennedy, E. Moran, D. Cox, E. Prosser, R. D. Thornes, *Drug Metab. Rev.* **1990**, *22*, 503.
- [7] S. D. Durgapal, R. Soni, S. Umar, B. Suresh, S. S. Soman, *Chem. Select* **2017**, *2*, 147.
- [8] A. I. Elkady, M. A. El-H. Salim, *Life Sci. J.* **2013**, *10*, 2529.
- [9] S. Chikara, K. Lindsey, H. Dhillon, S. Mamidi, J. Kittilson, M. Christofidou-Solomidou, K. M. Reindl, *Nutr. Cancer* **2017**, *69*, 652.
- [10] P. L. Olive, J. P. Ban ath, *Nat. Protoc.* **2006**, *1*, 23.
- [11] S. Pajaniradjie, K. Mohankumar, R. Pamidimukkala, S. Subramanian, R. Rajagopalan, *BioMed Res. Int.* **2014**, *2014*, 474953.
- [12] I. K. Maurya, S. Pathak, M. Sharma, H. Sanwal, P. Chaudhary, S. Tupe, M. Deshpande, V. S. Chauhan, R. Prasad, *Peptides* **2011**, *32*, 1732.
- [13] D. E. Paglia, W. N. Valentine, *Am. J. Clin. Pathol.* **1974**, *62*, 740.
- [14] S. Marklund, G. Marklund, *Eur. J. Biochem.* **1974**, *47*, 469.
- [15] A. K. Sinha, *Anal. Biochem.* **1972**, *47*, 389.
- [16] Q. Y. Chen, J. G. Shi, Q. H. Yao, D. M. Jiao, Y. Y. Wang, H. Z. Hu, Y. Q. Wu, J. Song, J. Yan, L. J. Wu, *Mol. Cell. Biochem.* **2012**, *359*, 389.
- [17] N. A. Franken, H. M. Rodermond, J. Stap, J. Haveman, C. Van Bree, *Nat. Protoc.* **2006**, *1*, 2315.
- [18] A. Lui, J. New, J. Ogony, S. Thomas, J. Lewis-Wambi, *BMC Cancer* **2016**, *16*, 487.
- [19] L. Yang, M. M. Lee, M. M. Leung, Y. H. Wong, *Cell. Signal.* **2016**, *28*, 1663.
- [20] K. J. Livak, T. D. Schmittgen, *Methods* **2001**, *25*, 402.
- [21] L. Khoshtabiat, M. Mahdavi, G. Dehghan, M. R. Rashidi, *Asian Pac. J. Cancer Prev.* **2016**, *17*, 4267.
- [22] K. A. Ahmad, K. B. Iskandar, J. L. Hirpara, M. V. Clement, S. Pervaiz, *Cancer Res.* **2004**, *64*, 7867.
- [23] L. Yang, W. Zeng, D. Li, R. Zhou, *Oncol. Rep.* **2009**, *22*, 121.
- [24] M. J. Wheelock, Y. Shintani, M. Maeda, Y. Fukumoto, K. R. Johnson, *J. Cell Sci.* **2008**, *121*, 727.
- [25] H. Peinado, D. Olmeda, A. Cano, *Nat. Rev. Cancer* **2007**, *7*, 415.
- [26] A. Kumar, A. C. Carrera, *Cell Cycle* **2007**, *6*, 1696.
- [27] A. C. Hsieh, M. L. Truitt, D. Ruggero, *Br. J. Cancer* **2011**, *105*, 329.
- [28] A. Parcellier, L. A. Tintignac, E. Zhuravleva, B. A. Hemmings, *Cell. Signal.* **2008**, *20*, 21.
- [29] W. Xu, Z. Yang, N. Lu, *Cell Adh. Migr.* **2015**, *9*, 317.
- [30] B. H. Jiang, J. Z. Zheng, M. Aoki, P. K. Vogt, *Proc. Natl. Acad. Sci. USA* **2000**, *97*, 1749.
- [31] M. L. Agarwal, W. R. Taylor, M. V. Chernov, O. B. Chernova, G. R. Stark, *J. Biol. Chem.* **1998**, *273*, 1.
- [32] K. Vermeulen, Z. N. Berneman, D. R. Van Bockstaele, *Cell Prolif.* **2003**, *36*, 165.
- [33] T. Abbas, A. Dutta, *Nat. Rev. Cancer* **2009**, *9*, 400.
- [34] G. Majno, I. Joris, *Am. J. Pathol.* **1995**, *146*, 3.
- [35] D. Trachootham, Y. Zhou, H. Zhang, Y. Demizu, Z. Chen, H. Pelicano, P. J. Chiao, G. Achanta, R. B. Arlinghaus, J. Liu, P. Huang, *Cancer Cell* **2006**, *10*, 241.
- [36] M. Ushio-Fukai, Y. Nakamura, *Cancer Lett.* **2008**, *266*, 37.
- [37] D. Trachootham, W. Lu, M. A. Ogasawara, N. Rivera-Del Valle, P. Huang, *Antioxid. Redox. Signal.* **2008**, *10*, 1343.
- [38] T. Ozben, *J. Pharm. Sci.* **2007**, *96*, 2181.
- [39] R. Reinehr, S. Becker, A. Eberle, S. Grether-Beck, D. H ussinger, *J. Biol. Chem.* **2005**, *280*, 27179.

- [40] A. J. Levine, W. Hu, Z. Feng, *Cell Death Differ.* **2006**, *13*, 1027.
- [41] M. R. Ramsey, N. E. Sharpless, *Nat. Cell Biol.* **2006**, *8*, 1213.
- [42] H. K. Lorenzo, S. A. Susin, J. Penninger, G. Kroemer, *Cell Death Differ.* **1999**, *6*, 516.
- [43] T. Cirman, K. Orešić, G. D. Mazovec, V. Turk, J. C. Reed, R. M. Myers, G. S. Salvesen, B. Turk, *J. Biol. Chem.* **2004**, *279*, 3578.
- [44] K. Kågedal, A. C. Johansson, U. Johansson, G. Heimlich, K. Roberg, N. S. Wang, J. M. Jürgensmeier, K. Öllinger, *Int. J. Exp. Pathol.* **2005**, *86*, 309.
- [45] M. Lechner, P. Lirk, J. Rieder, *Sem. Cancer Biol.* **2005**, *15*, 277.
- [46] L. Zhang, J. Liu, X. Wang, Z. Li, X. Zhang, P. Cao, X. She, Q. Dai, J. Tang, Z. Liu, *Curr. Mol. Med.* **2014**, *14*, 762.
- [47] C. S. Cobbs, J. E. Brenman, K. D. Aldape, D. S. Bredt, M. A. Israel, *Cancer Res.* **1995**, *55*, 727.
- [48] S. Loibl, A. Buck, C. Strank, G. von Minckwitz, M. Roller, H. P. Sinn, V. Schini-Kerth, C. Solbach, K. Strebhardt, M. Kaufmann, *Eur. J. Cancer* **2005**, *41*, 265.
- [49] S. Ekmekcioglu, J. A. Ellerhorst, V. G. Prieto, M. M. Johnson, L. D. Broemeling, E. A. Grimm, *Int. J. Cancer* **2006**, *119*, 861.
- [50] J. Jiang, J. Liu, J. Zhu, C. Yang, A. Zhang, *Chin. Med. J.* **2002**, *115*, 968.
- [51] A. M. Simeone, S. Ekmekcioglu, L. D. Broemeling, E. A. Grimm, A. M. Tari, *Mol. Cancer Ther.* **2002**, *1*, 1009.
- [52] B. M. Choi, H. O. Pae, S. I. Jang, Y. M. Kim, H. T. Chung, *BMB Rep.* **2002**, *35*, 116.
- [53] J. Jiang, Y. L. Tang, X. H. Liang, *Cancer Biol. Ther.* **2011**, *11*, 714.
- [54] P. Savagner, *BioEssays* **2001**, *23*, 912.
- [55] X. Lin, X. Shang, G. Manorek, S. B. Howell, *PLOS One* **2013**, *8*, e67496.
- [56] S. P. Wang, W. L. Wang, Y. L. Chang, C. T. Wu, Y. C. Chao, S. H. Kao, A. Yuan, C. W. Lin, S. C. Yang, W. K. Chan, K. C. Li, *Nat. Cell Biol.* **2009**, *11*, 694.
- [57] J. Xu, S. Lamouille, R. Derynck, *Cell Res.* **2009**, *19*, 156.
- [58] T. Vincent, E. P. Neve, J. R. Johnson, A. Kukalev, F. Rojo, J. Albanell, K. Pietras, I. Virtanen, L. Philipson, P. L. Leopold, R. G. Crystal, *Nat. Cell Biol.* **2009**, *11*, 943.
- [59] R. M. Liu, K. G. Pravia, *Free Radical Biol. Med.* **2010**, *48*, 1.
- [60] I. Ota, X. Y. Li, Y. Hu, S. J. Weiss, *Proc. Natl. Acad. Sci. USA* **2009**, *106*, 20318.
- [61] W. L. Hwang, M. H. Yang, M. L. Tsai, H. Y. Lan, S. H. Su, S. C. Chang, H. W. Teng, S. H. Yang, Y. T. Lan, S. H. Chiou, H. W. Wang, *Gastroenterology* **2011**, *141*, 279.
- [62] R. Du, K. V. Lu, C. Petritsch, P. Liu, R. Ganss, E. Passequé, H. Song, S. VandenBerg, R. S. Johnson, Z. Werb, G. Bergers, *Cancer Cell* **2008**, *13*, 206.
- [63] P. Mak, I. Leav, B. Pursell, D. Bae, X. Yang, C. A. Taglienti, L. M. Gouvin, V. M. Sharma, A. M. Mercurio, *Cancer Cell* **2010**, *17*, 319.
- [64] A. M. Lewis, S. Varghese, H. Xu, H. R. Alexander, *J. Transl. Med.* **2006**, *4*, 48.
- [65] D. Mukhopadhyay, L. Tsiokas, V. P. Sukhatme, *Cancer Res.* **1995**, *55*, 6161.
- [66] J. S. Silvestre, Z. Mallat, M. Duriez, R. Tamarat, M. F. Bureau, D. Scherman, N. Duverger, D. Branellec, A. Tedgui, B. I. Levy, *Circ. Res.* **2000**, *87*, 448.
- [67] Y. Shintani, A. Fujiwara, T. Kimura, T. Kawamura, S. Funaki, M. Minami, M. Okumura, *J. Thorac. Oncol.* **2016**, *11*, 1482.
- [68] G. S. Shang, L. Liu, Y. W. Qin, *Oncol. Lett.* **2017**, *13*, 4657.
- [69] E. Voronov, D. S. Shouval, Y. Krelin, E. Cagnano, D. Benharroch, Y. Iwakura, C. A. Dinarello, R. N. Apte, *Proc. Natl. Acad. Sci. USA* **2003**, *100*, 2645.
- [70] A. Thorburn, *Cell. Signal.* **2004**, *16*, 139.
- [71] Y. Lin, S. Choksi, H. M. Shen, Q. F. Yang, G. M. Hur, Y. S. Kim, J. H. Tran, S. A. Nedospasov, Z. G. Liu, *J. Biol. Chem.* **2004**, *279*, 10822.
- [72] C. C. Ma, Z. P. Liu, *Anti-Cancer Agents Med. Chem.* **2017**, *17*, 395.
- [73] L. Simonyan, T. T. Renault, M. J. da Costa Novais, M. J. Sousa, M. Côrte-Real, N. Camougrand, C. Gonzalez, S. Manon, *FEBS Lett.* **2016**, *590*, 13.
- [74] A. G. Abraham, E. O'Neill, *Biochem. Soc. Trans.* **2014**, *42*, 798.
- [75] K. O. Hong, J. H. Kim, J. S. Hong, H. J. Yoon, J. I. Lee, S. P. Hong, S. D. Hong, *J. Exp. Clin. Cancer Res.* **2009**, *28*, 28.
- [76] J. H. Zuo, W. Zhu, M. Y. Li, X. H. Li, H. Yi, G. Q. Zeng, X. X. Wan, Q. Y. He, J. H. Li, J. Q. Qu, Y. Chen, *J. Cell. Biochem.* **2011**, *112*, 2508.
- [77] D. Fang, D. Hawke, Y. Zheng, Y. Xia, J. Meisenhelder, H. Nika, G. B. Mills, R. Kobayashi, T. Hunter, Z. n Lu, *J. Biol. Chem.* **2007**, *282*, 11221.
- [78] B. H. Jiang, G. Jiang, J. Z. Zheng, Z. Lu, T. Hunter, P. K. Vogt, *Cell Growth Differ.* **2001**, *12*, 363.

#### SUPPORTING INFORMATION

Additional supporting information may be found online in the Supporting Information section.

**How to cite this article:** Umar S, Soni R, Durgapal SD, Soman S, Balakrishnan S. A synthetic coumarin derivative (4-fluorophenylacetamide-acetyl coumarin) impedes cell cycle at G0/G1 stage, induces apoptosis, and inhibits metastasis via ROS-mediated p53 and AKT signaling pathways in A549 cells. *J Biochem Mol Toxicol.* 2020:e22553. <https://doi.org/10.1002/jbt.22553>

## Medicinal Chemistry &amp; Drug Discovery

## Anticancer Activity and DNA Binding Studies of Novel 3,7-Disubstituted Benzopyrones

Sunil Dutt Durgapal,<sup>[a]</sup> Rina Soni,<sup>[a]</sup> Shweta Umar,<sup>[b]</sup> Balakrishnan Suresh,<sup>[b]</sup> and Shubhangi S. Soman<sup>\*[a]</sup>

We have designed and synthesized novel 7-substituted-3-acetyl-benzopyrones **9a-9g** and ethyl 7-substituted-3-carboxylate-benzopyrones **10a-10d** and screened for anticancer activity using MTT assay. Most of the tested compounds have shown very good activity against A549 cell line (lung cancer cell-line) and MCF7 cell line (breast cancer cell-line) compared to 5-Fluorouracil. Compound **9b** and **9e** exhibited excellent anticancer activity with IC<sub>50</sub> 0.16 nM against A549 cell line and

84.8 nM against MCF7 cell line respectively. Compounds **9b** and **9e** showed excellent anticancer activity at very low concentration, well falling in nanomolar region. Compounds **9b** and **9e** exhibited very good binding constant for DNA binding through intercalation in UV based DNA titration which was further confirmed by fluorescence based EtBr displacement assay in DNA-EtBr complex.

## Introduction

Cancer is one of the dreadful diseases after cardiovascular diseases and diabetes falling under category of non-communicable diseases all over the world. According to WHO, number of people affected by cancer will rise from 14 million in 2012 to 22 million within the next 20 years.<sup>[1]</sup> Most of the cancers are defined by uncontrolled growth of cells without differentiation due to the deregulation of essential enzymes and other proteins controlling cell division and proliferation.<sup>[2-3]</sup> Out of many therapeutic strategies, chemotherapy shows significant clinical responses. At the same time, these chemotherapeutic agents have a small therapeutic window with non-specificity and high-systemic toxicity. To get selective chemotherapeutics with very low side effects is a major challenge in treatment of cancer.<sup>[4]</sup> Second major problem after target selectivity in chemotherapy, is drug resistance to many anticancer agents. These have resulted in drug-induced toxicities and requirement of high doses of chemotherapeutic agents.<sup>[5-7]</sup> Therefore, discovering of new anticancer agent with high potency is urgent need in treatment of cancer.<sup>[8]</sup>

One of the important classes of natural products, coumarins are considered as useful source of potential drug candidates due to safety and efficacy exhibited by coumarin derivatives. The bioactivity of coumarin and more complex related

derivatives is mostly coming from coumarin nucleus. Coumarin derivatives are known with variety of pharmacological activities including anti-inflammatory,<sup>[9,10]</sup> antioxidant,<sup>[11,12]</sup> antithrombotic,<sup>[13,14]</sup> antiviral,<sup>[15,16]</sup> antimicrobial,<sup>[17,18]</sup> antituberculosis,<sup>[19]</sup> and antihyperlipidemic<sup>[20]</sup> activities. Due to the potential applications of coumarins in medicinal chemistry, many efforts have been made on the design and synthesis of new coumarin derivatives with improved biological activities. Coumarins exhibited antitumor activities at different stages of cancer formation through various mechanisms, for example blocking cell cycle, inducing cell apoptosis, modulating estrogen receptor (ER), or inhibiting the DNA-associated enzymes, such as topoisomerase.<sup>[21]</sup>

Coumarin derivatives containing a substituted hydroxyl group at the position 7 showed antibiotic and antifungal activities, while 7-hydroxycoumarin derivatives showed very good cytotoxicity and cytostatic activity.<sup>[22]</sup> Recent studies on a variety of synthetic coumarin derivatives have demonstrated the influence of the coumarin skeleton and substitutions at positions 3 and 7 on antitumor activities.<sup>[23]</sup> Maciejewska *et al* reported series of *O*-aminoalkyl substituted 7-hydroxycoumarins with anticancer activity.<sup>[24]</sup> Compound **1** showed good activity against various cancer cell lines such as leukemia CCRFCM, non-small cell lung cancer HOP92 and colon cancer HCC2998.

Antioxidant compounds play important role in biological system by removal of free radicals generated in body. Synthetic antioxidant compounds are showing toxicity and mutagenic effects. Several coumarin derivatives are reported with antioxidant activity. Recently, El-Hameed Hassan *et al* reported 7-hydroxycoumarin derivative **2** as very good antioxidant in DPPH assay with IC<sub>50</sub> value 213 µg/mL.<sup>[25]</sup> Most of the anticancer drugs including 5-fluorouracil, tamoxifen and paclitaxel exerts their cytotoxicity toward cancer cell by elevating cellular ROS production to a threshold level and this elevated ROS causes DNA damage and activate apoptotic pathway in cell.<sup>[26-29]</sup> To

[a] S. D. Durgapal, Dr. R. Soni, Prof. S. S. Soman  
Department of Chemistry  
The M. S University of Baroda  
Department of chemistry, Faculty of Science, Vadodara. 390002, India  
E-mail: shubhangiss@rediffmail.com

[b] S. Umar, Prof. B. Suresh  
Department of Zoology  
The M. S University of Baroda  
Department of Zoology, Faculty of Science, Vadodara. 390002, India

Supporting information for this article is available on the WWW under <http://dx.doi.org/10.1002/slct.201601361>

counterbalance the effect of ROS, cell have an antioxidant defence system which combat the effect of increased ROS in cell. Thus, the presence of antioxidant eradicates the anticancer effect of an anticancer drug which mostly exerts its effect by mean of ROS. Therefore, a potent anticancer drug should have low antioxidant property. Thus, screening of antioxidant activity provides useful insight into the mechanism of action of anticancer activity.

Anticancer drugs have traditionally been targeted to damage aberrantly dividing cells by interrupting the cell division process. Some of them are DNA intercalating agents or DNA cross linking agents. Coumarins form interstrand as well as intrastrand cross linkages and act as intercalating agents.<sup>[30–31]</sup> However, there are limited reports on such interactions for 3,7-disubstituted coumarins with DNA. The novel 3,7-disubstituted coumarin derivatives **9a–g** and **10a–d** were synthesized and screened for their anticancer activity, DNA binding studies and antioxidant activity (Figure 1).

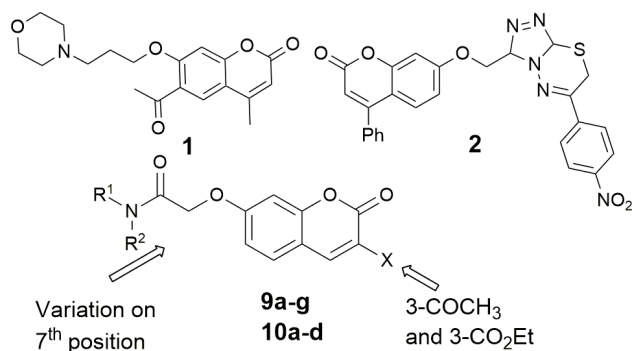
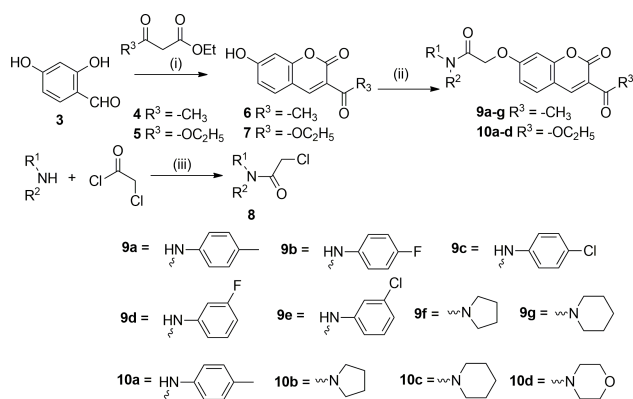


Figure 1. Coumarin derivatives with anticancer activity.

## Results and Discussion

### Chemistry

Novel 7-substituted-3-acetyl-benzopyrones **9a–9g** and ethyl 7-substituted-3-carboxylate-benzopyrones **10a–10d** (Scheme 1) were synthesized by reaction of 7-hydroxy-3-acetyl coumarin **6**, and ethyl 7-hydroxy-3-carboxylate coumarin **7** with different chloroacetamide derivatives. Knoevenagel Reaction of resorcaldehyde **3** with diethyl malonate **5** under similar conditions gave ethyl 7-hydroxy-3-carboxylate coumarin **7** as shown in **scheme 1**. The <sup>1</sup>H-NMR spectrum of compound **6** exhibited singlet for -OH at 11.14 ppm, all aromatic protons were observed at  $\delta$  8.56–6.72. The methyl protons were observed as a singlet at  $\delta$  2.53. In the <sup>13</sup>C-NMR spectrum, acetyl carbonyl carbon was observed at 195 ppm, the lactone carbonyl carbon of coumarin ring observed at  $\delta$  164, all aromatic carbons observed from  $\delta$  159–102 and methyl carbon at  $\delta$  30. The <sup>1</sup>H-NMR spectrum of compound **7** exhibited singlet for -OH at 11.10 ppm, all aromatic protons observed at  $\delta$  8.67–6.72. The ethyl protons of ester group exhibited quartet at  $\delta$  4.25 and triplet at  $\delta$  1.29 with coupling constant 7.2 Hz for -CH<sub>2</sub> and -CH<sub>3</sub>



**Scheme 1.** Synthesis of 3,7-disubstituted coumarin derivatives **9a–g** and **10a–d**. Reagents and conditions: (i) Piperidine catalytic, pyridine, bulb oven (100 W), 70–80 °C, 14 h, 74–87%; (ii) **8**, anhydrous K<sub>2</sub>CO<sub>3</sub>, KI pinch, DMF, 70–80 °C, 12–18 h, 43–91%; (iii) TEA, DCM, 0–5 °C, 30 min, rt, 24 h, 85–95%.

respectively. In the <sup>13</sup>C-NMR spectrum, the lactone carbonyl carbon of coumarin ring observed at  $\delta$  164 and ester carbonyl carbon was observed at  $\delta$  163 ppm, all aromatic carbons observed from  $\delta$  157–102 ppm and ethyl carbons at  $\delta$  61 and 14 ppm.

Various substituted amines on reaction with chloroacetyl chloride gave corresponding chloroacetamide derivatives **8** and these compounds were directly used for reaction with 7-hydroxy coumarins **6** and **7**. These chloroacetamide derivatives **8** were reacted with 7-hydroxy-3-substituted coumarins using anhydrous K<sub>2</sub>CO<sub>3</sub> in DMF at 70–80 °C in presence of catalytic amount of KI to give compounds **9a–g** and **10a–d**. The structures of 3,7-disubstituted coumarin derivatives **9a–g** and **10a–d** were confirmed by different analytical techniques such as <sup>1</sup>H-NMR, <sup>13</sup>C-NMR, IR, ESI-MS and X-ray Single Crystal. In general, the IR spectra of compounds **9a–g** exhibited three strong bands in the range of 1734–1723 cm<sup>-1</sup>, 1698–1681 cm<sup>-1</sup> and 1670–1611 cm<sup>-1</sup> for the lactone, ketone and amide carbonyl stretching frequency respectively. In the <sup>1</sup>H-NMR spectra of **9a–g**, peaks for methyl protons of acetyl group observed in range of  $\delta$  ~ 2.73–2.55, methylene protons observed in range of  $\delta$  ~ 4.92–4.71, aromatic protons observed in range of  $\delta$  6.82–8.64 depending on effect of different amine substituted on it. For compounds **9a–e**, -NH protons are observed in range of 10.41–10.25. For compound **9e** D<sub>2</sub>O exchange study was performed which showed disappearance of peak at  $\delta$  10.43 thus confirmed the peak for -NH proton at 10.43 ppm. In the <sup>13</sup>C-NMR spectra of **9a–g**, peak for methyl carbon of acetyl group observed around 30 ppm, methylene carbon around 67 ppm, aromatic carbons in range of 101–161 ppm, amide carbonyl carbon in range of 163–161 ppm, coumarin lactone carbonyl carbon in range of 166–164 ppm and acetyl carbonyl carbon around 195 ppm.

For compounds **10a–d**, the IR spectra exhibited three strong bands in range of 1757–1747 cm<sup>-1</sup>, 1708–1647 cm<sup>-1</sup> and 1623–1602 cm<sup>-1</sup> for the lactone, ester and amide carbonyls respectively. In the <sup>1</sup>H-NMR spectra of **10a–d**, peak for methyl protons of ester group observed in range of  $\delta$  ~ 1.42–1.30 as a

triplet and methylene protons observed in range of  $\delta$  ~4.42-4.27 as a quartet. Protons for methylene linkage are observed in range of 5.02-4.71 and aromatic protons observed in range of 6.82-8.72 depending on effect of different amine substitution on it. For compound **10a** -NH proton is observed at  $\delta$  8.15 ppm, which was confirmed by D<sub>2</sub>O exchange study. In the <sup>13</sup>CNMR spectra of **10a-d**, carbons for ethyl group observed around 14 ppm for methyl and 61 ppm for methylene. For compound **10a-d**, methylene linkage carbon observed around 67-66 ppm, aromatic carbon in range of 101-157 ppm, amide carbonyl group in range of 163-161 ppm, coumarin lactone carbonyl carbon in range of 163-164 ppm and ester carbonyl carbon at 165 ppm. All compounds **9a-g** and **10a-d** were analyzed by ESI-MS analysis to give [M+H]<sup>+</sup>/[M+Na]<sup>+</sup> peak corresponding to their molecular weight. Structure of compound **10d** was confirmed by X-ray single crystal analysis (CCDC 1522100). All these new chemical entities were subjected to *in-vitro* studies for anticancer activity by MTT assay method, DNA binding studies and antioxidant activity by DPPH assay.

### Anticancer Activity

Results from MTT assay were used to assess the growth inhibitory effect of the various compounds on A549 cancer cells (Lungs cancer cell line) and MCF7 (Breast cancer cell line). IC<sub>50</sub> values were calculated to determine the concentration of test compound at which 50% of the cells are killed (Table 1). Compounds were studied for their DNA binding interaction (Table 2) and for their anti-oxidant activity against DPPH assay with respect to ascorbic acid as standard (Table 3).

### Structure activity relationship (SAR) for anticancer activity

The MTT assay for 7-substituted-3-acetyl coumarin series showed better activity for compound **9a** with *p*-methyl substituent on aromatic amide against A549 and MCF7 with IC<sub>50</sub> 2.40  $\mu$ M and 0.65  $\mu$ M respectively. On replacement of *p*-methyl with halogen such as compounds **9b** and **9c** resulted in compounds with excellent activity (Table 1). Compound **9b** with 4-fluoro substituent showed excellent activity with IC<sub>50</sub> value 0.16 nM against A549 cell line, and showed good activity against MCF7 cell line with IC<sub>50</sub> 23.53  $\mu$ M. Moreover, compound **9c** with 4-chloro showed very good activity with IC<sub>50</sub> value 0.82  $\mu$ M and 13.02  $\mu$ M against A549 and MCF7 cancer cell lines respectively. Interestingly, changing position of halogen from *-para* to *-meta* in compound **9d** and **9e** resulted in drop of anticancer activity against A549 cell line. Compound **9d** with 3-fluoro group showed moderate activity with IC<sub>50</sub> value 9.16  $\mu$ M and 14.04  $\mu$ M, but compound **9e** showed very good anticancer activity against MCF7 cell line with IC<sub>50</sub> 84.8 nM, while moderate anticancer activity observed against A549 cell line. Further, replacement of aromatic ring with saturated nitrogen heterocycles such as pyrrolidine **9f** and piperidine **9g** resulted in compounds with moderate to very good activity against A549 cell line with IC<sub>50</sub> value 23.9  $\mu$ M and 5.06  $\mu$ M respectively. Against MCF7 cell line both compounds **9f** and **9g** showed

**Table 1.** Anticancer activity against A549 (Lungs cancer cell line), MCF7 (Breast cancer cell line) and anti-oxidant activity of compound **9a-g** and **10a-d**.

Compd no.	NR <sup>1</sup> R <sup>2</sup>	R <sup>3</sup>	A549 IC <sub>50</sub> <sup>a</sup>	MCF7 IC <sub>50</sub> <sup>a</sup>
9a		-CH <sub>3</sub>	2.40 $\mu$ M	0.65 $\mu$ M
9b		-CH <sub>3</sub>	0.16 nM	23.53 $\mu$ M
9c		-CH <sub>3</sub>	0.82 $\mu$ M	13.02 $\mu$ M
9d		-CH <sub>3</sub>	9.16 $\mu$ M	14.04 $\mu$ M
9e		-CH <sub>3</sub>	89.16 $\mu$ M	84.8 nM
9f		-CH <sub>3</sub>	23.9 $\mu$ M	3.08 $\mu$ M
9g		-CH <sub>3</sub>	5.06 $\mu$ M	1.11 $\mu$ M
10a		-OC <sub>2</sub> H <sub>5</sub>	NA	1.78 $\mu$ M
10b		-OC <sub>2</sub> H <sub>5</sub>	3.11 $\mu$ M	0.79 $\mu$ M
10c		-OC <sub>2</sub> H <sub>5</sub>	NA	NA
10d		-OC <sub>2</sub> H <sub>5</sub>	23.2 $\mu$ M	21.61 $\mu$ M
5-Fluoro-uracil			11.13 $\mu$ M	45.04 $\mu$ M

<sup>a</sup>IC<sub>50</sub> values were determined using Graph Pad Prism software by MTT assay using DMF. NA = Not active

**Table 2.** K<sub>b</sub> and K<sub>SV</sub> values for compound **9b** and **9e**.

Compd	$\lambda_{\text{max}}$ nm	K <sub>b</sub> (M <sup>-1</sup> ) UV based assay	Emission $\lambda_{\text{max}}$ nm	K <sub>SV</sub> (M <sup>-1</sup> ) Fluorescence assay
9b	359	2.64 x 10 <sup>4</sup>	609	4.69 x 10 <sup>3</sup>
9e	356	8.29 x 10 <sup>5</sup>	610	4.23 x 10 <sup>3</sup>

**Table 3.** Anti-oxidant activity of compounds **9a-e** and **10b-c**.

Compound no.	EC <sub>50</sub> $\mu$ g/mL <sup>a</sup>
9a	3436
9b	882
9d	48
9e	59
10b	46
10c	47
Ascorbic acid	11

<sup>a</sup>EC<sub>50</sub> values were determined using Graph Pad. Prism software by DPPH assay using DMF.

good activity with IC<sub>50</sub> value 3.08  $\mu$ M and 1.11  $\mu$ M respectively. Compounds **9a-9c**, **9g** and **10b** showed better anticancer activity in A549, while compounds **9a-g** and **10a-d** showed better activity in MCF7 compared to that of 5-Fluorouracil.

Compound **10a-10d** containing carboxylate group at third position of coumarin ring showed good to poor anticancer activity, compared to corresponding 3-acetyl coumarin analogues. Compound **10a** showed good activity against MCF7 cell line with  $IC_{50}$  1.78  $\mu$ M, however remain inactive against A549 cell line.

Carboxylate analogue of compound **9f** i.e compound **10b** showed good activity against both tested cell lines A549 and MCF7 with  $IC_{50}$  3.11  $\mu$ M and 0.79  $\mu$ M respectively. Compound **10c** remained inactive against both tested cell lines. However, morpholine analogue compound **10d** showed good activity against A549 and MCF7 cell lines. 5-Fluorouracil was used as standard and showed anticancer activity with  $IC_{50}$  45.04  $\mu$ M against MCF7 cell line

### Anticancer activity data from NCI-60

Structures of all compounds were submitted to Division of Cancer Treatment and Diagnosis, National Cancer Institute Bethesda, USA to be evaluated in the full panel of 60 different cell lines. Out of all two compounds, 2-[[3-acetyl-2-oxo-2H-chromen-7-yl]oxy]-N-(3-fluorophenyl)acetamide **9d** and ethyl 7-[2-(morpholin-4-yl)-2-oxoethoxy]-2-oxo-2H-chromene-3-carboxylate **10d** were selected for one dose analysis against 60 different cell lines. The growth inhibition (GI) was measured at the concentration of  $10^{-5}$  M.<sup>[32]</sup> The relative growth was evaluated from no drug control from time zero number of cell, NCI allows detection of both growth inhibition (value between 0 to 100) to cell lethality (value below zero). Compound **9d** showed anticancer activity against melanoma cell-lines including LOX-IMVI, UACC-62 and UACC-257 causing 41.38%, 23.23% and 9.15% cell death at  $10^{-5}$  M respectively. Whereas, showed no activity against ovarian cancer cell line and some cell lines of Breast cancer. Compound **10d** showed anticancer activity in prostate cancer cell line (DU145) with 34.74% cell death at  $10^{-5}$  M, but remained inactive against leukemia cancer cell line.

### DNA binding studies

Compounds **9b** and **9e** were selected for DNA-binding studies as they showed activity in nM concentration in MTT assay. For DNA binding UV based DNA titration and fluorescence emission study against DNA-EtBr complex were carried out as they provide more insight into mode of interaction of compounds with DNA.<sup>[21,33-34]</sup> UV absorption titrations for compounds **9b** and **9e** were performed with tris-HCl buffer (pH 7.2). The fixed concentration of compounds **9b** and **9e** were titrated against the known concentration of CT-DNA solution. Both the compounds showed good hypochromism shift (Figure 2a-2b). The strength of binding to CT-DNA was determined through the calculation of intrinsic binding constant  $K_b$  which is obtained by monitoring the changes in the absorbance of the compounds with increasing concentration of CT-DNA. Plot of  $[DNA]/(\epsilon_A - \epsilon_f)$  versus  $[DNA]$  (equation 1) is used to find out  $K_b$ .

$$[DNA]/(\epsilon_A - \epsilon_f) = [DNA]/(\epsilon_b - \epsilon_f) + 1/K_b(\epsilon_b - \epsilon_f) \quad (1)$$

Where  $[DNA]$  is the concentration of DNA,  $\epsilon_A = A_{\text{observed}}/[\text{compound}]$ ,  $\epsilon_f$  is the extinction coefficient for unbound compound and  $\epsilon_b$  is the extinction coefficient for the compound in the fully bound form. In plot of  $[DNA]/(\epsilon_A - \epsilon_f)$  versus  $[DNA]$ , slope is equal to  $1/(\epsilon_b - \epsilon_f)$  and Y-intercept is equal to  $1/K_b(\epsilon_b - \epsilon_f)$ .  $K_b$  is obtained from the ratio of slope to the Y-intercept (Figure 2c-2d).

Compounds **9b** and **9e** showed the hypochromism shift with the intrinsic binding values  $2.64 \times 10^4$  and  $8.29 \times 10^5$   $M^{-1}$  respectively in UV based DNA titrations which are indicative of DNA intercalative mode of binding (Table 2). To further confirm the mode of interaction of compounds **9b** and **9e** with DNA, fluorescence emission based Ethidium bromide (EtBr) displacement assay was carried out. The emission spectra of DNA-EtBr ( $\lambda_{\text{ex}} = 546$  nm) in the absence and presence of increasing amount of compounds were recorded (Figure 3a-3b). The data were plotted according to the Stern-Volmer equation (equation 2) where  $I_0$  and  $I$  are the fluorescence intensities in the absence and presence of compound.

$$I_0/I = 1 + K_{sv}[Q] \quad (2)$$

$K_{sv}$  is the Stern-Volmer quenching constant which can be obtained from the slope of straight line in plot of  $I_0/I$  versus  $[Q]$ . Quenching of fluorescence intensity was observed for compounds **9b** and **9e** with  $K_{sv}$   $4.69 \times 10^3$  and  $4.23 \times 10^3$   $M^{-1}$  respectively which supports the DNA intercalating property of these compounds (Table 2, Figure 3c-3d).

### Antioxidant activity

The drug which showed good anticancer activity have poor antioxidant activity which give emphasis that the anticancer activity may be due to reactive oxygen species.<sup>[35]</sup> Antioxidant activity of these entire synthesized compounds was screened by DPPH assay. Compounds which showed very good anticancer activity were found to be poor for antioxidant activity. Compounds **9a-9b** showed very poor antioxidant activity as compared to ascorbic acid (Table 3). Compounds **9d** and **9e** showed moderate anti-oxidant activity with  $EC_{50}$  48  $\mu$ g/mL and 59  $\mu$ g/mL respectively. Interestingly, 3-carboxylate coumarin compounds **10b** and **10c** showed good antioxidant activity with  $EC_{50}$  46 and 47  $\mu$ g/mL respectively. Compounds **9d-9e** and **10b-10c** showed scavenging activity similar to ascorbic acid at 100  $\mu$ M concentration. Compounds **9c, 9f, 9g, 10a** and **10d** remained inactive as antioxidant agent in DPPH assay.

### Conclusion

Our interest in synthesis of new 3,7-disubstituted coumarin derivatives is to develop more potent anticancer or antioxidant agents. All the newly synthesized compounds were obtained in good yields and characterized by spectral technique. Compounds **9a-9c, 9g** and **10b** showed better anticancer activity

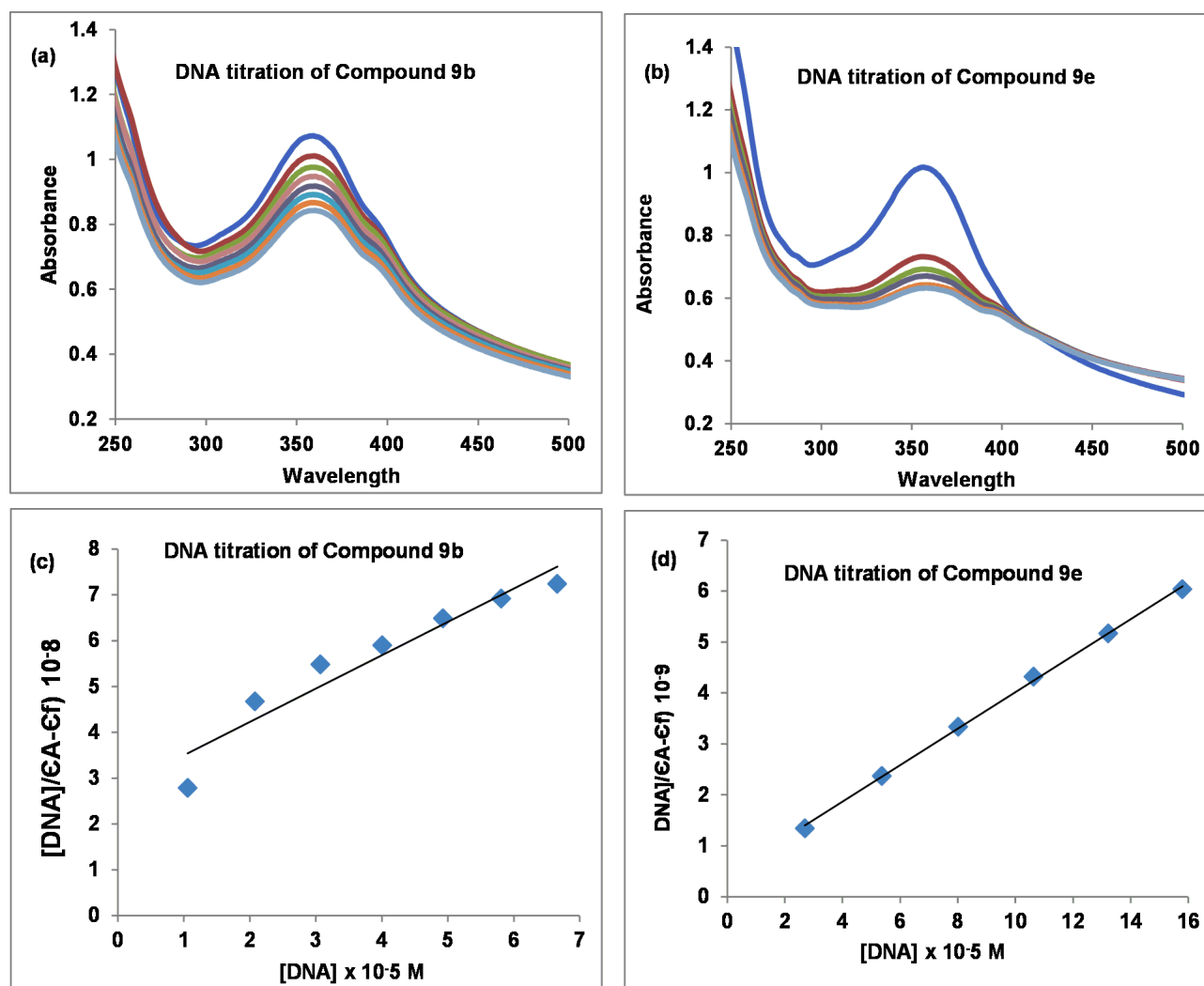


**Figure 2.** Titration plot of compounds **9b** and **9e** with DNA. Plot of Absorbance versus Wavelength (nm) for (a) compound **9b** and (b) compound **9e**. Plot of  $[DNA]/(\epsilon_A - \epsilon_f)$  versus  $[DNA]$  for (c) compound **9b** and (d) compound **9e**.

in A549 (Lungs cancer) cell line, while compounds **9a–g** and **10a–d** showed better activity in MCF7 (Breast cancer) cell line compared to that of 5-Fluorouracil.

Compounds **9b** and **9e** are showing excellent anticancer activity at very low concentration as compared to 5-Fluorouracil, well falling in nanomolar range. Both compounds **9b** and **9e** are exhibiting interaction with DNA through intercalation. The DNA interaction of compound **9e** is very good with intrinsic binding constant  $8.29 \times 10^5 \text{ M}^{-1}$  compared to that of compound **9b**  $2.64 \times 10^4 \text{ M}^{-1}$  in UV based DNA titration. Both compounds are showing good interaction with DNA by displacement of EtBr in DNA-EtBr complex by quenching its fluorescence. Further analysis is going on to confirm this finding that most of these derivatives also causing apoptosis in cancer cell line *via* p53 mediated induction of reactive oxygen species.

As per our target, structural modification of compound **3** was done to achieve more potent anticancer agent that has resulted in compound **9b** with excellent anticancer activity

against A549 cell line with  $IC_{50}$  0.16 nM. Thus strategy of modification of coumarin on 3<sup>rd</sup> position resulted in finding more active compound. Further work on identification of mechanism of anticancer activity is in progress.

### Acknowledgement

One of the authors (RS) is thankful to Department of Science & Technology, Government of India for financial support vide reference no. SR/WOS–A/CS-1028/2014 under Women Scientist Scheme to carry out this work. One of the authors (SU) is thankful to UGC, Government of India for UGC-JRF vide reference no. 22/06/2014(i)EU–V. Authors are thankful to The Head, Department of Chemistry and Department of Zoology, Faculty of Science, The M. S. University of Baroda for providing laboratory facilities and also thankful to DST-PURSE programme for X-ray single crystal analysis, Zydus Research Centre, Ahmedabad, for the ESI-MS analyses.

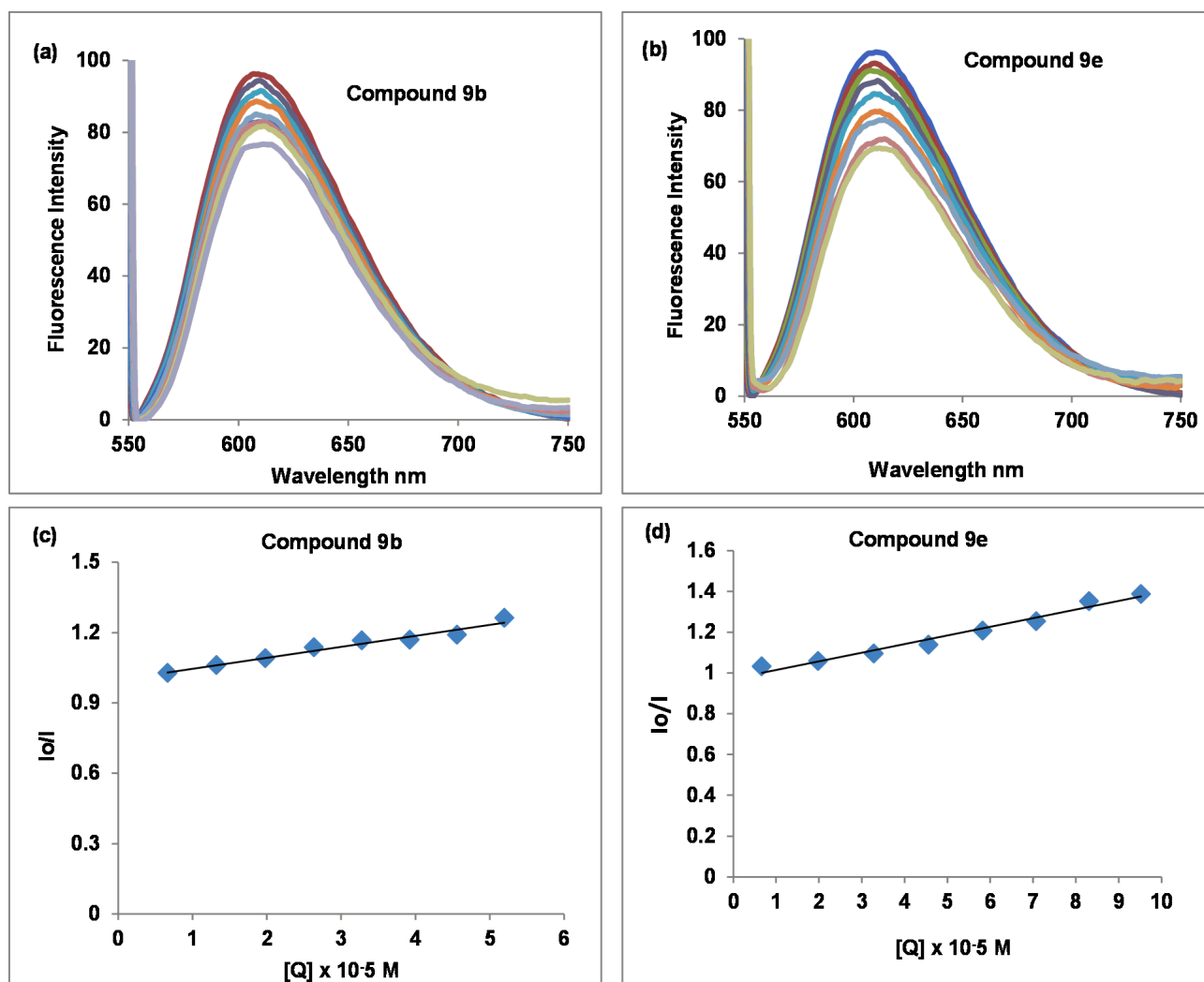


**Figure 3.** Plot of Fluorescence emission intensity  $I$  versus Wavelength (nm) for DNA-EtBr complex at different concentrations of (a) compound **9b** and (b) compound **9e**. Stern-Volmer quenching plot of DNA-EtBr for (c) compound **9b** and (d) compound **9e**.

## Conflict of Interest

The authors declare no conflict of interest.

**Keywords:** Anticancer · DNA Binding · Ethyl 7-substituted-3-carboxylate-benzopyrone · 7-Substituted-3-acetyl-benzopyrone

- [1] Cancer fact sheet No-297, World Health Organisation (2015) Feb 2015.
- [2] M. Mareel, A. Leroy, *Physiol. Rev.* **2003**, *83*, 337–376.
- [3] J. Wesche, K. Haglund, E. M. Haugsten, *Biochem. J.* **2011**, *437*, 199–213.
- [4] S. K. Grant, *Cell. Mol. Life Sci.* **2009**, *66*, 1163–1177.
- [5] G. I. Solyanik, *Exp. Oncol.* **2011**, *32*, 181–185.
- [6] S. Vijayaraghavalu, C. Peetla, S. Lu, V. Labhasetwar, *Mol. Pharm.* **2012**, *9*, 2730–2742.
- [7] H.-Y. Hung, E. Ohkoshi, M. Goto, K. F. Bastow, K. Nakagawa-Goto, K.-H. Lee, *J. Med. Chem.* **2012**, *55*, 5413–5424.
- [8] S. Riedl, D. Zweyck, K. Lohner, *Chem. Phys. Lipids* **2011**, *164*, 766–781.
- [9] Y. Bansal, P. Sethi, G. Bansal, *Med. Chem. Res.* **2013**, *22*, 3049–3060.
- [10] K. C. Fylaktakidou, D. J. Hadjipavlou-Litina, K. E. Litinas, D. N. Nicolaides, *Curr Pharm. Des.* **2004**, *10*, 3813–3833.
- [11] M. J. Matos, C. Terán, Y. Pérez-Castillo, E. Uriarte, L. Santana, D. Viña, *J. Med. Chem.* **2011**, *54*, 7127–7137.
- [12] A. Beillerot, J.-C. R. Dominguez, G. Kirsch, D. Bagrel, *Bioorg. Med. Chem. Lett.* **2008**, *18*, 1102–1105.
- [13] K. M. Amin, N. M. Abdel Gawad, D. E. Abdel Rahman, M. K. El Ashry, *Bioorg. Chem.* **2014**, *52*, 31–36.
- [14] M. Jain, W. R. Surin, A. Misra, P. Prakash, V. Singh, V. Khanna, S. Kumar, H. H. Siddiqui, K. Raj, M. K. Barthwal, *Chem. Biol. Drug Des.* **2013**, *81*, 499–505.
- [15] M. Curini, F. Epifano, F. Maltese, M. C. Marcotullio, S. P. Gonzales, J. C. Rodriguez, *Aust. J. Chem.* **2003**, *56*, 59–60.
- [16] J. R. Hwu, R. Singha, S. C. Hong, Y. H. Chang, A. R. Das, I. Vliegen, E. De Clercq, J. Neyts, *Antiviral Res.* **2008**, *77*, 157–162.
- [17] D. A. Ostrov, J. A. Hernandez Prada, P. E. Corsino, K. A. Finton, N. Le, T. C. Rowe, *Antimicrob. Agents Chemother.* **2007**, *51*, 3688–3698.
- [18] S. Emami, A. Foroumadi, M. A. Faramarzi, N. Samadi, *Arch. Pharm. Chem. Life Sci.* **2008**, *341*, 42–48.
- [19] A. Manvar, A. Bavishi, A. Radadiya, J. Patel, V. Vora, N. Dodia, K. Rawal, A. Shah, *Bioorg. Med. Chem. Lett.* **2011**, *21*, 4728–4731.
- [20] B. Yuce, O. Danis, A. Ogan, G. Sener, M. Bulut, A. Yarat, *Arzneim.-Forsch Drug Res.* **2009**, *59*, 129–134.
- [21] P. Bhattacharya, S. M. Mandal, A. Basak, *Eur. J. Org. Chem.* **2016**, 1439–1448.
- [22] D. Conley, E. M. Marshall, *Proc. Am. Assoc. Cancer Res.* **1987**, *28*, 63.

- [23] S. Emami, S. Dadashpour, *Eur. J. Med. Chem.* **2015**, *102*, 611–630.
- [24] J. T. Konc, E. Hejchman, H. Kruszewska, I. Wolska, D. Maciejewski, *Eur. J. Med. Chem.* **2011**, *46*, 2252–2263.
- [25] A. H. Halawa, A. A. E. Hassan, M. A. El-Nassag, M. M. A. El-Ail, G. E. El-Jaleel, E. M. Eliwa, A. H. Bedair, *Eur. J. Chem.* **2014**, *5*, 111–121.
- [26] V. Sosa, T. Moliné, R. Somoza, R. Paciucci, H. Kondoh, M. E. Lleornart, *Ageing Res Rev.* **2013**, *12*, 376–390.
- [27] S. Afzal, S. Jensen, J. Sørensen, T. Henriksen, A. Weimann, H. Poulsen, *Cancer Chemother. Pharmacol.* **2012**, *69*, 301–307.
- [28] J. Alexandre, Y. Hu, W. Lu, H. Pelicano, P. Huang, *Cancer Res.* **2007**, *67*, 3512–3517.
- [29] R. R. Nazarewicz, W. J. Zenebe, A. Parihar, S. K. Larson, E. Alidema, J. Choi, P. Ghafourifar, *Cancer Res.* **2007**, *67*, 1282–1290.
- [30] A. Thakur, R. Singla, V. Jaitak, *Eur. J. Med. Chem.* **2015**, *101*, 476–495.
- [31] Y. J. Li, C. Y. Wang, M. Y. Ye, G. Y. Yao, H. S. Wang, *Molecules* **2015**, *20*, 14791–14809.
- [32] For details: <http://dtp.nci.nih.gov> and <https://wiki.nci.nih.gov/display/NCIDTPdata/NCI-60+Growth+Inhibition+Data.html>
- [33] S. S. Mandal, U. Varshney, S. Bhattacharya, *Bioconjugate Chem.* **1997**, *8*, 798–812.
- [34] C. V. Kumar, E. H. Asunsion, *J. Am. Chem. Soc.* **1993**, *115*, 8547–8553
- [35] D. Dreher, A. F. Junod, *Eur. J. Cancer* **1996**, *32*, 30–38.

Submitted: September 20, 2016

Accepted: December 14, 2016

Rina Soni,<sup>a†</sup> Shweta Umar,<sup>b†</sup> Nirav N. Shah,<sup>a,c</sup> Suresh Balkrishnan,<sup>b</sup> and Shubhangi S. Soman<sup>a\*</sup>

<sup>a</sup>Department of Chemistry, Faculty of Science, The M. S. University of Baroda, Vadodara 390002, India

<sup>b</sup>Department of Zoology, Faculty of Science, The M. S. University of Baroda, Vadodara 390002, India

<sup>c</sup>GNFC, Bharuch, India

\*E-mail: shubhangiss@rediffmail.com

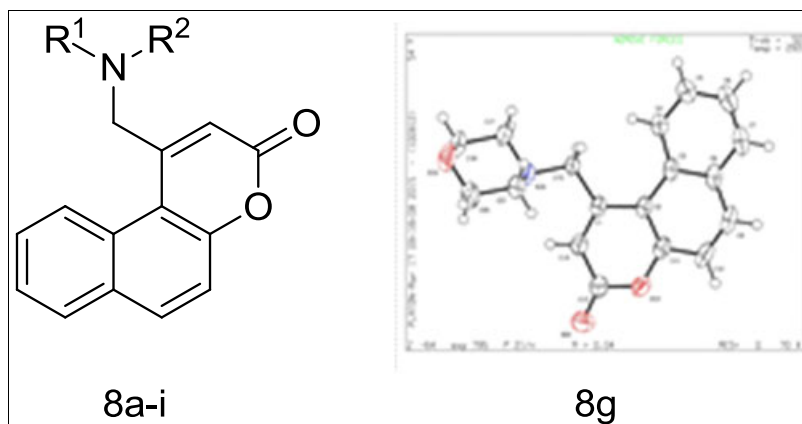
†Both authors contributed equally to this work.

Additional Supporting Information may be found in the online version of this article.

Received October 14, 2016

DOI 10.1002/jhet.2853

Published online 00 Month 2017 in Wiley Online Library (wileyonlinelibrary.com).



A series of substituted aminomethylbenzocoumarin derivatives **8a-i** have been synthesized, characterized, and structure of compound **8g** was confirmed by X-ray single crystal analysis. All the synthesized compounds were tested for their anticancer activity against cancer cell lines A549 (lung carcinoma cell line), MCF7 (breast cancer cell line), and A375 (melanoma cell line). Compounds **8a**, **8f**, and **8h** showed excellent growth inhibitory activity against all three cell lines, respectively. Compounds **8a** and **8f** were also found to be quite promising at very low concentration as an anticancer agent against MCF7 and A549 cell lines. Compounds **8g** and **8i** showed excellent antimitotic activity with  $IC_{50}$  0.32 and 19.98 nM for A549 cell line.

*J. Heterocyclic Chem.*, **00**, 00 (2017).

## INTRODUCTION

Coumarin, also known as benzopyrone, is a class of compound found in nature with wide range of applications. It falls under the flavonoid class of plant as a secondary metabolite and found as bioactive compounds in fruits, vegetables, spices, and herbs [1–4]. As coumarins are associated with low toxicity, considerable interest has been increased to find their beneficial effects on human health [1,5]. Coumarins naturally present in many plants showed interesting pharmacological properties like anticoagulant, antimicrobial, antioxidant, anti-inflammatory, and anti-allergic properties [6–8]. Recent studies have created interest in this class of compounds as they have shown diverse biological activities such as anti-human immunodeficiency virus, dyslipidemic, and anticancer [9–13].

Cell division and cell death is the essential requirement for the homeostatic balance of cell; any loss of this balance leads to many fatal diseases such as cancer. Cancer usually affects multiple targets simultaneously

and being the leading cause of death, requiring a great attention and adequate medication for its eradication. Available drug either fails to eliminate it completely or has very high side effect on resident cells. Therefore, more potent and drug-specific to only cancer cell is need of the day: hence, scientific researchers and commercial bodies are trying their best to discover anticancer drugs with good potency, safety, and selectivity.

As coumarins have ability to get bind either noncovalently or electrostatically to DNA through intercalation between the base pairs of DNA via major and minor groove through 3,4-position, therefore, it can be utilized for treating rapid proliferating cancer cells with certain modification [14–16].

Lee *et al.* reported a coumarin derivative neotanshinlactone **1**, (Fig. 1) with inhibition for two ER+ human breast cancer cell lines with 20-fold more potency compared with Tamoxifen [17]. Bariwal *et al.* reported 4-substituted coumarin derivatives as cytotoxic agents against MCF7 cell line [18]. 8-Methyl-4-substituted coumarin derivatives **2a** and **2b** (Fig. 1) showed very good

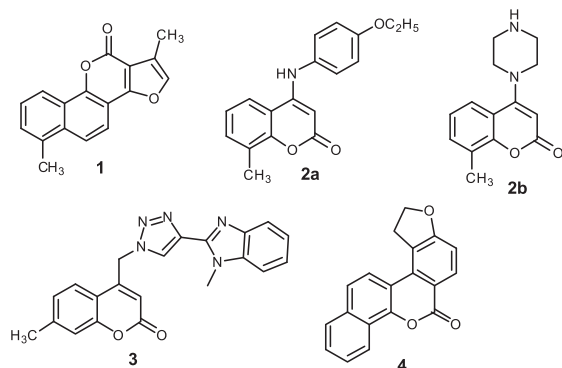


**Figure 1.** Some potent coumarin derivatives with anticancer activity.

potency as cytotoxic agents with  $IC_{50}$  value 6.25 and  $6.50 \mu M$  respectively against MCF7 breast cancer cell line.

Raić-Malić *et al.* reported triazole-based 4-substituted coumarin as cytotoxic agents. *N*-methyl benzimidazole derivative **3** showed very good cytotoxicity against HepG2 cell line with  $IC_{50}$   $0.9 \mu M$  [19]. Basak *et al.* synthesized 6H-benzo[*c*]chromen-6-one derivatives as DNA intercalating agents with moderately good activity [20]. Naphthyl derivative compound **4** (Fig. 1) induced maximum fluorescence quenching EB-DNA binding assay.

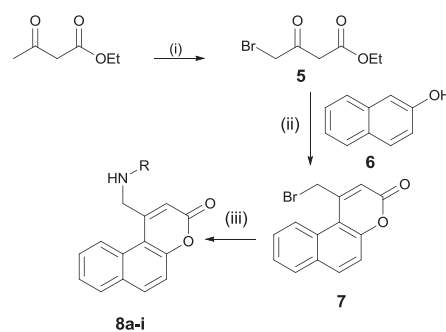
Synthetic coumarin derivatives have been reported with wide range of biological activities along with beneficial effects on human health [21–24]. Since coumarin moiety binds with DNA through 3,4-positions while extended benzene ring increases hydrophobicity and cytotoxicity, these new developments have encouraged us to design new 4-substituted aminomethyl coumarin derivatives that may increase binding ability with DNA along with extended aromatic ring that may increase cytotoxicity. On the basis of these facts and in continuation of our work on synthesis of coumarin derivatives as anticancer and antimicrobial agents [25–27], we have designed 4-aminomethyl substituted coumarin derivatives **8a–i** and report herein their synthesis, characterization, and anticancer activity.

## RESULTS AND DISCUSSION

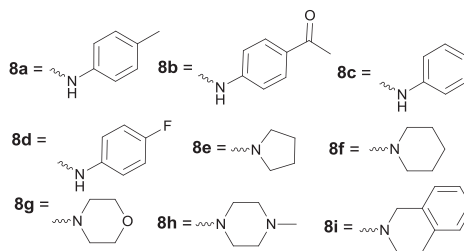
**Chemistry.** The 1-(substitutedaminomethyl)-3H-benzo[*f*]chromen-3-one **8a–i** (Scheme1) was synthesized by substitution reaction of 1-(bromomethyl)-3H-benzo[*f*]chromen-3-one **7** with different amines.

$\beta$ -Naphthol on Pechmann reaction with ethyl acetoacetate gave 1-methyl-3H-benzo[*f*]chrome-3-one. Allylic bromination of 1-methyl-3H-benzo[*f*]chrome-3-one using *N*-bromosuccinimide was failed to give desired product because of solubility problem of starting compound in  $CCl_4$ , when reaction was carried out in

**Scheme 1.** Synthesis of substituted aminomethyl naphthopyrone derivatives **8a–i**.



Reaction & Conditions: (i)  $Br_2$ ,  $0^\circ C$  to r.t. 18 h; (ii) **6**, Conc.  $H_2SO_4$ ,  $0^\circ C$  to r.t. 48 h; (iii) primary or secondary amine, TEA, DMF, r.t. 16 h.



$CHCl_3$  resulted in vinylic bromination instead of desired allylic bromination as reported [28].

In alternate approach, bromination of ethyl acetoacetate using  $Br_2$  gave ethyl 4-bromo-3-oxobutanoate **5** as a red oil [29]. Thus, obtained compound **5** was used as such for Pechmann reaction with  $\beta$ -naphthol **6** in conc.  $H_2SO_4$  to obtain 1-(bromomethyl)-3H-benzo[*f*]chromen-3-one **7** [30].  $^1H$ -NMR for compound **7** showed presence of singlet at  $\delta$  4.90 for two protons indicated presence of  $-CH_2Br$  group and all other aromatic protons appeared in the range of  $\delta$  6.6–8.5, thereby confirming the formation of **7**. This compound **7** was used to carry out substitution reaction with different amines using triethylamine in dimethylformamide (DMF) to form substituted aminomethyl naphthopyrone derivatives **8a–i**.

The infrared (IR) spectrum of compound **8a** exhibited strong band at  $3355 \text{ cm}^{-1}$  for the  $-NH$  proton, another strong band at  $1720 \text{ cm}^{-1}$  for lactone carbonyl group of coumarin ring. In the  $^1H$ -NMR spectrum of **8a**, all aromatic protons observed at  $\delta$  8.40–6.53. The methylene protons were observed as a doublet at  $\delta$  4.91 because of the coupling with the amine proton. In the  $^{13}C$ -NMR spectrum, the lactone carbonyl carbon of coumarin ring observed at  $\delta$  161, all aromatic carbons observed from  $\delta$  155–113, methylene carbon at  $\delta$  50, and methyl carbon at  $\delta$  20. In the electrospray ionization–mass spectrometry (ESI–MS) spectrum of **8a**, a peak at  $m/z$  315.8 for  $[M+H]^+$  confirmed its formation.

The structures of substituted aminomethyl naphthopyrones **8a–i** were confirmed by different

analytical techniques such as  $^1\text{H-NMR}$ ,  $^{13}\text{C-NMR}$ , IR, and ESI-MS. For compound **8g**, single crystal was developed by using system Pet. Ether: EtOAc (1:1) via slow evaporation of solvents for several days and studied its structure by X-ray single crystal analysis (Fig. 2a) (CCDC no. 1054564). Crystal data and structure refinement parameters for compound **8g** are given in Table 1. Crystal structure analysis of compound **8g** showed presence of such four molecules per unit cell (Fig. 2b), and pi-pi stacking observed along axis a with separation of 3.712 Å (Fig. 2c).

In general, the IR spectra of compounds **8a-i** exhibited one strong band in range of 1724–1711  $\text{cm}^{-1}$  for the lactone carbonyl group of coumarin ring. In the  $^1\text{H-NMR}$  spectra of **8a-i**, peak for the methylene protons observed in range of  $\delta$  approximately 5.01–3.91 depending on the effect of different amine substitution on it. All these new chemical entities were subjected to in vitro studies.

**Biological evaluation.** The 3-(4,5-dimethylthiazol-2-yl)-2,5-diphenyltetrazolium bromide (MTT) assay was

performed to screen test compounds **8a-i** (Table 2) for their activity against cancer cell lines, namely, A549 (lung cancer cell line), MCF7 (breast cancer cell line), and A375 (melanoma cell line).  $\text{IC}_{50}$  ( $\mu\text{M}$ ) values were determined using GRAPHPAD PRISM software (San Diego, CA) for compounds **8a-i**, and the results are presented in Table 2.

Results from MTT assay were used to assess the growth inhibitory effect of the various compounds on three types of cancer cell lines (A549, MCF7, and A375) and found that most of the compounds are active only in two cell lines viz. A549 and MCF7. Hence, we took forward the only two cell lines for further study with the compounds **8a**, **8f**, and **8h** as these compounds showed activity at lowest conc.  $\text{IC}_{50}$  values were calculated to determine the concentration of test compound at which 50% of the cells growth is inhibited.

From the MTT assay, it could be deduced that the compound **8a** worked better in all three cell lines as a growth inhibitor against A375 with  $\text{IC}_{50}$  4.29  $\mu\text{M}$ , MCF7

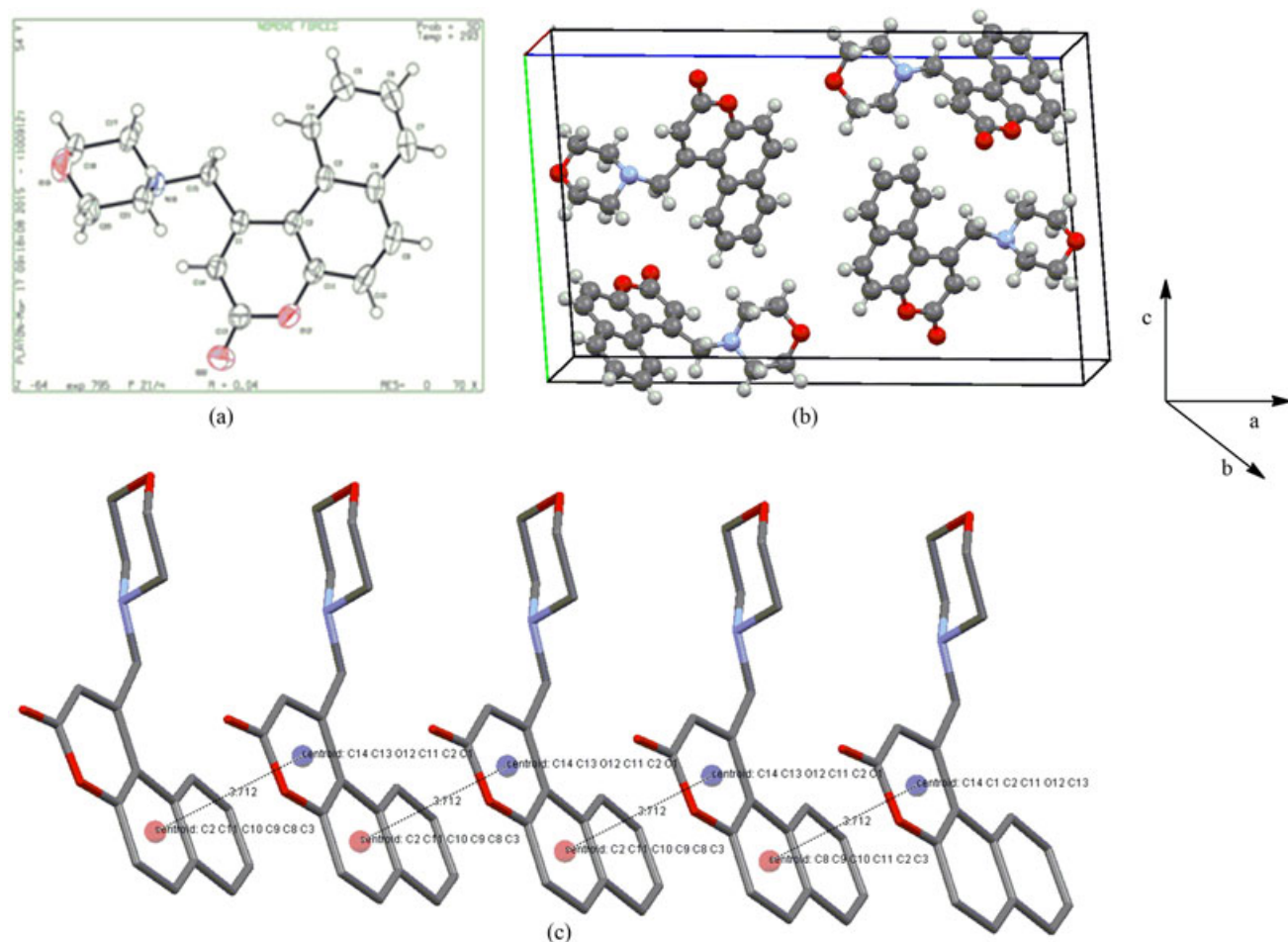


**Figure 2.** (a) X-ray crystal structure of compound **8g**; (b) molecular packing in unit cell; (c) pi-pi stacking in crystal structure. [Color figure can be viewed at [wileyonlinelibrary.com](http://wileyonlinelibrary.com)]

Table 1

Crystal data and structure refinement parameters for compound **8g**.

Chemical formula	C <sub>19</sub> H <sub>22</sub> NO <sub>3</sub>
Molecular weight	292.40
Crystal system	Monoclinic
Space group	P2 <sub>1</sub> /n
a/Å	4.5843(3)
b/Å	13.6007(10)
c/Å	22.9961(15)
α/°	90.00
β/°	95.429(6)
γ/°	90.00
V/Å <sup>3</sup>	1427.37(17)
Z	4
ρ <sub>calc</sub> /mg/mm <sup>3</sup>	1.361
Θ	6.96 to 58.02°
H	-5 to 5
k	-10 to 17
L	-30 to 28
Total reflections	7373
Independent reflections	3237
Used no. of reflections	3237
R <sup>a</sup>	0.0982
Absorption coefficient (m/Å)	0.082
R <sub>int</sub>	0.0153
Peak and hole	1.40 and -0.68 Å Å <sup>3</sup>

with IC<sub>50</sub> 5.17 μM, and A549 cell line with IC<sub>50</sub> 9.02 μM. When methyl substituent on aromatic ring was replaced by acetyl group in compound **8b**, it resulted in loss of activity against MCF7 cell line, but increased activity in A549 cell line with IC<sub>50</sub> value 2.32 μM. Replacement of methyl group with halogens, compound **8c** with -Cl, and compound **8d** with -F resulted in compounds with poor solubility in dimethyl sulfoxide (DMSO); hence, these compounds were screened against A549 cell line dissolved in DMF. However, both **8c** and **8d** were found ineffective as an anticancer agent against A549 cell line.

Replacement of aromatic amine with pyrrolidine ring as in compound **8e** showed good activity against A549 cancer cell line with IC<sub>50</sub> 6.20 μM, while no anticancer activity was observed when applied against MCF7 and A375 cell lines. Interestingly, piperidine substituted compound **8f** showed very good activity pattern against all tested cancer cell lines. Compound **8f** gave IC<sub>50</sub> 1.12 μM for A549 cell line and 0.83 μM for MCF7 cell line. Further, replacement of piperidine with *N*-methylpiperazine in compound **8h** resulted in very good growth inhibitory activity against A549 cancer cell line with IC<sub>50</sub> 0.74 μM, while good activity was observed against MCF7 and A375 cancer cell line with IC<sub>50</sub> 14.24 and 13.96 μM, respectively. On the other hand, replacement of piperidine moiety with morpholine in compound **8g** and tetrahydroisoquinoline in compound **8i** gave compounds with poor solubility in DMSO; hence, these compounds were screened against A549 cell line using DMF as diluent. Compound **8g** showed excellent antimitotic

activity with IC<sub>50</sub> 0.32 nM for A549 cell line; similarly, compound **8i** showed very good activity with IC<sub>50</sub> 19.98 nM. Compounds **8a** and **8f** showed promising inhibitory potential with IC<sub>50</sub> values falling in micromolar region and good solubility in DMSO; hence, these compounds further investigated for the lactic dehydrogenase (LDH) assay and ethidium bromide/acridine orange (ETBr/AO). The results are shown in Figure 3.

The release of cytosolic LDH enzyme has been used historically to understand the extent of plasma membrane damage that is a hallmark of necrotic cell death. The analysis of the results proved beyond doubt that the selected derivatives induced cell death in cancer cell lines via one of the innocuous mechanisms, namely, apoptosis rather than necrosis that used to inflame the surrounding cells and causes unwanted immunological inflammation. Compound **8f** showed much lower LDH release than **8a** in both the cell lines: however, a dose-dependent increase in membrane damage was noticed, and at higher concentration, these compounds exerted cytotoxicity via necrosis. Further, ETBr/AO assay, which is based on the morphological analysis of cell, confirmed the aforementioned results as shown in Figure 4. AO is a vital dye that stains both live and dead cells; however, ETBr stains only the cells that have lost the membrane integrity. Late apoptotic cells also incorporate ETBr and show condensed and often fragmented nuclei. Necrotic cells nevertheless stain red.

There are many mechanisms by which a compound induces cell death, and it has been reported that the several coumarin derivatives use reactive oxygen species (ROS)-mediated apoptotic pathway for inducing cytotoxicity. In order to understand the mechanism behind apoptosis by these compounds, intracellular ROS was measured using dichlorofluorescein diacetate fluorescence dye. The computational analyses of the images revealed that the intracellular ROS production in coumarin-treated cells was significantly higher compared with that of untreated control cells as shown in Figure 5.

Fluorescence is proportional to the ROS concentration in cell, treated cells were showing higher fluorescence than normal control, fluorescence intensity was analyzed using IMAGE J software (USA).

Therefore, it could be construed that the observed increase in ROS intermediates could be the reason for the induction of apoptosis in coumarin-treated cancer cell lines. It has been reported that the increased ROS production destabilizes the mitochondrial membrane and causes the cytochrome-C release; this in turn activates caspases and downregulate Bcl2 that ultimately leads to apoptosis [31].

It has been observed that when *p*-toluidine, piperidine, morpholine, and tetrahydroisoquinoline were used as substituents on fourth position of coumarin such as in

**Table 2**  
Anticancer activity of substituted aminomethyl naphthopyrones **8a-i**.

Compound	-NR <sup>1</sup> R <sup>2</sup>	IC <sub>50</sub> <sup>a</sup>			IC <sub>50</sub> <sup>b</sup>
		A549	MCF7	A375	A549
<b>8a</b>		4.29 μM	5.17 μM	9.02 μM	
<b>8b</b>		2.32 μM	47.80 μM	15.46 μM	
<b>8c</b>		NS	NS	NS	56.75 μM
<b>8d</b>		NS	NS	NS	59.14 μM
<b>8e</b>		6.20 μM	77.90 μM	84.45 μM	
<b>8f</b>		1.12 μM	0.83 μM	5.26 μM	
<b>8g</b>		NS	NS	NS	0.32 nM
<b>8h</b>		0.74 μM	14.24 μM	13.61 μM	
<b>8i</b>		NS	NS	NS	19.98 nM
<b>5-Fluorouracil</b>		11.13 μM	45.04 μM		

NS, Not soluble in DMSO.

<sup>a</sup>IC<sub>50</sub> values were determined using GRAPHPAD PRISM software by MTT assay using DMSO.

<sup>b</sup>IC<sub>50</sub> values were determined using GRAPHPAD PRISM software by MTT assay using DMF.

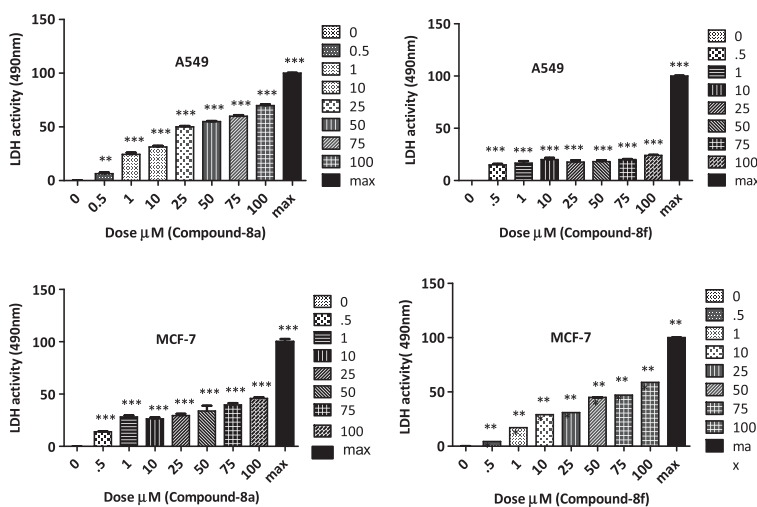


**Figure 3.** (a) Representation of cytosolic enzyme LDH in A549 cell line; activity of LDH in A549 cell line treated with different concentrations of compounds **8a** and **8f**. Graph plotted against LDH release versus dose. (\*\*\*)  $P \leq .001$ , (\*\*\*)  $p < .01$  significance one-way ANOVA (Tukey–Kramer). (b) Representation of cytosolic enzyme LDH in MCF7 cell line; activity of LDH in MCF7 cell line treated with different concentrations of compounds **8a** and **8f**. Graph plotted against LDH release versus dose. (\*\*\*)  $P \leq .001$ , (\*\*\*)  $p < .01$  significance one-way ANOVA (Tukey–Kramer). ANOVA, analysis of variance; LDH, lactic dehydrogenase

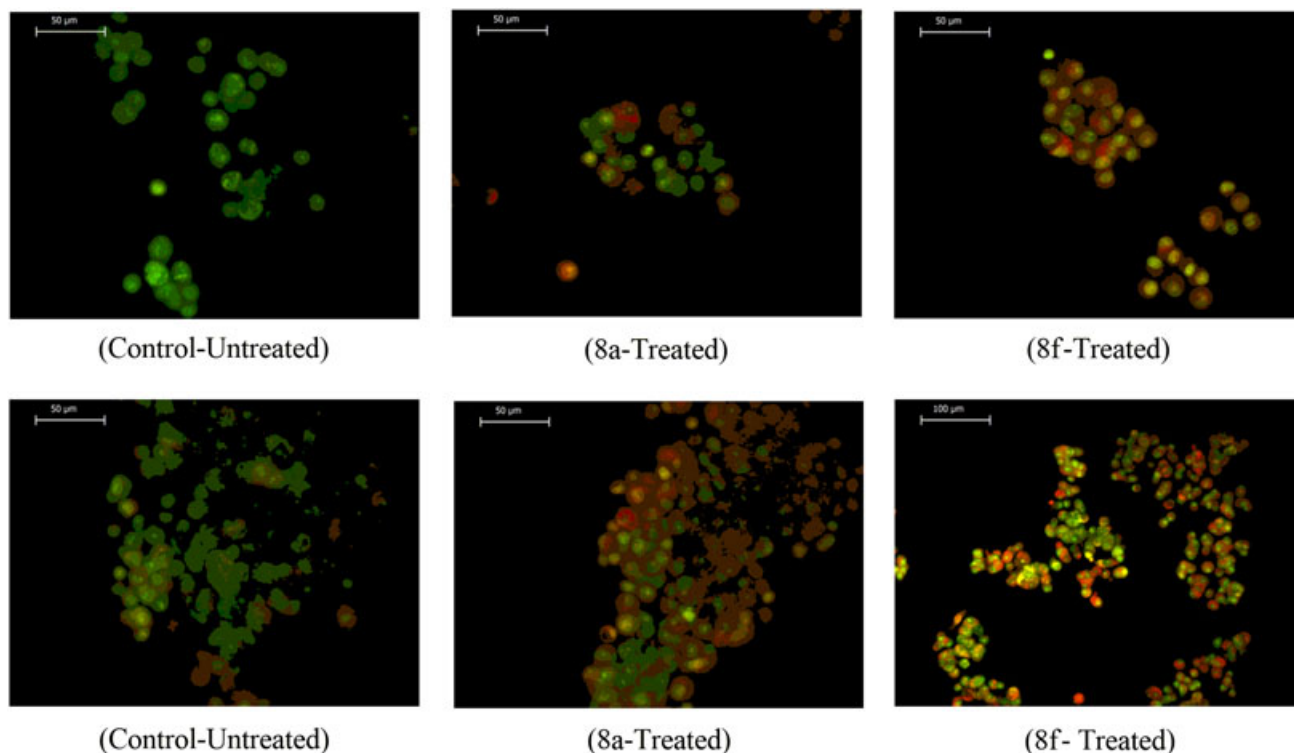


**Figure 4.** (a) Ethidium bromide/acridine orange staining: induction of apoptosis in A549 cell lines when treated with  $IC_{50}$  ( $\mu M$ ) concentration of compounds. (b) Ethidium bromide/acridine orange staining: induction of apoptosis in MCF7 cell lines when treated with  $IC_{50}$  ( $\mu M$ ) concentration of compounds. [Color figure can be viewed at [wileyonlinelibrary.com](#)]

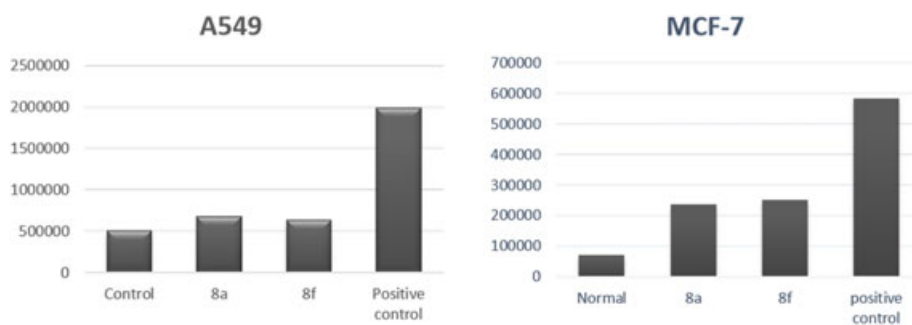


**Figure 5.** Representation of intracellular reactive oxygen species production in treated cell lines; reactive oxygen species production was measured using 2,7-dichlorodihydrofluorescein diacetate dye. [Color figure can be viewed at [wileyonlinelibrary.com](#)]

compounds **8a**, **8f**, **8g**, and **8i**, they showed very good anticancer activity compared with other substituents and even standard drug Fluorouracil. From the LDH assay, ETBr/AO assay, and intracellular ROS production assay, it can be concluded that these derivatives are responsible for apoptosis pathway for anticancer activity.

## CONCLUSION

In conclusion, we report here the design and synthesis of substituted aminomethyl naphthopyrone derivatives

**8a–8i** and their anticancer activity. Compounds **8a**, **8f**, and **8g** have shown promising anticancer activity against A549 (lung cancer cell line), MCF7 (breast cancer cell line), and A375 (melanoma cell line). Compound **8f** proved to be very good anticancer agent against A549 and MCF7 with  $IC_{50}$  values 1.12 and 0.83  $\mu M$ , respectively. Both compounds **8g** and **8i** tested against A375 have been excellent in checking cell growth with  $IC_{50}$  values of 0.32 and 19.98 nM, respectively, after solubilizing in DMF. From the LDH assay and ETBr/AO assay of compounds **8a** and **8f**, it could be deduced that the new coumarin derivatives,

studied here, exert their cytotoxic effect via apoptosis that is known to be less inflammatory to subsiding cells at a lower concentration by altering the redox homeostasis of cell.

## EXPERIMENTAL

**Chemistry.** Reagent grade chemicals and solvents were purchased from commercial supplier and used after purification. Thin-layer chromatography was performed on silica gel F254 plates (Merck & Co., Kenilworth, NJ, USA). Acme's silica gel (60–120 mesh) was used for column chromatographic purification. All reactions were carried out in nitrogen atmosphere. Melting points are uncorrected and were measured in open capillary tubes, using a Rolex melting point apparatus. IR spectra were recorded as KBr pellets on Perkin Elmer RX 1 spectrometer.  $^1\text{H-NMR}$  and  $^{13}\text{C-NMR}$  spectral data were recorded on Advance Bruker 400 spectrometer (400 MHz) with  $\text{CDCl}_3$  or  $\text{DMSO-d}_6$  as solvent and tetramethylsilane as internal standard.  $J$  values are in Hz. Mass spectra were determined by ESI-MS, using a Shimadzu LCMS 2020 apparatus (Shimadzu Scientific Instruments, Inc., USA). 2,7-dichlorodihydrofluorescein diacetate, MTT, ETBr, and AO were purchased from Sigma-Aldrich (St. Louis, MO, USA). DMSO, LDH assay kit (Thermo Scientific Pierce) and Dulbecco's modified Eagle's medium, fetal bovine serum, Penicillin–Streptomycin, trypsin–ethylene diamine tetraacetic acid obtained from G.

**Preparation of ethyl 4-bromo-3-oxobutanoate (5).** To an ice-cold solution of ethyl acetoacetate (25.24 mL), liquid bromine (10.25 mL) added dropwise over a period of 10–15 min. The resulting solution stirred at 0–5°C for 30 min and at room temperature for 24 h. The mixture thus obtained was diluted with ice-cold water and neutralized with saturated sodium bicarbonate ( $\text{Na}_2\text{CO}_3$ ) solution in saturated sodium chloride ( $\text{NaCl}$ ) solution. The organic layer separated, filtered through calcium chloride ( $\text{CaCl}_2$ ) to give reddish brown oil. The ethyl 4-bromo-3-oxobutanoate **5** thus obtained (25 g) used directly for the next step.

**Preparation of 1-(bromomethyl)-3H-benzof[f]chromen-3-one (7).** To an ice-cold solution of conc.  $\text{H}_2\text{SO}_4$  (30 mL), ethyl 4-bromo-3-oxobutanoate **5** (9 mL) was added slowly followed by portionwise addition of  $\beta$ -naphthol **6** (8.5 g) over a period of 10–15 min. Resulting mixture was stirred at room temperature for 48 h. The reaction mixture poured on crushed ice. The solid obtained was filtered and recrystallized from acetic acid to obtain compound **7** as golden yellow crystals. Yield: 79.81%; M.P: 180°C; IR (KBr): 3060, 1725, 1545, 1515, 1210, 1007, 928, 899, 825, 710  $\text{cm}^{-1}$ ;  $^1\text{H-NMR}$  (400 MHz,  $\text{CDCl}_3$ ): 4.90 (s, 2H), 6.66 (s, 1H), 7.51 (d,  $J = 9.2$  Hz, 1H), 7.61 (m, 1H), 7.63

(m, 1H), 7.97 (d,  $J = 9.2$  Hz, 1H), 8.05 (d,  $J = 8.8$  Hz, 1H), 8.54 (d,  $J = 8.4$  Hz, 1H);  $^{13}\text{C-NMR}$  (100 MHz,  $\text{CDCl}_3$ ): 32.73, 112.36, 117.89, 118.21, 125.35, 125.86, 128.54, 128.76, 129.89, 131.37, 134.46, 151.78, 155.34, 159.97; ESI-MS: 290.11[M+2] $^+$ , 287.63 [M] $^+$ .

**General procedure for the preparation of compounds (8a–8i).** 4-Bromomethylnaphthopyrone **7** (500 mg) dissolved in DMF (20–30 mL) and substituted amine (1.1 eq), along with base triethylamine (1.5 eq) was added to it. The resulting mixture was stirred at room temperature for 16 h and then poured into cold water. The aqueous layer thus obtained was extracted using ethyl acetate and/or dichloromethane (checked by TLC) and solvent evaporated to give crude product. The product thus, obtained was purified by column chromatography using pet ether:ethyl acetate.

**1-(*p*-Tolylamino) methyl)-3H-benzof[f]chromen-3-one (8a).** Yield: 38.95%; M.P:180°C; IR (KBr): 3859, 3616, 3355, 2840, 2384, 1779, 1720, 1617, 1550, 1519, 1447, 1399, 1373, 1333, 1300, 1256, 1195, 1130, 1089, 998, 925, 865, 821, 807, 779, 745, 640, 588  $\text{cm}^{-1}$ ;  $^1\text{H-NMR}$  (400 MHz,  $\text{CDCl}_3$ ):  $\delta$  2.26 (s, 3H), 4.23 (br s, 1H), 4.90 (d,  $J = 5.2$  Hz, 2H), 6.84 (s, 1H), 7.02 (d,  $J = 8.0$  Hz, 2H), 7.51 (d,  $J = 8.8$  Hz, 1H), 7.58 (m, 1H), 7.65 (m, 1H), 7.99 (m, 1H), 8.40 (d, 1H);  $^{13}\text{C-NMR}$  (100 MHz,  $\text{CDCl}_3$ ):  $\delta$  ppm 20.43, 49.72, 113.03, 113.55, 114.28, 117.93, 125.51, 125.60, 127.95, 128.28, 129.56, 129.88, 129.98, 131.41, 133.85, 144.23, 155.03, 160.68; ESI-MS: 315.8 [M] $^+$ ; Anal. Calcd for  $\text{C}_{21}\text{H}_{17}\text{NO}_2$ : C, 79.98; H, 5.43; N, 4.44. Found: C, 79.95; H, 5.45; N, 4.41%.

**1-(((4-Acetylphenyl)amino)methyl)-3H-benzof[f]chromen-3-one (8b).** Yield: 53.76%; M.P: 194°C; IR (KBr): 3069, 2969, 2784, 1724, 1676, 1560, 1549, 1458, 1342, 1302, 1269, 1236, 1190, 1149, 987, 919, 858, 825, 738  $\text{cm}^{-1}$ ;  $^1\text{H-NMR}$  (400 MHz,  $\text{CDCl}_3$ ): 2.40 (s, 3H), 5.05 (d,  $J = 5.3$  Hz, 2H), 6.50 (s, 1H), 6.67 (d,  $J = 8.6$  Hz, 2H), 7.39 (t,  $J = 5.3$  Hz, 1H), 7.65–7.60 (m, 2H), 7.70 (d,  $J = 7.2$  Hz, 1H), 7.74 (d,  $J = 8.6$  Hz, 2H), 8.11 (d,  $J = 8.0$  Hz, 1H), 8.25 (d,  $J = 8.8$  Hz, 1H), 8.51 (d,  $J = 8.8$  Hz, 1H);  $^{13}\text{C-NMR}$  (100 MHz,  $\text{CDCl}_3$ ):  $\delta$  ppm 26.43, 47.68, 111.77, 112.97, 113.73, 117.98, 126.14, 126.42, 126.64, 128.82, 129.51, 130.10, 131.02, 131.51, 134.65, 152.26, 154.85, 155.94, 160.00, 195.74; ESI-MS: 342 [M–1] $^+$ ; Anal. Calcd for  $\text{C}_{22}\text{H}_{17}\text{NO}_3$ : C, 76.95; H, 4.99; N, 4.08. Found: C, 76.99; H, 4.95; N, 4.09%.

**1-(((4-Chlorophenyl)amino)methyl)-3H-benzof[f]chromen-3-one (8c).** Yield: 42%; M.P:195°C; IR (KBr): 3365, 1692, 1602, 1550, 1506, 1446, 1335, 1270, 1088, 1002, 819, 749  $\text{cm}^{-1}$ ;  $^1\text{H-NMR}$  (400 MHz,  $\text{CDCl}_3$ ):  $\delta$  4.84 (d,  $J = 5.3$  Hz, 2H), 6.22 (t,  $J = 5.3$  Hz 1H), 6.44 (d,  $J = 8.8$  Hz, 2H), 6.61 (s, 1H), 6.96 (d,  $J = 8.8$  Hz, 2H), 7.42 (d,  $J = 8.8$  Hz, 2H), 7.50 (t,  $J = 7.4$  Hz, 1H), 7.14 (m, 1H), 7.91 (d,  $J = 8.0$  Hz, 1H), 8.00

(d,  $J = 9.2$  Hz, 1H), 8.33 (d,  $J = 8.4$  Hz, 1H);  $^{13}\text{C-NMR}$  (100 MHz,  $\text{CDCl}_3$ ):  $\delta$  ppm 53.51, 117.81, 118.41, 118.53, 122.44, 126.06, 130.47, 130.59, 133.15, 133.72, 134.28, 134.66, 136.14, 138.84, 150.96, 159.54, 160.52, 165.28; ESI-MS: 336.8  $[\text{M}+1]^+$ ; *Anal.* Calcd for  $\text{C}_{20}\text{H}_{14}\text{ClNO}_2$ : C, 71.54; H, 4.20; N, 4.17. Found: C, 71.52; H, 4.18; N, 4.15%.

**1-((4-Fluorophenylamino)methyl)-3H-benzof[chromen]-3-one (8d).** Yield: 54%; M.P: 175°C; IR (KBr): 3369, 2897, 1690, 1550, 1515, 1447, 1336, 1223, 1212, 1002, 818, 746  $\text{cm}^{-1}$ ;  $^1\text{H-NMR}$  (400 MHz,  $\text{CDCl}_3$ ):  $\delta$  4.10 (d,  $J = 5.2$  Hz, 2H), 5.52 (br t, 1H), 5.75–5.76 (m, 2H), 5.85 (s, 1H), 6.04–6.08 (m, 2H), 6.73 (d,  $J = 8.8$  Hz, 1H), 6.80 (t,  $J = 7.4$  Hz, 1H), 6.88 (t,  $J = 7.4$  Hz, 1H), 7.24 (d,  $J = 8.0$  Hz, 1H), 7.36 (d,  $J = 9.2$  Hz, 1H), 7.66 (d,  $J = 8.4$  Hz, 1H);  $^{13}\text{C-NMR}$  (100 MHz,  $\text{CDCl}_3$ ):  $\delta$  ppm 43.54, 107.49, 107.84, 108.26, 110.11, 110.33, 112.25, 120.39, 120.70, 123.07, 124.03, 124.48, 125.93, 128.81, 138.78, 149.26, 150.88, 154.88; ESI-MS: 320.2  $[\text{M}+1]^+$ ; *Anal.* Calcd for  $\text{C}_{20}\text{H}_{14}\text{FNO}_2$ : C, 75.22; H, 4.42; N, 4.39. Found: C, 75.19; H, 4.39; N, 4.40%.

**1-(Pyrrolidin-1-ylmethyl)-3H-benzof[chromen]-3-one (8e).** Yield: 27.63%; M.P: 128°C; IR (KBr): 3068, 2966, 2784, 1724, 1676, 1654, 1560, 1549, 1518, 1458, 1342, 1236, 1190, 1149, 1112, 987, 919, 858, 825, 738  $\text{cm}^{-1}$ ;  $^1\text{H-NMR}$  (400 MHz,  $\text{CDCl}_3$ ): 1.86 (br s, 4H), 2.73 (br s, 4H), 4.10 (s, 2H), 6.79 (s, 1H), 7.47 (d,  $J = 8.8$  Hz, 1H), 7.55 (t,  $J = 7.5$  Hz, 1H), 7.65 (t,  $J = 7.5$  Hz, 1H), 7.90 (d,  $J = 8.0$  Hz, 1H), 7.97 (d,  $J = 8.8$  Hz, 1H), 8.66 (d,  $J = 8.8$  Hz, 1H);  $^{13}\text{C-NMR}$  (100 MHz,  $\text{CDCl}_3$ ):  $\delta$  ppm 23.72, 54.04, 60.76, 114.38, 115.97, 117.76, 125.49, 126.52, 127.79, 129.36, 129.76, 131.28, 133.54, 154.84, 154.86, 160.96; ESI-MS: 279.9  $[\text{M}+\text{H}]^+$ ; *Anal.* Calcd for  $\text{C}_{18}\text{H}_{17}\text{NO}_2$ : C, 77.40; H 6.13; N, 5.01. Found: C, 77.37; H, 6.09; N, 4.98%.

**1-(Piperidine-1-ylmethyl)-3H-benzof[chromen]-3-one (8f).** Yield: 57.7%; M.P: 138°C; IR (KBr): 3056, 2924, 2838, 2809, 2764, 1711, 1646, 1570, 1516, 1453, 1403, 1373, 1334, 1270, 1236, 1190, 1129, 1108, 1037, 996, 927, 885, 810, 740, 673, 609, 571;  $^1\text{H-NMR}$  (400 MHz,  $\text{CDCl}_3$ ):  $\delta$  ppm 1.51 (br s, 2H), 1.65 (m, 4H), 2.59 (m, 4H), 3.91 (s, 2H), 6.84 (s, 1H), 7.48 (d,  $J = 8.8$  Hz, 1H), 7.56 (m, 1H), 7.65 (m, 1H), 7.91 (m, 1H), 7.97 (d,  $J = 8.8$  Hz, 1H), 8.67 (d,  $J = 8.8$  Hz, 1H);  $^{13}\text{C-NMR}$  (100 MHz,  $\text{CDCl}_3$ ):  $\delta$  ppm 24.02, 26.02, 54.68, 63.70, 114.60, 116.15, 117.76, 125.48, 126.64, 127.65, 129.34, 129.77, 131.27, 133.50, 154.23, 154.86, 160.9; ESI-MS: 293.20  $[\text{M}]^+$ ; *Anal.* Calcd for  $\text{C}_{19}\text{H}_{19}\text{NO}_2$ : C, 77.79; H, 6.53; N, 4.77. Found: C, 77.63; H, 6.43; N, 4.61%.

**1-(Morpholinomethyl)-3H-benzof[chromen]-3-one (8g).** Yield: 57.35%; M.P: 186°C; IR (KBr): 3059, 2955, 2887, 2839, 1712, 1623, 1549, 1515, 1454, 1428, 1373,

1315, 1250, 1192, 1113, 1000, 911, 883, 861, 817, 738  $\text{cm}^{-1}$ ;  $^1\text{H-NMR}$  (400 MHz,  $\text{CDCl}_3$ ): 2.67 (br s, 4H), 3.78 (br s, 4H), 3.99 (s, 2H), 6.84 (s, 1H), 7.56 (s, 1H), 7.59 (m, 1H), 7.66 (m, 1H), 7.92–7.94 (m, 1H), 7.98 (d,  $J = 8.8$  Hz, 1H), 8.59 (d,  $J = 8.8$  Hz, 1H);  $^{13}\text{C-NMR}$  (100 MHz,  $\text{CDCl}_3$ ):  $\delta$  ppm 53.61, 63.16, 66.91, 114.30, 116.27, 117.77, 125.59, 126.25, 127.77, 129.49, 129.61, 131.29, 133.74, 152.98, 154.96, 160.67; ESI-MS: 294.88  $[\text{M}]^+$ ; *Anal.* Calcd for  $\text{C}_{18}\text{H}_{17}\text{NO}_3$ : C, 73.20; H, 5.80; N, 4.74. Found: C, 73.09; H, 5.72; N, 4.68%. For compound **8g**, single crystal was developed by using system Pet. Ether: EtOAc (1:1) via slow evaporation of solvents for several days and studied its structure by X-ray single crystal analysis (Fig. 2a) (CCDC no. 1054564).

**1-((4-Methylpiperazin-1-yl)methyl)-3H-benzof[chromen]-3-one (8h).** Yield: 41.97%; M.P: 124°C; IR (KBr): 3859, 3843, 3444, 3054, 2931, 2836, 2790, 2755, 2700, 2363, 1713, 1621, 1550, 1517, 1455, 1375, 1285, 1193, 1137, 1015, 999, 985, 887, 812, 777, 742, 674, 591, 573  $\text{cm}^{-1}$ ;  $^1\text{H-NMR}$  (400 MHz,  $\text{CDCl}_3$ ):  $\delta$  ppm 2.32 (s, 3H), 2.53 (br s, 4H), 2.71 (brs, 4H), 3.98 (s, 2H), 6.84 (s, 1H), 7.48 (d,  $J = 8.8$  Hz, 1H), 7.54–7.58 (m, 1H), 7.65 (m, 1H); 7.91 (d,  $J = 8.0$  Hz, 1H), 7.97 (d,  $J = 8.8$  Hz, 1H), 8.59 (d,  $J = 8.8$  Hz, 1H);  $^{13}\text{C-NMR}$  (100 MHz,  $\text{CDCl}_3$ ):  $\delta$  ppm 46.01, 53.015, 55.04, 62.73, 114.42, 116.23, 117.77, 125.54, 126.40, 127.75, 129.42, 129.67, 131.28, 133.64, 153.51, 154.91, 160.78; ESI-MS: 308.75  $[\text{M}]^+$ ; *Anal.* Calcd for  $\text{C}_{19}\text{H}_{20}\text{N}_2\text{O}_2$ : C, 74.00; H, 6.54; N, 9.08. Found: C, 73.96; H, 6.57; N, 9.05%.

**1-((3,4-Dihydroisoquinolin-2(1H)-yl)methyl)-3H-benzof[chromen]-3-one (8i).** Yield: 48.57%; M.P: 172°C; IR (KBr): 3022, 2908, 2828, 2799, 1713, 1645, 1570, 1552, 1532, 1452, 1426, 1336, 1268, 1194, 1130, 1095, 1054, 1000, 930, 883, 855, 813, 780, 739  $\text{cm}^{-1}$ ;  $^1\text{H-NMR}$  (400 MHz,  $\text{CDCl}_3$ ): 2.99 (s, 4H), 3.87 (s, 2H), 4.10 (s, 2H), 6.90 (s, 1H), 7.06 (m, 1H), 7.16 (m, 3H), 7.51, (d,  $J = 8.8$  Hz, 1H); 7.52–7.58 (m, 1H), 7.63–7.67 (m, 1H) 7.91 (d, 1H), 8.1 (d, 1H), 8.7 (d, 1H);  $^{13}\text{C-NMR}$  (100 MHz,  $\text{CDCl}_3$ ):  $\delta$  ppm 29.21, 51.01, 55.90, 62.84, 125.55, 125.82, 126.41, 126.56, 127.83, 128.73, 129.44, 129.71, 131, 133, 134.08, 134.12, 153, 155, 160; ESI-MS: 342.1  $[\text{M}+\text{H}]^+$ ; *Anal.* Calcd for  $\text{C}_{23}\text{H}_{19}\text{NO}_2$ : C, 80.92; H, 5.61; N, 4.10. Found: C, 80.89; H, 5.58; N, 4.13%.

**Biological activity screening. 3-(4,5-Dimethylthiazol-2-yl)-2,5-diphenyltetrazolium bromide assay.** The compounds were tested for their cytotoxic potential on three types of cancer cells, namely, A549 (lung cancer cell line), MCF7 (breast cancer cell line), and A375 (melanoma cell line). The MTT assay was used to determine the effect of each compound on the proliferation of cancer cells. A549, MCF7, and A375 cultures were purchased from

National Centre for Cell Science, Pune, India. All growth media, supplements, and reagents were purchased from HiMedia Labs, Mumbai, India. For the assay, cells were seeded at  $10^5$  cells/mL in a 96-well plate in Dulbecco's modified minimum essential medium supplemented with 10% fetal bovine serum. To each well, test compound was added at six different concentrations of 100, 50, 10, 5, 1, and 0.5  $\mu$ M. Each concentration was tested in triplicates. The cells were incubated with these compounds at 37°C under 5% CO<sub>2</sub> for 48 h. Following this, MTT was added to each well at a final concentration of 0.5 mg/mL. Cells were incubated with this tetrazolium dye for 4 h. Subsequently, purple crystals of formazan were observed in each well, formed as a metabolic product of MTT. These crystals were dissolved in Isopropanol, and the absorbance in each well was recorded at 570 nm in a microplate reader (Metertech Sigma 360). Absorbance at 570 nm directly correlates with cell viability. IC<sub>50</sub> ( $\mu$ M) values were determined using GRAPHPAD PRISM software.

**Lactate dehydrogenase assay.** Cytotoxicity was assayed by measuring the activity of cytosolic enzyme LDH that released into culture medium when plasma membrane damage occurs because of necrosis [32]. Cells were seeded on 96-well plate ( $1 \times 10^6$  cells/mL) and allowed to attach for overnight; the next day, cells were treated with various concentrations (0.5, 1, 10, 25, 50, 75, 100  $\mu$ M) of coumarin derivatives and incubated for 48 h. LDH activity was measured using manufacturer's protocol (Pierce LDH Cytotoxicity Assay Kit). Absorbance was measured at 490 nm, and background was measured at 680 nm. % LDH release was measured using manufacturer's formula.

**Acridine orange/ethidium bromide dual staining.** Morphological analysis of apoptosis and necrosis was performed using ETBr/AO staining [33]. Cells were plated on 6-well plate and treated with IC<sub>50</sub> conc for 48 h. A ratio of 1:1 of AO and ETBr (100  $\mu$ g/mL in PBS) was prepared; 25  $\mu$ L of cell suspension ( $1-2 \times 10^5$  cells/mL) was incubated for 1 min with 1  $\mu$ L of AO/ETBr. Cell suspension of 10  $\mu$ L was placed on microscopic slide, and image was taken by fluorescent microscope at 40 $\times$  (Leica DM2500, LAS EZ V1.6.0 software).

**Dichlorofluorescein diacetate staining.** Intracellular ROS production was measured with 2',7'-dichlorodihydrofluorescein diacetate (H<sub>2</sub>-DCFDA; Sigma-Aldrich). For this, cells were plated on 6-well plate ( $1 \times 10^5$  cells/well) and incubated with IC<sub>50</sub> concentration of derivatives; after 48 h of incubation, cells were trypsinized, and 10  $\mu$ M of H<sub>2</sub>-DCFDA was added, washed with PBS, and incubated: after 30 min, cell suspension was placed on microscopic slide, and image was evaluated, from fluorescent microscope (Leica

DM2500, LAS EZ V1.6.0 software). For positive control, H<sub>2</sub>O<sub>2</sub> treatment was given.

**Acknowledgments.** One of the authors (R.S.) is thankful to the Department of Science & Technology, Government of India, for financial support vide reference no. SR/WOS-A/CS-1028/2014 under Women Scientist Scheme to carry out this work. One of the authors (S.U.) is thankful to UGC, Government of India, for UGC-JRF vide reference no. 22/06/2014(i)EU-V. Authors are thankful to The Head, Department of Chemistry and Department of Zoology Faculty of Science, The M. S. University of Baroda for providing laboratory facilities, Zydus Research Centre, Ahmedabad, for the ESI-MS analyses, DST-PURSE for X-Ray crystallography facility. One of the author N.N.S. is thankful to M/S GNFC LTD for kind support.

## REFERENCES AND NOTES

- [1] Kennedy, R. O.; Thorne, R. D. *Coumarins. Biology, Applications and Mode of Action*; Wiley: New York, 1997.
- [2] Almeida, I. M.; Barreira, J. C.; Oliveira, M. B.; Ferreira, I. C. *Food Chem Toxicol* 2011, 49, 3232.
- [3] Barros, L.; Duenas, M.; Carvalho, A. M.; Ferreira, I. C.; Santos-Buelga, C. *Food Chem Toxicol* 2012, 50, 1576.
- [4] Pinela, J.; Barros, L.; Carvalho, A. M.; Ferreira, I. C. *Food Chem Toxicol* 2012, 50, 829.
- [5] Hoult, J. R. S.; Paya, M. *Gen Pharmacol* 1996, 27, 713.
- [6] Kidane, A. G.; Salacinski, H.; Tiwari, A.; Bruckdorfer, K. R.; Seifalian, A. M. *Biomacromolecules* 2004, 5, 798.
- [7] Cheng, J. H.; Hung, C. F.; Yang, S. C.; Wang, J. P.; Won, S. J.; Lin, C. N. *Bioorg Med Chem* 2008, 16, 7270.
- [8] Ma, T.; Liu, L.; Xue, H.; Li, L.; Han, C.; Wang, L.; Chen, Z.; Liu, G. *J Med Chem* 2008, 51, 1432.
- [9] Sashidhara, K. V.; Rosaiah, J. N.; Kumar, A.; Bhatia, G.; Khanna, A. K. *Bioorg Med Chem Lett* 2010, 20, 3065.
- [10] Wang, X.; Nakagawa-Goto, K.; Bastow, K. F.; Don, M. -J.; Lin, Y. -L.; Wu, T.-S.; Lee, K.-H. *J Med Chem* 2006, 49, 5631.
- [11] Myers, R. B.; Parker, M.; Grizzle, W. E. *J Cancer Res Clin Oncol* 1994, 12, 11.
- [12] Yacquot, Y.; Belmont, L.; Giorgi, H.; Refouvet, B.; Adessi, G.; Daubrosse, E.; Xicluna, A. *Eur J Med Chem* 2001, 36, 127.
- [13] Gibbs, J. B. *Science* 2000, 287, 1969.
- [14] Paul, A.; Bhattacharya, S. *Curr Sci* 2012, 102, 212.
- [15] Wood, A. W.; Huang, M.-T.; Chang, R. L.; Newmark, H. L.; Lehr, R. E.; Yagi, H.; Sayer, J. M.; Jerina, D. M.; Conney, A. H. *Proc Natl Acad Sci U S A* 1982, 79, 5513.
- [16] Li, Y. J.; Wang, C. Y.; Ye, M. Y.; Yao, G. Y.; Wang, H. S. *Molecules* 2015, 20, 14791.
- [17] Dong, Y.; Shi, Q.; Liu, Y.-N.; Wang, X.; Bastow, K. F.; Lee, K.-H. *J Med Chem* 2009, 52, 3586.
- [18] Kaur, P.; Gill, R. K.; Singh, G.; Bariwal, J. *J Heterocyclic Chem* 2016, 53, 1519.
- [19] Kraljević, T. G.; Harej, A.; Sedić, M.; Pavelić, S. K.; Stepanić, V.; Drenjančević, D.; Talapko, J.; Raić-Malić, S. *Eur J Med Chem* 2016, 124, 794.
- [20] Bhattacharya, P.; Mandal, S. M.; Basak, A. *Eur J Org Chem* 2016 1439.
- [21] Chen, Z.; Bi, J.; Su, W. *Chin J Chem* 2013, 31, 507.
- [22] Manidhar, D. M.; Kesharwani, R. K.; Reddy, B. N.; Reddy, S. C.; Misra, K. *Med Chem Res* 2013, 22, 4146.
- [23] Nasr, T.; Bondock, S.; Youns, M. *Eur J Med Chem* 2014, 76, 539.

- [24] Dandriyal, J.; Singla, R.; Kumar, M.; Jaitak, V. *Eur J Med Chem* 2016, 119, 141.
- [25] Soni, J. N.; Soman, S. S. *Eur J Med Chem* 2014, 75, 77.
- [26] Soman, S. S.; Soni, J. N.; Inamdar, G. S.; Robertson, G. P. *Der Pharma Chemica* 2013, 5, 201.
- [27] Soman, S. S.; Thaker, T. H. *Med Chem Res* 2013, 22, 4223.
- [28] Soman, S. S.; Thaker, T. H. *J Chem Res* 2010, 34, 502.
- [29] Sousa, C. M.; Berthet, J.; Delbaere, S.; Coelho, P. J. *J Org Chem* 2012, 77, 3959.
- [30] Dey, B. B.; Sankaranarayan, Y. *J Ind Chem Soc* 1934, 11, 687.
- [31] Chuang, J. Y.; Huang, Y. F.; Lu, H. F.; Ho, H. C.; Yang, J. S.; Li, T. M.; Chang, N. W.; Chung, J. G. *In Vivo* 2007, 21, 1003.
- [32] Danpure, C. I. *Cell Biochem* 1984, 72, 144.
- [33] Kasibhatla, S.; Amarante-Mendes, G. P.; Finucane, D.; Brunner, T.; Bossy-Wetzels, E.; Green, D. R. *Cold Spring Harb Protoc* 2006 3.



UNIVERSITY AND INSTITUTE  
OF ADVANCED RESEARCH  
THE PURI FOUNDATION FOR EDUCATION IN INDIA

**NATIONAL SYMPOSIUM ON  
CURRENT RESEARCH IN CANCER BIOLOGY & THERAPY**

School of Biological Sciences and Biotechnology

UIAR, Koba, Gandhinagar, Gujarat

7<sup>th</sup>-8<sup>th</sup> October 2016

**CERTIFICATE OF PARTICIPATION**

This is to certify that *Dr./Mr./Ms. Shweta Uma*.....

has Participated and presented an Oral Talk/ Poster in the Symposium.

**Prof. Guna Magesan**  
Vice Chancellor, UIAR

**Dr. Chandramani Pathak**  
Convener, CRCBT-2016



# Certificate

This is to certify that

*Shweta Umar*

has Delivered an **Oral Presentation** entitled  
*In vitro and in silico study of 4-flouropherylacetamide-acetyl  
coumarin induced cytotoxicity in A549 cell line via ROS mediated  
p53 dependent pathway*

in the **UGC Supported National Conference on  
'Current Trends in Biological Sciences - V'  
(CTBS – 2020)**

UGC - CENTRE OF ADVANCED STUDY  
Saturday, February 15, 2020

Organized By

**Post Graduate Department of Biosciences, Centre of Advanced Study**  
Sardar Patel University, Satellite Campus, Bakrol,  
Gujarat, India

**Prof. K. C. Patel**  
President

**Prof. R. B. Subramanian**  
Coordinator

**Dr. Hetalkumar Panchal**  
Organizing Secretary